Doctoral Dissertation
Doctoral Program in Complex Systems for Life Sciences (32^{nd}cycle)

Particle-based models reproducing collective dynamics of animal groups

By

Sara Bernardi

******

Supervisors:

Prof. Luigi Preziosi
Prof. Marco Scianna

Università degli Studi di Torino - Politecnico di Torino (DISMA)
2019 - 2020

Declaration

I hereby declare that, the contents and organization of this dissertation constitute my own original work and does not compromise in any way the rights of third parties, including those relating to the security of personal data.

Sara Bernardi

* This dissertation is presented in partial fulfillment of the requirements for the degree of ***Philosophiæ Diploma*** **(PhD degree)** in **Complex Systems for Life Sciences**.

Contents

Chapter 1

Preface

Collective migration in biological systems is a fascinating phenomenon observed at different levels, i.e., from the cellular scale to the case of animal populations. The First Part of this Thesis focuses on an emblematic example of coordinated multi-agent movement and organization: the swarming of honeybees. In particular, the dynamics of a bee colony is guided by a small group of scout individuals, which are informed of the target destination (e.g., the new nest). However, little is known on the mechanisms underlying this leader-follower system: i.e., in particular it is not clear the specific behavior that allows the leader to point out the flight direction and how this information then diffuses within the poopulation. These aspects are investigated in this dissertation with a discrete particle-based mathematical approach. In more details, each bee is here represented by a material point and assigned a role within the colony. Furthermore, it is set to move according to individual strategies and social interactions, the former involving the desire to reach a target destination and to communicate the flight direction, the latter accounting for repulsive/attractive stimuli and alignment processes.

Entering in more details, after the introduction of the biological phenomenon and of the modeling framework, we first study whether a single leader bee is able to transmit the direction of movement to the rest of the population, testing both topological and metric-based alignments. The former amounting to a synchronization to a given number of bees, regardless of distance; the latter to a synchronization to all bees within a set region. As a result, we observe that an efficient guidance is obtained under (i) a sufficiently large alignment region (i.e., defined by a radius encompassing the entire bee cloud) for metric alignments or (ii) for sufficiently high numbers of groupmates under topological alignment.

The second goal of the first Part of the Thesis is then to prise out how the subtlety of scout visibility and behaviour hypotheses impact on swarm efficiency. Specifically, we propose alternative assumptions on the flight synchronization mechanism of uninformed individuals and on the characteristic dynamics of the scout insects. In this respect, numerical realizations point out the combinations of behavioral hypotheses resulting in collective productive movement. Specifically, alignment mechanisms involving a control over groupmate velocity do not certainly imply directionally productive and collective swarm dynamics. An efficient and coordinate flight is instead reproduced if the follower individuals synchronize their movement (i) to all insects sufficiently close to their position and (ii) only to close enough uninformed and leader groupmates, provided the fact that the leaders stop upon reaching the front of the cloud. Further, the correlation between scout percentage on total swarm size and guidance efficiency is investigated, with larger swarms demanding a smaller fraction of scouts to achieve comparable targeting. An analysis of the phenomenology of the swarm in domains with environmental complexity is also performed, and reproduces realistic morphological evolution of the cloud of insects, i.e. needed to circumnavigate structural elements.

Finally, experiments relative to the disruption of coordinated swarming behavior due to the confusing presence of high density traffic lines of forager bees are reproduced. In this respect, our results suggest that among the previously proposed combinations of behavioral assumptions, the most reliable set of hypotheses involves follower bees synchronising their movement to all the insects sufficiently close to their position regardless of their status, provided that the leaders slowly come back from the front to the rear edge of the bee cloud.

In the Second Part of this Thesis, another particle-based model is presented, which is able to capture self-organization and movement of a generic group of animals. Again, each agent moves following a first-order ODE, however this approach distinguishes individual speed and orientation. In particular, the latter is the result of the balance of a given set of behavioral stimuli, each of them defined by a direction and a weight, that quantifies its relative importance. Working in the limit of fast orientation dynamics, such a second modeling is intrinsically based on a minimal set of parameters and is able to capture and classify, in terms of pattern and type of motion, a number of collective group evolutions emerging from different individual preferred dynamics. This approach is then here extended to account for group heterogeneity, i.e., for the presence of predators with different hunting strategies (i.e., confused vs. not confused) which impacts on the behavior of a prey population. The proposed dissertation is also equipped by a review on the pertinent literature dealing with collective animal dynamics with a particular emphasis on discrete models. Along the

dissertation some hints for possible developments and future perspectives of the proposed approaches are given. Comments on the numerical results are provided as well.

Papers related to this Ph.D. Thesis:

1. Bernardi S., Colombi A., Scianna M., *A discrete particle model reproducing collective dynamics of a bee swarm*, Computers in biology and medicine, 93, 158 –174, 2018, IRIS AperTo ID (handle) No. 2318/1711576

2. Bernardi S., Colombi A., Scianna, M., *A particle model analysing the behavioural rules underlying the collective flight of a bee swarm towards the new nest*, Journal of biological dynamics, 12.1, 632 – 662, 2018, IRIS AperTo ID (handle) No. 2318/1711566

3. Bernardi S., Colombi A., *A particle model reproducing the effect of a conflicting flight information on the honeybee swarm guidance, Communications in Applied and Industrial Mathematics*, 9.1, 159 – 173, 2018, IRIS AperTo ID (handle) No. 2318/1711573

4. Bernardi S., Scianna M., *An agent-based approach for modelling collective dynamics in animal groups distinguishing individual speed and orientation*, 2019, submitted to Philosophical Transaction of the Royal Society B.

Chapter 2

A brief review on selected modeling approaches for collective migration

The description of the collective and coordinated dynamics of groups of animals is a challenging topic for theoretical researchers. Populations of intelligent living entities are in fact *complex systems*, since the component individuals are not passively dragged by external forces but rather they undergo active decision-based dynamics, so that the use of classical passive mechanics is no longer sufficient. The overall evolution of the group in fact emerges from the rules governing the individual behavior. The mathematical and computational literature in this field presents indeed a particularly wide range of approaches.

For instance, *microscopic* models (also called individual-based models, IBMs) describe a group of animals as a collection of isolated agents: each of them is individually considered, assimilated for instance to a point particle or a quasi-rigid disk and followed during motion. More specifically, a first subgroup of microscopic models is represented by the so-called *cellular automata* (CA), where each animal is set to behave according to phenomenological algorithmic rules, that depend on its individuality and/or on the surrounding environment. Another subtype of microscopic approach involves instead *discrete* models: they rely on classical Newtonian laws of point mechanics, as the motion of each agent is defined by a first- or a second-order ordinary differential equation (ODE). Microscopic approaches are typically able to provide a detailed description of the dynamics of each agent and therefore represent a natural tool to investigate animal world-related collective phenomena (see, for instance, [20, 26, 27, 32, 39, 44, 47, 58, 67]).

However, when the number of component individuals is significantly large, as in the case of fishes [64] or myxobacteria [99, 51], microscopic methods become computationally expensive and therefore different approaches are needed. In this respect, *continuous models*, characteristic of a *macroscopic* point of view, rely on the definition of a proper density of agents, which evolves following (typically nonlinear) partial differential equations (PDEs), which implement conservation laws and require phenomenological assumptions for their closure, see for example [11, 93–95]. It is useful to remark that the rules of motion underlying discrete and continuous approaches often coincide: however, in the former case, they are related to the individual behavior of single agents, whereas, in the second case, they account for the dynamics of the overall population density, treated as an undifferentiated element.

A bridge between the microscopic word and the macroscopic representation of animal systems is represented by *kinetic* models. Characteristics of a *mesoscopic* point of view, they are able to derive, employing hydrodynamic arguments, Boltzmann-like evolution laws for statistical distribution functions, which describe position and velocity of the components of the population of interest [12, 16, 52].

As said in the Abstract, the models presented in this dissertation belong to the class of microscopic/discrete methods. This choice is justified by the fact that (i) we typically deal with bee swarm or animal populations formed by a number of individuals that can be easily approached from a numerical perspective and (ii) the topic of the Thesis is to shed light on individual behavioral assumptions that result in selected collective dynamics.

Part I

A particle-based model analyzing honeybee swarming

Chapter 3

Biological background

The aim of describing emerging *collective* dynamics of populations of interacting individuals, such as birds, fishes, insects and certain mammals, from individual behaviors has increased in the last decades the multidisciplinary interest of various research communities, e.g., biologists, ecologists, sociologists, physicists, and applied mathematicians.

For instance, the coordinated behavior of bee swarms represents an interesting problem to be studied. Such insect populations, which are typically composed by the old queen and by 10000 to 30000 worker individuals, in fact undergo a synchronized flight with the specific purpose of reaching a new nest site [87]. All colonies are subject to this natural phenomenon, and every year beekeepers have to deal with it in late spring and early summer. In this period, as the weather warms up and flowers begin to bloom, the colony is in fact at the peak of its capacity and ready to produce a new hive.

In this respect, each bee swarm has to face two challenges: it first needs to identify a suitable new location using a process of community site selection and then it has to move towards the chosen destination. Entering in more details, when the migrating bees leave the original hive they first temporarily settle on a tree branch a few meters away from the old nest. There, they cluster around the queen, and a small fraction of bees (called *scouts*) starts exploring the surrounding area. Specifically, the latter represent only the $3\% - 5\%$ of the whole swarm, i.e. the swarming process relies on the guidance of very few informed bees. These individuals inspect possible locations for the new nest to assess their quality, in terms of volume, aspect, size and height of entrance, and presence of structures left by other bee colonies [87, 89]. Then, they return to the rest of the population and perform a waggle dance to broadcast information on the characteristics of the explored sites. Nest

Figure 3.1 Bees congregate on a tree branch after swarming from their hive, waiting for a new nest to be found by the scout bees. Picture taken from `http://sciamiapi.blogspot.com/2015/03/recupero-sciami-di-api.html`

proposals coming from the scout bees may be different but, after some hours (sometimes days), an agreement is finally found.

The whole swarm finally takes off and compactly flies towards the chosen destination, following the guidance of the informed/scout individuals. In this respect, various assumptions have been proposed to account for the migration mechanisms underlying this leader-follower system. First, it was hypothesized that the scout bees can guide the cloud of insects to the new home by producing the Nasonov pheromone, [2]. However, a subsequent experimental study revealed that such a chemical substance is not really involved in the flight guidance process, while it is crucial to help the uninformed/follower individuals to find the entrance of the new nest [6].

A different family of possible explanations instead involves selected visual signals. For instance, the *streaker hypothesis* is based on the empirical observations experienced by Lindauer. Specifically, in 1955 he suggested that the scout insects can transmit the direction of movement by a characteristic flight through the swarm [73]. In particular, such informed bees are observed to streak at high speed from the back of the swarm to its front. However, once they have reached the front of the cloud, their behavior is still unknown. In this respect, in [85, 87], two possible dynamics are suggested: (i) they may slowly fly back towards the rear edge of the swarm or (ii) they may stop and wait to be passed by the rest of the groupmates. In both cases, the scout bees then start again to streak towards the leading edge of the insect cloud and the process is iterated. How the follower individuals acquire the information of the correct migration direction under the scout guidance is debated as well. More specifically, each different hypothesis on their flight synchronization

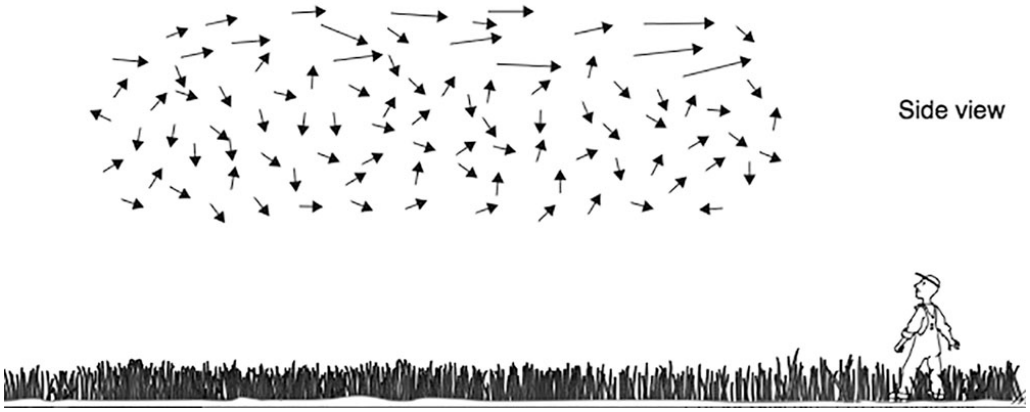

Figure 3.2 Schematic view of the flight patterns of bees in a swarm flying to the right. Lindauer reported the presence of streaker bees flying within the swarm cloud, [87].

mechanism involves the alignment with a distinct set of groupmates, composed, e.g., by faster individuals, or by closer individuals, or only by informed individuals. The First Part of this Thesis aims to mathematically investigate these aspects in order to elucidate individual behaviour underlying this interesting collective migration.

Chapter 4

General modeling framework

This chapter will introduce the modeling framework that will be employed to describe bee swarming with particular emphasis on the math notation.

4.1 Bee representation and characteristics

Swarm dynamics is constantly modeled in two-dimensional domains $\Omega \subseteq \mathbb{R}^2$, whose dimensions will be specified later on. We indeed consider a planar section, parallel to the ground, of a typical bee swarm, see Fig. 4.1. The target destinations of the insects are then assumed to be constituted by subregions of the domain. Each insect $i = 1, ..., N$, being N the total number of individuals, is an autonomous discrete agent, represented by a material point with concentrated mass. In particular, the generic i-th bee is uniquely defined by the following set of variables:

$$(\mathbf{x}_i(t), \mathbf{v}_i(t), s_i(t)) \in \Omega \times \mathbb{R}^2 \times \mathcal{S}. \tag{4.1}$$

Specifically, the vectors $\mathbf{x}_i(t)$ and $\mathbf{v}_i(t)$ denote individual position and velocity, respectively, whereas $s_i(t)$ is a state variable which defines the role that the insect of interest has within the swarm, e.g. U('uninformed'), L('leader') or F('forager'), being $\mathcal{S}$ the set containing all its possible specifications.

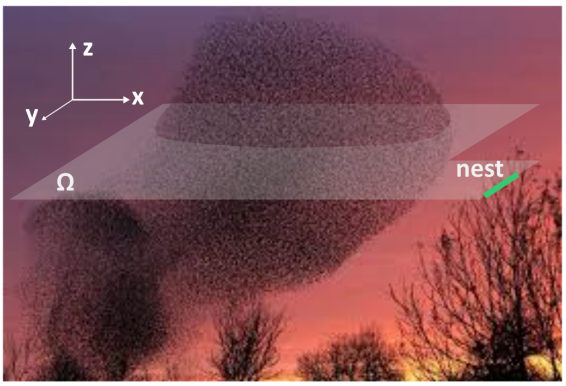

Figure 4.1 The virtual population of bees is modeled in a two-dimensional domain $\Omega \subseteq \mathbb{R}^2$, i.e., we are taking into account a planar section of a typical swarm. The aim of the insect population is to reach a new nest, which is constituted by a subregion of the domain. The domain may represent a large open-space or it may account for environmental elements, such as trees or buildings.

4.2 Bee dynamics

The dynamics of a generic bee i can be described starting from a general second-order particle model:

$$m_i \frac{d^2\mathbf{x}_i}{dt^2}(t) + \lambda_i \frac{d\mathbf{x}_i}{dt}(t) = \mathbf{F}_i(t), \tag{4.2}$$

where m_i is the individual mass and λ_i a friction coefficient. $\mathbf{F}_i$ denotes instead the resultant of the forces that affect insect behavior. However, it is worth to notice that bees (such as most living entities, e.g., from cells and bacteria to big animal species and humans) are not passively prone to the Newtonian laws of inertia. They are in fact intelligent individuals able to actively develop behavioral strategies, which depend both on intrinsic stimuli and on the interactions with the surrounding environment. For instance, bees can control their movement without undergoing inertial effects: in other words, they can suddenly decide to stop and change direction of motion, at least for reasonable speeds. These concepts allow to neglect the inertial term in Eq. (4.2), i.e., to assume, in mathematical terms, that $\lambda_i >> m_i$ and to obtain

$$\underbrace{\frac{m_i}{\lambda_i}}_{\to 0} \frac{d^2\mathbf{x}_i}{dt^2}(t) + \frac{d\mathbf{x}_i}{dt}(t) = \frac{\mathbf{F}_i(t)}{\lambda_i} \qquad \Rightarrow \qquad \frac{d\mathbf{x}_i}{dt}(t) = \frac{\mathbf{F}_i(t)}{\lambda_i} = \underbrace{\widetilde{\mathbf{v}}_i(t)}_{\substack{\text{bee} \\ \text{velocity}}}. \tag{4.3}$$

Eq. (4.3) gives the so-called *overdamped force-velocity response* relation, which states that the velocity of an individual, and not his/her acceleration, is proportional to the acting forces: it is employed in a number of discrete/IBM approaches (see [23, 29, 41, 86] and references therein for comments) and allows to describe selected bee behavior by a direct phenomenological postulation of the velocity contributions, i.e., by a first-order model.

Remark. The choice of a more general second-order model would imply greater persistence of particle motion with respect to a first-order description. In fact, the inertial term would have the effect of smoothing the trajectories, e.g. of preventing particles to carry out a right angle bend; rather they perform a parabolic curve. As a consequence, in the presence of inertia, the agent-based system would need a larger time to reach the asymptotic configurations.

The individual velocity $\widetilde{\mathbf{v}}_i$ has then to be characterized by a realistic modulus, i.e. subjected to physical constraints and limitations, and an orientation. In this respect, the equation of motion of the generic bee i is finally assumed to be

$$\frac{d\mathbf{x}_i(t)}{dt} = \widetilde{\mathbf{v}}_i(t) = \min\left\{ v_{\max}^{s_i(t)}(t), |\mathbf{v}_i(t)| \right\} \frac{\mathbf{v}_i(t)}{|\mathbf{v}_i(t)|}, \tag{4.4}$$

where $v_{\max}^{s_i(t)}$ denotes the maximal speed of the i-th individual according to its actual status, avoiding also unrealistically high speeds. The velocity of each individual is defined by the superposition of different possible velocity contributions, i.e.,

$$\mathbf{v}_i(t) = \underbrace{\mathbf{v}_i^{\mathrm{dir}}(t)}_{\text{individual strategy}} + \underbrace{\mathbf{v}_i^{\mathrm{rep}}(t) + \mathbf{v}_i^{\mathrm{attr}}(t) + \mathbf{v}_i^{\mathrm{align}}(t)}_{\text{social interactions}} + \underbrace{\mathbf{v}_i^{\mathrm{rand}}(t)}_{\text{noise}} + \underbrace{\dots}_{\text{other behaviors}} \tag{4.5}$$

The first term in Eq. (4.5) describes the strategic behavior of each bee (e.g., the attempt to reach a target destination while minimizing the effort, covering the shortest possible path at a comfort speed, but other strategies may of course be taken into account). The social contribution results from different individual behaviors. Specifically, the repulsive component $\mathbf{v}_i^{\mathrm{rep}}$ models the tendency of the generic i-th bee of staying sufficiently far away from its neighbours, typically in order to avoid physical collisions, while maintaining a minimal comfort space within the swarm. The third contribution in Eq. (4.5) implements the desire of each individual to keep a connection with the groupmates, i.e., to be close enough to the rest of the population. Finally, the social velocity term $\mathbf{v}_i^{\mathrm{align}}$ describes the alignment process of bees, i.e., the adaptation and synchronization of their movement with

at least a given part of the swarm. Finally, the random fluctuation term implements the impossibility of an individual to apply the ideal set of rules, e.g., to take the correct and productive decision in a very short time. Other behavioural contributions may be easily added to the model framework.

Entering in more details, the repulsive/attractive behavior of the i-th bee is described by proper kernels $\mathbf{H}_{ij}^{\text{rep}}, \mathbf{H}_{ij}^{\text{attr}} : \mathbb{R}^2 \times \mathbb{R}^2 \longmapsto \mathbb{R}^2$, which define its pairwise interaction instances with the generic j-th individual falling within a given neighbourhood, say $\mathcal{N}_i^{\text{rep}}$ and $\mathcal{N}_i^{\text{attr}}$, respectively. We then assume that (i) the above-introduced kernels do not depend on the specific couple of bees, i.e., $\mathbf{H}_{ij}^{\text{rep}} = \mathbf{H}^{\text{rep}}$ and $\mathbf{H}_{ij}^{\text{attr}} = \mathbf{H}^{\text{attr}}$ for any (i, j), (ii) the resulting velocity contributions have an effect on the direction ideally connecting the interacting insects and (iii) they depend on individual relative distance. In this respect, we can write:

$$\mathbf{v}_i^{\text{rep}}(t) = \sum_{j \in \mathcal{N}_i^{\text{rep}}(t)} \mathbf{H}^{\text{rep}}(\mathbf{x}_j(t), \mathbf{x}_i(t)) = \sum_{j \in \mathcal{N}_i^{\text{rep}}(t)} h^{\text{rep}}(|\mathbf{r}_{ij}(t)|) \frac{\mathbf{r}_{ij}(t)}{|\mathbf{r}_{ij}(t)|}; \tag{4.6}$$

$$\mathbf{v}_i^{\text{attr}}(t) = \sum_{j \in \mathcal{N}_i^{\text{attr}}(t)} \mathbf{H}^{\text{attr}}(\mathbf{x}_j(t), \mathbf{x}_i(t)) = \sum_{j \in \mathcal{N}_i^{\text{attr}}(t)} h^{\text{attr}}(|\mathbf{r}_{ij}(t)|) \frac{\mathbf{r}_{ij}(t)}{|\mathbf{r}_{ij}(t)|}, \tag{4.7}$$

where $\mathbf{r}_{ij}(t) := \mathbf{x}_j(t) - \mathbf{x}_i(t)$ and the continuous and Lebesgue integrable functions $h^{\text{rep}}, h^{\text{attr}} : \mathbb{R}_+ \longmapsto \mathbb{R}$ are such that

$$h^{\text{rep}}(|\mathbf{r}_{ij}(t)|) \leq 0; \tag{4.8}$$

$$h^{\text{attr}}(|\mathbf{r}_{ij}(t)|) \geq 0, \tag{4.9}$$

for all pairs of bees (i, j) and corresponding positions $(\mathbf{x}_i, \mathbf{x}_j)$. In this perspective, in Eqs. (4.6) - (4.7) the notation $j \in \mathcal{N}_i^{\bullet}(t)$ has to be intended as $j : \mathbf{x}_j(t) \in \mathcal{N}_i^{\bullet}(t)$, where $\bullet \in \{\text{“rep”}, \text{“attr”}\}$.

The alignment contribution in the dynamics of the generic i-th bee results instead from a mean over the velocity of a given set of its neighbours that, as we will see in the following, has to be specified according to biological assumptions.

The proposed approach is intrinsically multiparametric. In particular, the model coefficients can be classified in two groups: those that have a direct and measurable biological meaning (e.g., speed values) and those that are more technical, i.e., that only subsume experimental dynamics, such as the interaction coefficients. We will indeed derive a composite parameter setting, obtained by observations and data present both in

the experimental and in the theoretical literature and, when necessary, by preliminary numerical realizations.

Given the above-described general math framework, in the next Chapters we will study different hypotheses on the individual bee movement. In particular, we will test different assumptions on the velocity terms included in Eq. (4.5), in order to elucidate selected biological mechanisms underlying bee swarming behavior.

Chapter 5

Analysis of the collective dynamics of a swarm guided by a single leader

In this Chapter, we will test combinations of alternative assumptions related to flight alignment mechanisms and bee pairwise interactions. The obtained theoretical results will be also used to reduce the free space of possible parameter variations.

Entering in more details, the rest of this Chapter is organized as follows. In Section 5.1, we clarify the assumptions on which our mathematical approach is based and we present the model components. Section 5.2 deals with different assumptions underlying flight synchronization mechanisms. In particular, we focus either on an Euclidean metric-based or on a topological neighborhood metric-based alignment process within the swarm. In this respect, we discuss how these two mutually exclusive hypotheses impact on the repulsion/attraction velocity contributions (which in turn have to satisfy a stability condition to assure a realistic crystalline patterning of the particle system). Different series of numerical realizations then analyze the swarm behavior in different parameter regimes and show that our approach is able to capture selected experimentally-observed swarm phenomenology (e.g., flight synchronization and productive motion). After discussing in Section 5.3 the effect of the inclusion of random contributions on the particle system, we review in Section 5.4 the results obtained in this Chapter.

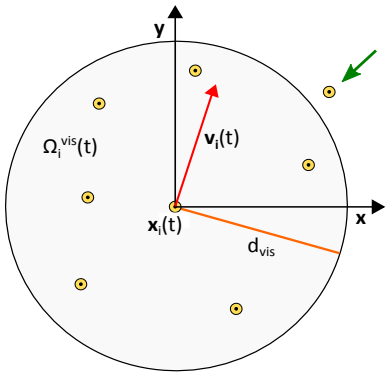

Figure 5.1 Each bee i is represented as a material point. Given its actual position $\mathbf{x}_i(t)$ and velocity $\mathbf{v}_i(t)$, for each insect we define a visual region $\Omega_i^{\text{vis}}(t)$, i.e., a round area determined by the bee visual depth d_{vis}. The inclusion of a visual field implies that each bee is not able to see and therefore to interact with the entire set of their groupmates (see the individual indicated by the green arrow). For representative purposes, hereafter the virtual bees will be indicated by rigid disks centered at their actual position.

5.1 Modeling details

Bee characteristics. In this case the domain Ω coincides with the entire space $\mathbb{R}$. The simulated swarm accounts for a leader bee that guides the rest of follower individuals, i.e. the status set is given by

$$\mathcal{S} = \{U(\text{'uninformed'}); L(\text{'leader'})\} \tag{5.1}$$

We further define, for each insect i, a proper visual/perception region, as reproduced in Fig. 5.1:

$$\Omega^{\text{vis}}(t) = \left\{\mathbf{y} \in \mathbb{R}^2 : |\mathbf{y} - \mathbf{x}_i(t)| \leq d_{\text{vis}}\right\}. \tag{5.2}$$

It is a round region centered at $\mathbf{x}_i(t)$ with radius d_{vis}, that represents the bee vision depth.

Bee dynamics. The group of insects behaves following the system (4.4). For simplicity, we set $v_{\max}^U = v_{\max}^L = v_{\max}$, i.e., as first modeling step we assume that the maximal speed does not depend on the bee status. In particular, the differentiated, i.e., status-dependent, rules of motion read as

$$\mathbf{v}_1(t) = \mathbf{v}_1^{\text{targ}}(t) + \mathbf{v}_1^{\text{rep}}(t) + \mathbf{v}_1^{\text{attr}}(t), \quad \text{with } s_1(t) = L \tag{5.3}$$

$$\mathbf{v}_i(t) = \mathbf{v}_i^{\text{align}}(t) + \mathbf{v}_i^{\text{rep}}(t) + \mathbf{v}_i^{\text{attr}}(t), \quad \text{with } s_i(t) = U, \quad \forall\, i = 2,3,\ldots,N. \tag{5.4}$$

Eqs. (5.3)-(5.4) state that all bees are characterized by repulsive/attractive interactions. Further, only one bee, identified with the index 1 and with the leader status is set to have a target velocity component, i.e., it is the only one *informed* of the destination of the entire swarm (e.g., of the location of the new nest). The presence of a small group of leader bees within a swarm, which are able to guide the rest of the population is widely known from the ecological literature [87]. Entering in more details, assuming $\mathbf{x}_{\text{nest}}$ as the target point, we set

$$\mathbf{v}_1^{\text{targ}}(t) = v_{\max} \frac{\mathbf{x}_{\text{nest}} - \mathbf{x}_i(t)}{|\mathbf{x}_{\text{nest}} - \mathbf{x}_i(t)|}, \tag{5.5}$$

i.e., the leader bee aims to cover the shortest possible path towards the destination at the possible maximal speed. On the opposite, all the other individuals undergo alignment process. Specifically, this contribution is given by a mean over the velocity of a given set of its neighbours, i.e., for the i-th follower

$$\mathbf{v}_i^{\text{align}}(t) = < \mathbf{v}_j(t) >_{j \in \mathcal{N}_i^{\text{align}}(t)}, \tag{5.6}$$

where the notation $j \in \mathcal{N}_i^{\text{align}}(t)$ stands for $j : \mathbf{x}_j(t) \in \mathcal{N}_i^{\text{align}}(t)$.

5.2 Social velocity components: Assumptions and simulations

We now test different hypotheses on the alignment velocity component, in particular on the synchronization region $\mathcal{N}^{\text{align}}$, which impact also on the repulsive/attractive contributions.

5.2.1 Euclidean metric-based alignment mechanism

We first assume that the alignment mechanism, as well as the individual repulsive/attractive behavior, relies on Euclidean metric arguments, i.e., for any $i = 1, \ldots, N$, it involves all the bees $j = 1, \ldots, N$, with $i \neq j$, whose distance from the i-th insect falls within a given range. In particular, we identify three concentric regions such that each of them characterizes one of the social velocity components (see Fig. 5.2, left panel):

$$\mathcal{N}_i^{\text{rep}}(t) \quad = \quad \left\{ j = 1, \ldots, N, j \neq i : \mathbf{x}_j(t) \in \Omega_i^{\text{vis}}(t), 0 < |\mathbf{r}_{ij}(t)| \leq d_{\text{rep}} \right\}; \tag{5.7}$$

$$\mathcal{N}_i^{\text{align}}(t) = \left\{ j = 1,\dots,N, j \neq i : \mathbf{x}_j(t) \in \Omega_i^{\text{vis}}(t), d_{\text{rep}} < |\mathbf{r}_{ij}(t)| \leq d_{\text{align}} \right\}; \quad (5.8)$$

$$\mathcal{N}_i^{\text{attr}}(t) = \left\{ j = 1,\dots,N, j \neq i : \mathbf{x}_j(t) \in \Omega_i^{\text{vis}}(t), d_{\text{align}} < |\mathbf{r}_{ij}(t)| \leq d_{\text{attr}} \right\}, \quad (5.9)$$

where $\Omega_i^{\text{vis}}(t)$ is the actual visual field of the i-th bee, as defined in Eq. (5.2) and again $\mathbf{r}_{ij}(t) := \mathbf{x}_j(t) - \mathbf{x}_i(t)$.

To completely determine individual dynamics, we have finally to define the interaction kernels. In this respect, although there are several possible options, we take advantage of some published results [24, 25] and set, for each couple of bees (i, j):

$$h^{\text{rep}}(|\mathbf{r}_{ij}(t)|) = \begin{cases} f_{\text{rep}} \left(\dfrac{1}{d_{\text{rep}}} - \dfrac{1}{|\mathbf{r}_{ij}(t)|} \right), & \text{if } 0 < |\mathbf{r}_{ij}(t)| \leq d_{\text{rep}}; \\ 0, & \text{otherwise;} \end{cases} \quad (5.10)$$

$$h^{\text{attr}}(|\mathbf{r}_{ij}(t)|) = \begin{cases} -\dfrac{4 f_{\text{attr}} (|\mathbf{r}_{ij}(t)| - d_{\text{attr}}) (|\mathbf{r}_{ij}(t)| - d_{\text{align}})}{(d_{\text{attr}} - d_{\text{align}})^2}, & \text{if } d_{\text{align}} < |\mathbf{r}_{ij}(t)| \leq d_{\text{attr}} \\ 0, & \text{otherwise.} \end{cases} \quad (5.11)$$

For instance, such Newtonian-type short-range hyperbolic kernel has been used by Diwold and coworkers to reproduce the collective flight of red dwarf honeybees (cf. [39], Eq. (1)) and by Chen and Kolokolnikov to study predator-swarm interactions (cf. [19], Eq. (1.1) and the references below). Repulsive kernels with similar trends (i.e., which go to infinity as $|\mathbf{r}_{ij}|^{\alpha}$, with $\alpha < 0$, when $|\mathbf{r}_{ij}| \to 0$, being $|\mathbf{r}_{ij}|$ the distance between two interacting agents) have been implemented also in the case of discrete approaches for zebrafish embryogenesis [38] and endothelial patterning on polymers [60]. Further, we do not use linear Hooke-like attraction laws, such as those introduced in some of the previously cited works dealing with swarming, e.g., [19, 39], since we hypothesize that the attractive stimulus is negligible when two bees are very close and, after a maximum, it decreases again to zero at d_{attr}, which is taken to be the margin of the visual field. Finally, according to us, it is plausible that pairs of insects falling substantially apart one from each other do not have a significant mutual influence. Analogous attraction functions has been used in the case of other particle models relative to bee and cell dynamics, see [23–25] and references therein.

The functions defined in Eqs. (5.10)-(5.11), and plotted in Fig. 5.2 (right panel), are intrinsically multiparametric, since they are characterized by the following set of

coefficients:

$$(d_{\text{rep}}, d_{\text{align}}, d_{\text{attr}}, f_{\text{rep}}, f_{\text{attr}}) \in \mathbb{R}^5_+.$$

To decrease the complexity of the problem, we can reduce the dimension of the free parameter space with phenomenological arguments and observations. First of all, d_{rep} can be intended as the comfort distance that each bee tends to preserve in order to fly without colliding with other components of the swarm. According to several experimental measurements, we estimate $d_{\text{rep}} = 0.3$ m [87]. On the opposite, d_{attr} is the extension of the long-range attraction, i.e., of the desire of each individual to remain sufficiently close to the rest of the population. In this respect, it is consistent to assume $d_{\text{attr}} = d_{\text{vis}} = 10$ m, i.e., each bee is attracted by the groupmates that it is able to see (and that do not fall within the alignment and repulsion regions). In this respect, given the estimated extension of the three interaction neighborhoods, we have that

$$\mathcal{N}_i^{\text{rep}}(t) \cup \mathcal{N}_i^{\text{align}}(t) \cup \mathcal{N}_i^{\text{attr}}(t) = \Omega_i^{\text{vis}}(t),$$

for each insect i and time t, see again Fig. 5.2 (left panel).

The above considerations allow us to reduce the parameter space of the problem to

$$(d_{\text{align}}, f_{\text{rep}}, f_{\text{attr}}) \in [d_{\text{rep}}, d_{\text{attr}}] \times \mathbb{R}^2_+.$$

Given the form of $h^{\text{attr}}(r)$, $f_{\text{attr}} \in [0, v_{\max}]$ can be interpreted as the maximal attraction speed, whereas $f_{\text{rep}} > 0$ determines the slope of the hyperbolic part of $h^{\text{rep}}(r)$ (cf. Fig. 5.2, right panel).

Further, the swarm has to maintain a realistic crystalline configuration during the collective flight. In this respect, it has been shown that the large-time asymptotic collective pattern of discrete particle systems depends on the stability characteristics of the potential relative to individual pairwise interactions [84]. In particular, we use and extend to our case the criterium introduced in [13], applied to the case of cell aggregates in [14], in order to identify the regions of the free parameter space that assure the H-stability of a particle system. We can indeed prove:

Theorem 5.2.1. *If the following parametric relation*

$$\frac{f_{\text{rep}}}{f_{\text{attr}}} > \frac{2(d_{\text{attr}} - d_{\text{align}})}{5(d_{\text{rep}})^2} \left(3(d_{\text{align}})^2 + 4 d_{\text{attr}} d_{\text{align}} + 3(d_{\text{attr}})^2\right) \tag{5.12}$$

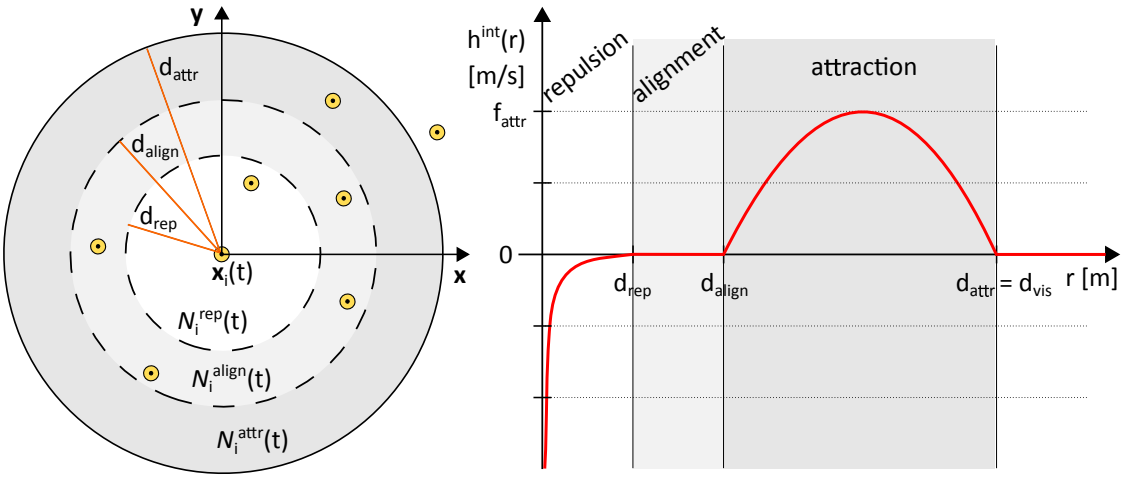

Figure 5.2 Euclidean metric-based alignment mechanism. Left panel: Representation of the three interaction regions: the repulsive neighborhood $\mathcal{N}_i^{\text{rep}}(t)$ (see Eq. (5.7)), the alignment neighborhood $\mathcal{N}_i^{\text{align}}(t)$ (see Eq. (5.8)), and the attractive neighborhood $\mathcal{N}_i^{\text{attr}}(t)$ (see Eq. (5.9)). In particular, assuming $d_{\text{attr}} = d_{\text{vis}}$, we have that the three interaction regions entirely cover the visual field of each animal, i.e., $\mathcal{N}_i^{\text{rep}}(t) \cup \mathcal{N}_i^{\text{align}}(t) \cup \mathcal{N}_i^{\text{attr}}(t) = \Omega_i^{\text{vis}}(t)$. Right panel: Plot of the pairwise interaction kernel $h^{\text{int}} : \mathbb{R}_+ \longmapsto \mathbb{R}$ given by the sum of the repulsive and attractive functions defined in Eqs. (5.10)-(5.11), i.e., $h^{\text{int}}(r) = h^{\text{rep}}(r) + h^{\text{attr}}(r)$.

holds, the potential related to the pairwise interaction kernel $h^{\text{int}}(r) = h^{\text{rep}}(r) + h^{\text{attr}}(r)$, with $r = |\boldsymbol{r}_{ij}(t)| = |\boldsymbol{x}_j(t) - \boldsymbol{x}_i(t)|$, defined in Eqs. (5.10)-(5.11) is H-stable. As shown in [13, 18, 40], for a finite number of agents, as in the case of our interest, this implies that, at each time $t \in \mathbb{R}_+$, there exist two finite and positive quantities $d_{\min}(t) = \min_{\substack{i,j=1,\dots,N \\ i \neq j}} |\boldsymbol{x}_i(t) - \boldsymbol{x}_j(t)|$ and $d_{\max}(t) = \max_{\substack{i,j=1,\dots,N \\ i \neq j}} |\boldsymbol{x}_i(t) - \boldsymbol{x}_j(t)|$ such that $d_{\min}(t) \leq |\boldsymbol{x}_i(t) - \boldsymbol{x}_j(t)| \leq d_{\max}(t)$ for all pairs (i, j) of bees, i.e., at each time $t \in \mathbb{R}_+$ the swarm does not collapse nor explode. In particular, for $t \to +\infty$, the minimal relative distance between bees $d_{\min}(t)$ tends to the limit value d_∞, whereas the maximal relative distance $d_{\max}(t)$ (which also represents the diameter of the swarm) tends to the value D_∞: in other words, the particle population asymptotically organizes in a stable crystalline-like pattern.

Proof. Following the analytical study in [13] and the calculations introduced in [14], we have first to define a potential $u^{\text{int}} : \mathbb{R} \longmapsto \mathbb{R}$ associated to our pairwise interaction kernels,

i.e.,

$$u^{\text{int}}(r) = \int h^{\text{int}}(r)dr = \int h^{\text{rep}}(r)dr + \int h^{\text{attr}}(r)dr =$$

$$= \begin{cases} f_{\text{rep}}\left(\dfrac{r}{d_{\text{rep}}} - \log r\right) + C_1, \\ \text{if } 0 < r \leq d_{\text{rep}}; \\ \\ C_2, \\ \text{if } d_{\text{rep}} < r \leq d_{\text{align}}; \\ \\ -\dfrac{2 f_{\text{attr}}\left(2r^3 - 3\left(d_{\text{attr}} + d_{\text{align}}\right) r^2 + 6 d_{\text{attr}} d_{\text{align}} r\right)}{3(d_{\text{attr}} - d_{\text{align}})^2} + C_3, \\ \text{if } d_{\text{align}} < r \leq d_{\text{attr}}; \\ \\ C_4, \\ \text{otherwise}, \end{cases}$$

where the constants C_1, C_2, C_3, C_4 have to satisfy the following conditions

$$\begin{cases} C_1 = C_2 - f_{\text{rep}}\left(1 - \log d_{\text{rep}}\right); \\ C_2 = C_3 - \dfrac{2 f_{\text{attr}}\left(2\left(d_{\text{align}}\right)^3 - 3\left(d_{\text{attr}} + d_{\text{align}}\right)\left(d_{\text{align}}\right)^2 + 6 d_{\text{attr}}\left(d_{\text{align}}\right)^2\right)}{3\left(d_{\text{attr}} - d_{\text{align}}\right)^2}; \\ C_3 = C_4 + \dfrac{2 f_{\text{attr}}\left(2\left(d_{\text{attr}}\right)^3 - 3\left(d_{\text{attr}} + d_{\text{align}}\right)\left(d_{\text{attr}}\right)^2 + 6\left(d_{\text{attr}}\right)^2 d_{\text{align}}\right)}{3\left(d_{\text{attr}} - d_{\text{align}}\right)^2}, \end{cases}$$

to assure its continuity. To fully apply the characterization of H-stable potentials given in [13], u^{int} has to be essentially negligible for large interparticle distances (i.e., $\lim_{r\to\infty} u^{\text{int}}(r) = 0$). Without loss of generality, we indeed assume $C_4 = 0$. As a consequence, with simple algebraic calculations, we have that

$$\begin{cases} C_3 = -\dfrac{2 f_{\text{attr}}(d_{\text{attr}})^2\left(d_{\text{attr}} - 3 d_{\text{align}}\right)}{3\left(d_{\text{attr}} - d_{\text{align}}\right)^2}; \\ C_2 = -\dfrac{2}{3} f_{\text{attr}}\left(d_{\text{attr}} - d_{\text{align}}\right); \\ C_1 = -\dfrac{2}{3} f_{\text{attr}}\left(d_{\text{attr}} - d_{\text{align}}\right) - f_{\text{rep}}\left(1 - \log d_{\text{rep}}\right). \end{cases}$$

The pairwise interaction potential therefore rewrites in the following explicit form

$$u^{\text{int}}(r) = \begin{cases} f_{\text{rep}}\left(\dfrac{r}{d_{\text{rep}}} - \log\left(\dfrac{r}{d_{\text{rep}}}\right) - 1\right) - \dfrac{2}{3} f_{\text{attr}}\,(d_{\text{attr}} - d_{\text{align}}), \\ \text{if } 0 < r \leq d_{\text{rep}}; \\ \\ -\dfrac{2}{3} f_{\text{attr}}\,(d_{\text{attr}} - d_{\text{align}}), \\ \text{if } d_{\text{rep}} < r \leq d_{\text{align}}; \\ \\ -\dfrac{2 f_{\text{attr}}\left(2r^3 - 3(d_{\text{attr}} + d_{\text{align}})r^2 + 6 d_{\text{attr}} d_{\text{align}} r + (d_{\text{attr}})^2\left(d_{\text{attr}} - 3 d_{\text{align}}\right)\right)}{3(d_{\text{attr}} - d_{\text{align}})^2}, \\ \text{if } d_{\text{align}} < r \leq d_{\text{attr}}; \\ \\ 0, \\ \text{otherwise.} \end{cases} \tag{5.13}$$

Now, recalling Definition 1.1 in [13], we can say that u^{int} (and consequently h^{int}) is H-stable if

$$\int_0^{+\infty} u^{\text{int}}(r)\, r\, dr > \frac{1}{2} \lim_{r \to +\infty} u^{\text{int}}(r) = 0.$$

In this respect, let us calculate the value of the integral of interest:

$$\begin{aligned} &\int_0^{+\infty} u^{\text{int}}(r) r\, dr \; = \\ &= \int_0^{d_{\text{rep}}} \left(f_{\text{rep}}\left(\frac{r^2}{d_{\text{rep}}} - r \log\left(\frac{r}{d_{\text{rep}}}\right) - r\right) - \frac{2}{3} f_{\text{attr}}(d_{\text{attr}} - d_{\text{align}}) r \right) dr \\ &\quad - \int_{d_{\text{rep}}}^{d_{\text{align}}} \left(\frac{2}{3} f_{\text{attr}}(d_{\text{attr}} - d_{\text{align}}) r \right) dr \\ &\quad - \int_{d_{\text{align}}}^{d_{\text{attr}}} \left(\frac{2 f_{\text{attr}}\left(2r^4 - 3(d_{\text{attr}} + d_{\text{align}}) r^3 + 6 d_{\text{attr}} d_{\text{align}} r^2 + (d_{\text{attr}})^2\left(d_{\text{attr}} - 3 d_{\text{align}}\right) r\right)}{3(d_{\text{attr}} - d_{\text{align}})^2} \right) dr \\ &= \frac{f_{\text{rep}}(d_{\text{rep}})^2}{12} - \frac{f_{\text{attr}}}{30}(d_{\text{attr}} - d_{\text{align}})\Big(3(d_{\text{align}})^2 + 4 d_{\text{attr}} d_{\text{align}} + 3(d_{\text{attr}})^2\Big), \end{aligned}$$

which is non-negative (assuring indeed the H-stability of the system) if the parametric relation in Eq. (5.12) holds. □

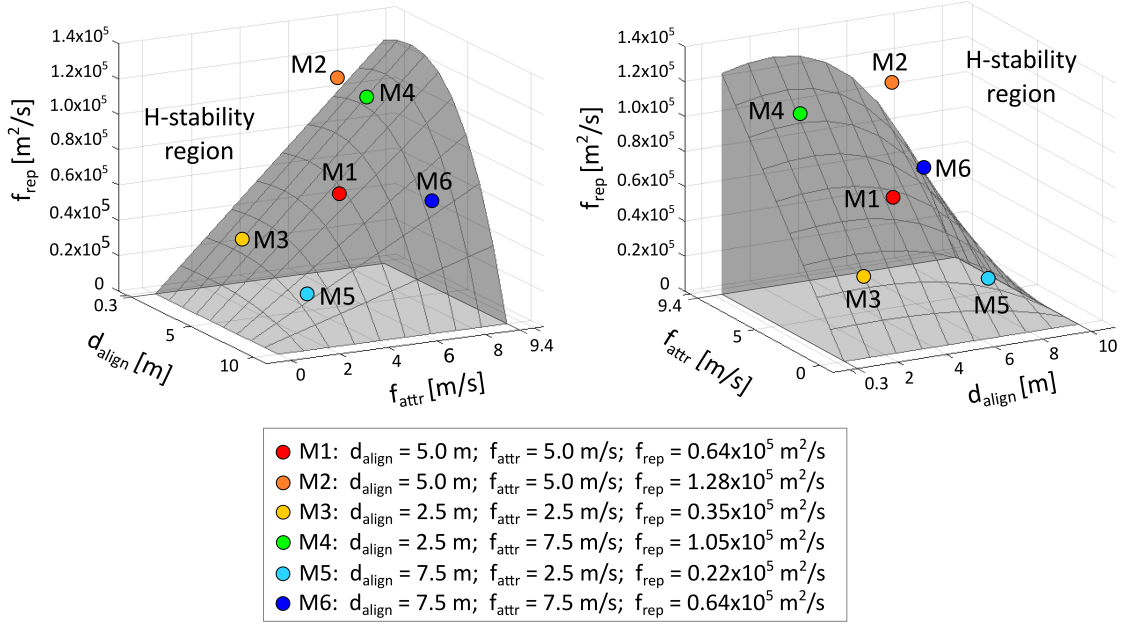

Figure 5.3 Euclidean metric-based alignment mechanism. Different views of the permitted parameter region, i.e., where h^{int} is H-stable. The space of free model coefficients is given by $(d_{\text{align}}, f_{\text{rep}}, f_{\text{attr}}) \in \mathbb{R}^3_+$. In particular, biological considerations allows the following restrictions: $d_{\text{align}} \in [d_{\text{rep}}, d_{\text{attr}}]$ and $f_{\text{attr}} \in [0, v_{\max}]$. The H-stability criterium in Eq. (5.12) further reduces the possible variations of parameter values to the region above the grey surface. Of the remaining combination of coefficients, we focus on the six sets Mk, where $k = 1, ..., 6$, since they are sufficiently distributed, thereby covering large enough parameter regimes.

Theorem 5.2.1 allows to better identify the parameter space, that is drawn in Fig. 5.3 (for the sake of clarity, we recall that $d_{\text{attr}} = 10$ m and that $d_{\text{rep}} = 0.3$ m). Specifically, only the points above the plotted surface are able to satisfy both experimental observations and the relation (5.12) (that assures the H-stability of the system). Each point of this area leads, in principle, to a different system evolution.

In this respect, we now turn to analyze swarm dynamics upon permitted variations of the model coefficients, i.e., within the region of H-stability. In particular, we study the behavior of a population formed by $N = 100$ bees, with 99 followers and 1 leader, according to the following classification of the particle system evolution:

Definition 5.2.2. The population of uninformed bees has a time asymptotic collective *swarming* behavior (with respect to the informed individual) if the following condition is

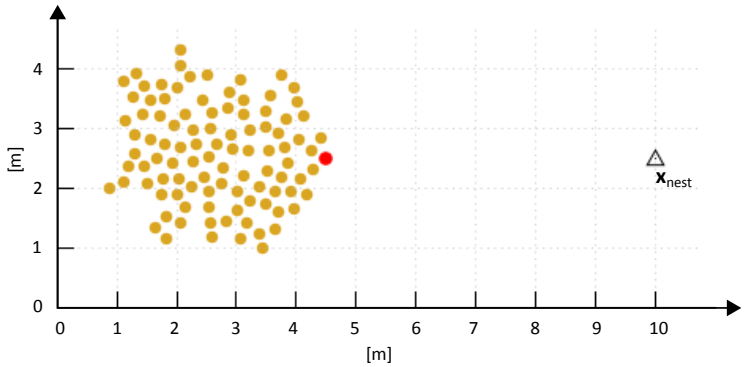

Figure 5.4 Initial spatial configuration of the swarm. The red disk denotes the position of the informed (leader) bee, while the follower individuals are represented by yellow disks. The target destination $\mathbf{x}_{\text{nest}}$ =(10 m, 2.5 m) is here represented by a triangle.

Table 5.1 Model parameters and corresponding references.

Parameter	**Description**	**Value [Unit]**	**Reference**
d_{vis}	bee visual depth	10 [m]	estimated
d_{rep}	repulsion range	0.3 [m]	[87]
d_{attr}	attraction range	10 [m]	estimated
$v_{\max}$	bee maximal speed	9.4 [m/s]	[87]
N	number of bees	100	

satisfied:

$$\lim_{t\to\infty} V_{\text{swarm}}(t) = \lim_{t\to\infty} \sqrt{\sum_{i=2}^{N} |\mathbf{v}_i(t) - \mathbf{v}_1(t)|^2} = 0. \tag{5.14}$$

The swarm undergoes a collective *productive motion* if the following condition is satisfied:

$$\lim_{t\to\infty} X_{\text{swarm}}(t) = \lim_{t\to\infty} \left| \frac{\sum_{i=2}^{N} \mathbf{x}_i(t)}{N-1} - \mathbf{x}_{\text{nest}} \right| = 0, \tag{5.15}$$

i.e., if the population of uninformed individuals (in terms of barycenter displacement) approaches the target destination. Representative sketches of the distinct behavior of the bee population are given in Figs. 5.5 - 5.6.

The swarm is initially arranged in an almost round pattern of radius equal to 2 m and centered at $(2.5\text{ m}, 2.5\text{ m})$, i.e., we initially account for a reasonable density of ≈ 8 bees/m^2 [87] (see Fig. 5.4).

The parameter values used in the simulations are summarized in Table 5.1.

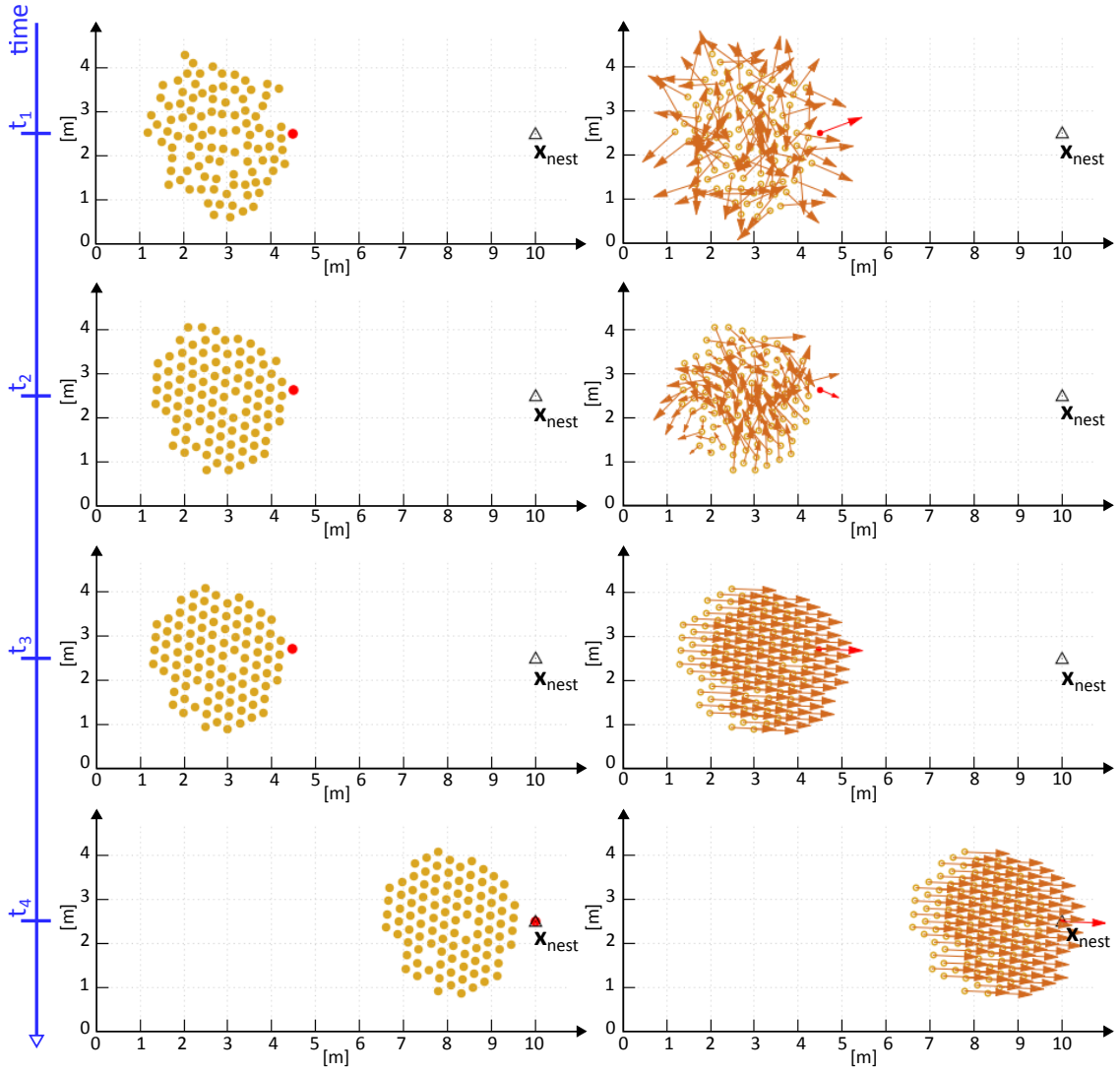

Figure 5.5 Representative evolution of the bee population in the case of swarming and productive movement. Left panels show the position of the insects at selected different times, right panels show also their direction of motion (i.e., the unit vector of their velocity, indicated by the orange arrow) at the same instants. It is possible to see that the bee cloud first undergoes crystallization (i.e., $t_1 \rightarrow t_2$) and then flight alignment and productive movement, i.e., behind the leader individual towards the target destination (i.e., $t_3 \rightarrow t_4$). Such a representative system evolution is obtained with the parameter combination $M6$: however, it is completely consistent for all the other analogous cases.

Among the possible combinations of the free model parameters $d_{\text{align}}, f_{\text{rep}}$, and f_{attr}, we hereafter focus on six representative sets, which are indicated in Fig. 5.3 by the points Mk

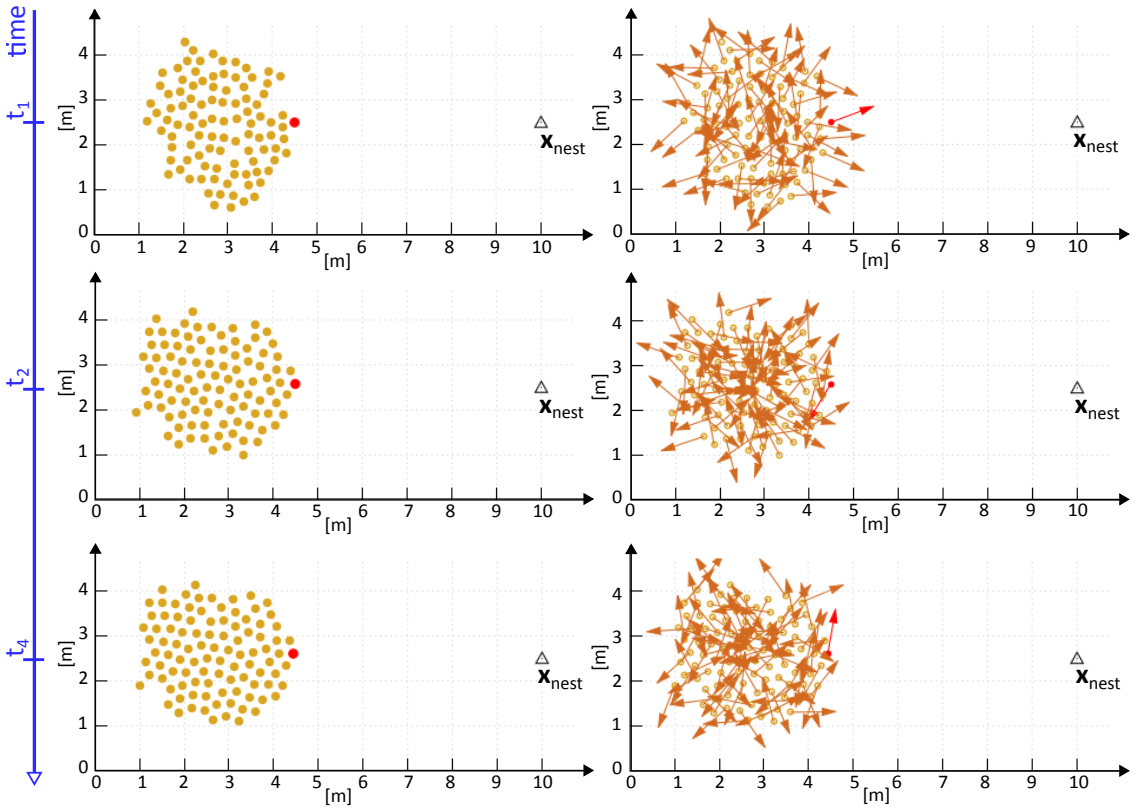

Figure 5.6 Representative evolution of the bee population in the case of uncorrelated and non productive behavior. Left panels show the position of the insects at selected different times, right panels show also their direction of motion (i.e., the unit vector of their velocity, indicated by the orange arrow) at the same instants. It is possible to see that the bee cloud still organizes in a crystalline pattern (i.e., $t_1 \to t_2$), however the insect velocities do not align: therefore, the bee cloud almost fluctuates around the initial position (compare the position of the insects at the final time t_4 here and in the previous Fig. 5.5). Such a representative system evolution is obtained with the parameter combination $M4$: however, it is completely consistent for all the other analogous cases.

(where $k = 1, ..., 6$): they are in fact sufficiently distributed and allow the classification of swarm dynamics in large enough parameter regimes.

We first observe that in all cases the swarm organizes in a crystalline-like configuration: as shown in Fig. 5.7, $d_{\min}$, i.e., the measure of the distance between pairs of first closest bees, in fact quickly stabilizes to the asymptotic threshold $d_\infty = 0.3$ m, which results in a overall swarm diameter of about $D_\infty = 3.75$ m. Such values are consistent with d_{rep}, i.e., the approximated extension of the comfort space that each insect desires to maintain during its flight, as commented in the experimental literature [87]. In this respect, we

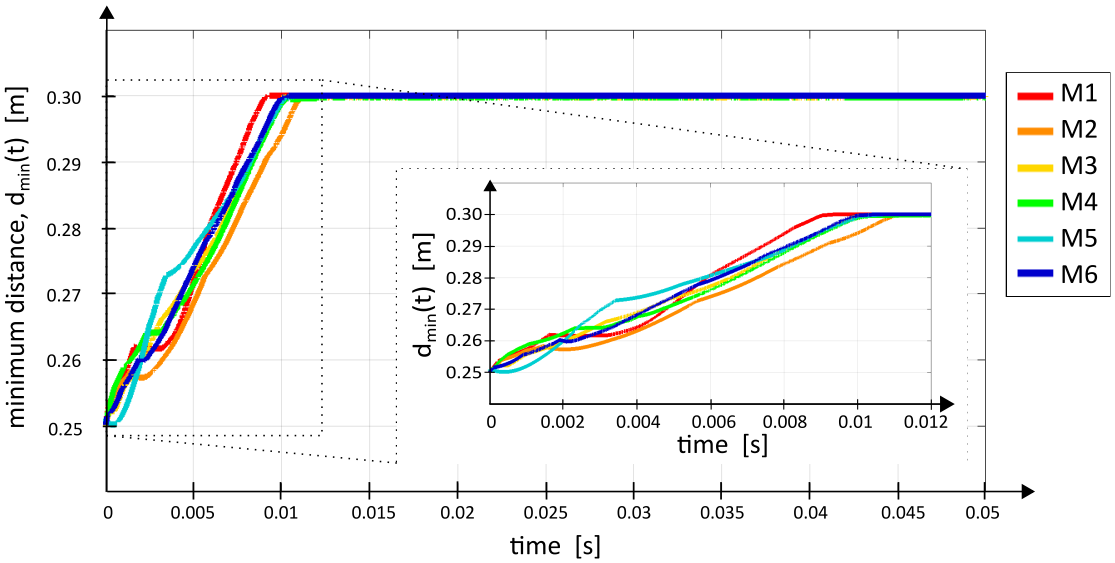

Figure 5.7 Euclidean metric-based alignment mechanism. Time evolution of the minimal distance between pairs of bees, i.e., $d_{\min}(t)$, observed in selected combinations of parameters. We can first notice that, in all cases, $d_{\min}$ converges to $d_\infty = 0.3$ m, the swarm constantly organizes in a crystalline-like configuration. This is consistent to the fact that all sets of coefficients satisfy the criterium in Eq. (5.12) for the H-stability of the system. The specific parameter values instead affect the convergence dynamics: for instance, comparing the cases $M1$ and $M2$, it emerges that higher values of f_{rep} increase the time needed by the swarm to stabilize in the crystalline pattern.

further observe that increments in f_{rep} result in increments in the time needed to the particle system to reach the stable configuration (see, for instance, the cases $M1$ and $M2$ in Fig. 5.7). This behavior, which is independent from the specific value of the other model parameters, is due to the enhanced role of the repulsive force which, at the initial stages of the system evolution, i.e., when the bee cloud is more compact, overcomes the other velocity contributions, pushing away the insects one from each other and therefore delaying the achievement of a stable pattern. In this respect, we remark that the obtained asymptotic crystalline configuration of the swarm is consistent with, and predicted by, the analytical results of Theorem 5.2.1, given that the sets of parameter values employed in this series of simulations satisfy relation (5.12), which assures the H-stability of the pairwise interaction kernels and therefore of the overall particle system.

We then turn to analyze the migratory determinants of the swarm. From Fig. 5.8, it is possible to observe that, regardless of the values of f_{rep} and f_{attr}, the bee cloud undergoes swarming with productive motion (i.e., towards the target destination) only if the extension

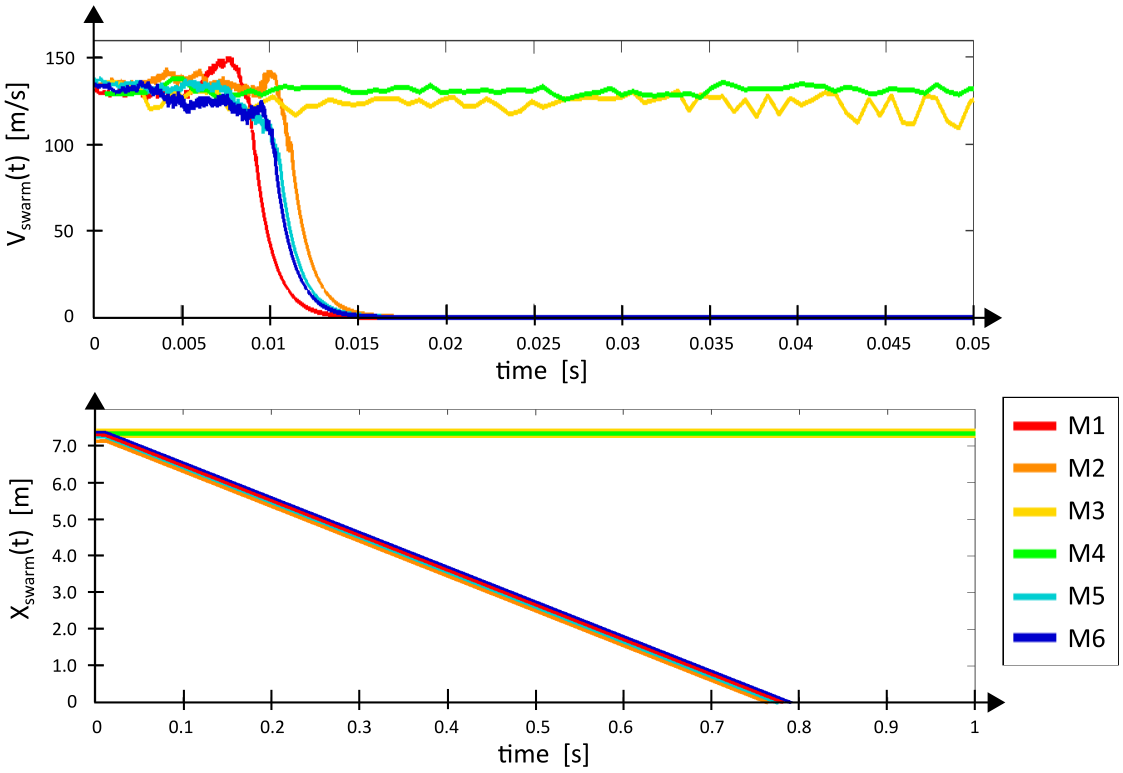

Figure 5.8 Euclidean metric-based alignment mechanism. Time evolution of V_{swarm} (top panel) and X_{swarm} (bottom panel), introduced in Eqs. (5.14-5.15), observed in selected combinations of parameters. It is possible to notice that the bee population undergoes swarming and productive motion only in the cases $M1$, $M2$, $M5$, and $M6$, which are characterized by a sufficiently large d_{align}, i.e., larger than $D_\infty = 3.75$ m.

of the alignment region, i.e., d_{align}, is sufficiently large (see the parameter settings $M1$, $M2$, $M5$, and $M6$). Otherwise, the insect cloud is characterized by uncorrelated individual movement (see the parameter settings $M3$ and $M4$). Entering in more details, let us compare Figs. 5.7 and 5.8: it is straightforward to notice that the flight synchronization process starts at $t \approx 0.01$, i.e., just after the stabilization of the bee configuration. In this perspective, our simulations point out that a value of d_{align} not smaller than the asymptotic diameter of the insect cloud $D_\infty = 3.75$ is needed to have swarming and productive motion, i.e., it is necessary that each bee has, at the same time, almost the rest of the groupmates (included the leader) within its flight synchronization region.

We can indeed conclude that, under our first hypothesis on the alignment process, the swarm is characterized by two-steps dynamics: in the first stages, the bee cloud organizes in a crystalline configuration (regardless of the parameter values, provided the H-stability

condition); in the later phases, if d_{align} is large enough (i.e., $\geq D_\infty$), the component insects synchronize their velocity and the overall population undergoes productive directional movement.

5.2.2 Topological neighborhood metric-based alignment mechanism

In our second hypothesis, the alignment mechanism of bees involves a topological neighborhood metric. In more details, the i-th insect tracks and synchronizes its movement with the a-th seen closest individuals, regardless of their position, and not with all (or only) the individuals placed within a given alignment region. In this respect, we set

$$\mathcal{N}_i^{\text{align}}(t) = \left\{ j : \mathbf{x}_j(t) \in \Omega_i^{\text{vis}}(t) \text{ and } j \text{ is one of the } a\text{-th closest neighbors of } i \right\}, \quad (5.16)$$

where a can be interpreted as a sort of interindividual *communication rate*.

On the opposite, the repulsive/attractive velocity components still rely on an Euclidean metric, i.e., they involve the couples of bees whose relative distance falls within a given range. In particular, the interaction regions slightly differ from the previous case (see Fig. 5.9, left panel):

$$\mathcal{N}_i^{\text{rep}}(t) = \left\{ \mathbf{x} \in \Omega_i^{\text{vis}}(t) : 0 < |\mathbf{x} - \mathbf{x}_i(t)| \leq d_{\text{rep}} \right\}; \quad (5.17)$$

$$\mathcal{N}_i^{\text{attr}}(t) = \left\{ \mathbf{x} \in \Omega_i^{\text{vis}}(t) : d_{\text{rep}} < |\mathbf{x} - \mathbf{x}_i(t)| \leq d_{\text{attr}} \right\}. \quad (5.18)$$

The interaction kernels, in particular the adhesive part, have then to adapt to the new hypothesis as well (see Fig. 5.9, right panel):

$$h^{\text{rep}}(|\mathbf{r}_{ij}(t)|) = \begin{cases} f_{\text{rep}} \left(\dfrac{1}{d_{\text{rep}}} - \dfrac{1}{|\mathbf{r}_{ij}(t)|} \right), & \text{if } 0 < |\mathbf{r}_{ij}(t)| \leq d_{\text{rep}}; \\ 0, & \text{otherwise;} \end{cases} \quad (5.19)$$

$$h^{\text{attr}}(|\mathbf{r}_{ij}(t)|) = \begin{cases} -\dfrac{4 f_{\text{attr}} \left(|\mathbf{r}_{ij}(t)| - d_{\text{attr}} \right) \left(|\mathbf{r}_{ij}(t)| - d_{\text{rep}} \right)}{(d_{\text{attr}} - d_{\text{rep}})^2}, & \text{if } d_{\text{rep}} < |\mathbf{r}_{ij}(t)| \leq d_{\text{attr}}; \\ 0, & \text{otherwise,} \end{cases} \quad (5.20)$$

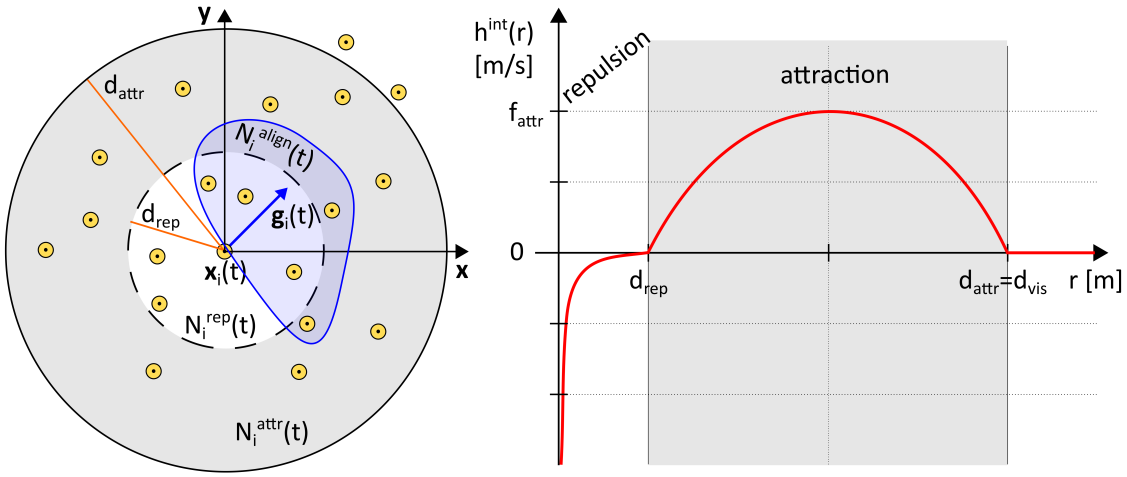

Figure 5.9 Topological neighborhood metric-based alignment mechanism. Left panel: Representation of the attractive and repulsive regions, defined in Eqs. (5.17)-(5.18), and of the alignment set, introduced in Eq. (5.16). In particular, assuming $d_{\text{attr}} = d_{\text{vis}}$, we have that $\mathcal{N}^{\text{rep}}(t) \cup \mathcal{N}^{\text{attr}}(t) = \Omega_i^{\text{vis}}(t)$ for all bees $i = 1, \ldots, N$ and for any t. Right panel: Plot of the pairwise interaction kernel $h^{\text{int}} : \mathbb{R}_+ \longmapsto \mathbb{R}$ given by the sum of the repulsive and attractive functions defined in Eqs. (5.19)-(5.20), i.e., $h^{\text{int}}(r) = h^{\text{rep}}(r) + h^{\text{attr}}(r)$.

where again $d_{\text{rep}} = 0.3$ m and $d_{\text{attr}} = d_{\text{vis}} = 10$ m. In this case we have indeed that $\mathcal{N}_i^{\text{rep}}(t) \cup \mathcal{N}_i^{\text{attr}}(t) = \Omega_i^{\text{vis}}(t)$ for each insect i and time t.

Remark We underline that, according to our second hypothesis, the social behavior of a bee can *simultaneously* involve alignment and attractive (or repulsive) stimuli due to the presence of the same groupmates. On the opposite, in the case of our first hypothesis, the j-th animal was only permitted to affect one of the social velocity contributions of the i-insect (i.e., j could fall within only one of the interaction regions of i), compare Figs. 5.2 and 5.9 (left panels).

According to the second type of assumptions, the space of free parameters regulating bee dynamics now reads as

$$(f_{\text{rep}}, f_{\text{attr}}, a),$$

where $f_{\text{rep}} \in \mathbb{R}_+$, $f_{\text{attr}} \in [0, v_{\max}]$, and $a \in \{1, \ldots, N-1\}$, being N the total number of insects. In this respect, the assumption of H-stability of the system allows to have a functional relation between the coefficients f_{rep} and f_{attr}, as stated by the following

Theorem 5.2.3. *If the following parametric relation*

$$\frac{f_{\text{rep}}}{f_{\text{attr}}} > \frac{2(d_{\text{attr}} - d_{\text{rep}})}{5(d_{\text{rep}})^2}\left(3(d_{\text{rep}})^2 + 4d_{\text{attr}}d_{\text{rep}} + 3(d_{\text{attr}})^2\right) \tag{5.21}$$

holds, the potential related to the pairwise interaction kernel $h^{\text{int}}(r) = h^{\text{rep}}(r) + h^{\text{attr}}(r)$, *with* $r = |\boldsymbol{r}_{ij}(t)| = |\boldsymbol{x}_j(t) - \boldsymbol{x}_i(t)|$, *defined in Eqs. (5.19)-(5.20) is H-stable. As shown in [13, 18, 40], for a finite number of agents, as in the case of our interest, this implies that, at each time* $t \in \mathbb{R}_+$, *there exist two finite and positive quantities* $d_{\min}(t) = \min_{\substack{(i,j)\in\{1,\dots,N\}\\ i\neq j}} |\boldsymbol{x}_i(t) - \boldsymbol{x}_j(t)|$ *and* $d_{\max}(t) = \max_{\substack{(i,j)\in\{1,\dots,N\}\\ i\neq j}} |\boldsymbol{x}_i(t) - \boldsymbol{x}_j(t)|$ *such that* $d_{\min}(t) \leq |\boldsymbol{x}_i(t) - \boldsymbol{x}_j(t)| \leq d_{\max}(t)$ *for all pairs* (i, j) *of bees, i.e., at each time* $t \in \mathbb{R}_+$ *the swarm does not collapse nor explode. In particular, for* $t \to +\infty$, *the minimal relative distance between bees* $d_{\min}(t)$ *tends to the limit value* d_∞, *whereas the maximal relative distance* $d_{\max}(t)$ *(which also represents the diameter of the swarm) tends to the value* D_∞*: in other words, the particle population asymptotically organizes in a stable crystalline-like pattern.*

Proof. The proof closely resembles the one of Theorem 5.2.1 which, as already explained, relies on the analytical study in [13] and on the calculations firstly introduced in [14] to the case of cell aggregates. Entering in more details, the potential $u^{\text{int}} : \mathbb{R} \longmapsto \mathbb{R}$ associated to the pairwise interaction kernels defined in (5.19)-(5.20) has the form

$$u^{\text{int}}(r) = \int h^{\text{int}}(r)dr = \int h^{\text{rep}}(r)dr + \int h^{\text{attr}}(r)dr =$$

$$= \begin{cases} f_{\text{rep}}\left(\dfrac{r}{d_{\text{rep}}} - \log r\right) + A_1, \\ \text{if } 0 < r \leq d_{\text{rep}}; \\ \\ -\dfrac{2\,f_{\text{attr}}\left(2r^3 - 3\,(d_{\text{attr}} + d_{\text{rep}})\,r^2 + 6\,d_{\text{attr}}\,d_{\text{rep}}\,r\right)}{3(d_{\text{attr}} - d_{\text{rep}})^2} + A_2, \\ \text{if } d_{\text{rep}} < r \leq d_{\text{attr}}; \\ \\ A_3, \\ \text{otherwise,} \end{cases}$$

where the constants A_1, A_2, A_3 have to satisfy the following conditions

$$\begin{cases} A_1 &= A_2 - \dfrac{2f_{\text{attr}}\left(2(d_{\text{rep}})^3 - 3(d_{\text{attr}}+d_{\text{rep}})(d_{\text{rep}})^2 + 6d_{\text{attr}}(d_{\text{rep}})^2\right)}{3(d_{\text{attr}}-d_{\text{rep}})^2} \\ &- f_{\text{rep}}(1-\log d_{\text{rep}}); \\ \\ A_2 &= A_3 + \dfrac{2f_{\text{attr}}\left(2(d_{\text{attr}})^3 - 3(d_{\text{attr}}+d_{\text{rep}})(d_{\text{attr}})^2 + 6(d_{\text{attr}})^2 d_{\text{rep}}\right)}{3(d_{\text{attr}}-d_{\text{rep}})^2}, \end{cases}$$

to assure its continuity. As done for Theorem 5.2.1, let us now assume that $u^{\text{int}}(r) \to 0$ when $r \to \infty$ and set $A_3 = 0$. We have indeed that

$$\begin{cases} A_2 &= -\dfrac{2f_{\text{attr}}(d_{\text{attr}})^2\left(d_{\text{attr}} - 3d_{\text{rep}}\right)}{3(d_{\text{attr}}-d_{\text{rep}})^2}; \\ \\ A_1 &= -\dfrac{2}{3} f_{\text{attr}}(d_{\text{attr}}-d_{\text{rep}}) - f_{\text{rep}}(1-\log d_{\text{rep}}). \end{cases}$$

The particle interaction potential is therefore given by

$$u^{\text{int}}(r) = \begin{cases} f_{\text{rep}}\left(\dfrac{r}{d_{\text{rep}}} - \log\left(\dfrac{r}{d_{\text{rep}}}\right) - 1\right) - \dfrac{2}{3} f_{\text{attr}}\,(d_{\text{attr}} - d_{\text{rep}}), \\ \text{if } 0 < r \le d_{\text{rep}}; \\ \\ -\dfrac{2\,f_{\text{attr}}\left(2r^3 - 3(d_{\text{attr}}+d_{\text{rep}})r^2 + 6d_{\text{attr}}d_{\text{rep}}r + (d_{\text{attr}})^2\left(d_{\text{attr}} - 3d_{\text{rep}}\right)\right)}{3(d_{\text{attr}}-d_{\text{rep}})^2}, \\ \text{if } d_{\text{rep}} < r \le d_{\text{attr}}; \\ \\ 0, \\ \text{otherwise.} \end{cases} \tag{5.22}$$

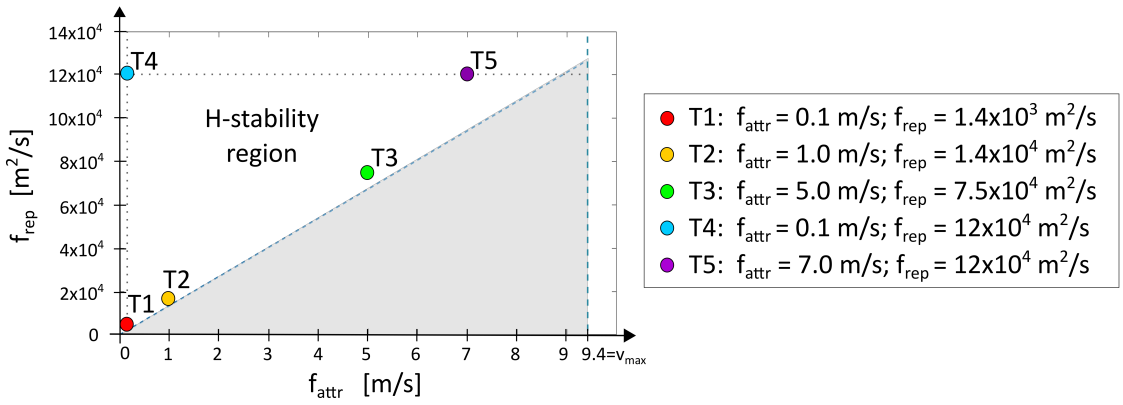

Figure 5.10 Topological neighborhood metric-based alignment mechanism. The space of free model coefficients is given by $(f_{\text{rep}}, f_{\text{attr}}, a) \in \mathbb{R}^2_+ \times \{1, \ldots, N-1\}$, being N the total number of insects. In particular, biological considerations allows also the following restriction: $f_{\text{attr}} \in [0, v_{\max}]$. The H-stability-related criterium in Eq. (5.21) further reduces the possible variations of parameter values to the white region of the plane $(f_{\text{rep}}, f_{\text{attr}})$. a can instead vary without affecting the system stability. Of the remaining combination of coefficients, we focus on the sets Tk, where $k = 1, \ldots, 5$, since they are sufficiently distributed, thereby covering large enough parameter regimes.

Recalling again the criterium given in [13], the potential u^{int} defined in (5.22) is H-stable if the already-introduced relation $\int_0^{+\infty} u^{\text{int}}(r)\, r\, dr > 0$ holds. In this respect, let us calculate

$$
\begin{aligned}
&\int_0^{+\infty} u^{\text{int}}(r) r\, dr \;= \\
&= \int_0^{d_{\text{rep}}} \left(f_{\text{rep}} \left(\frac{r^2}{d_{\text{rep}}} - r \log\left(\frac{r}{d_{\text{rep}}} \right) - r \right) - \frac{2}{3} f_{\text{attr}} (d_{\text{attr}} - d_{\text{rep}}) r \right) dr + \\
&\quad - \int_{d_{\text{rep}}}^{d_{\text{attr}}} \left(\frac{2 f_{\text{attr}} \left(2r^4 - 3(d_{\text{attr}} + d_{\text{rep}}) r^3 + 6 d_{\text{attr}} d_{\text{rep}} r^2 + (d_{\text{attr}})^2 \left(d_{\text{attr}} - 3 d_{\text{rep}} \right) r \right)}{3 (d_{\text{attr}} - d_{\text{rep}})^2} \right) dr \\
&= \frac{f_{\text{rep}} (d_{\text{rep}})^2}{12} - \frac{f_{\text{attr}}}{30} (d_{\text{attr}} - d_{\text{rep}}) \left(3 (d_{\text{rep}})^2 + 4 d_{\text{attr}} d_{\text{rep}} + 3 (d_{\text{attr}})^2 \right),
\end{aligned}
$$

which is non-negative (assuring indeed the H-stability of the system) if the parametric relation defined in Eq. (5.21) is satisfied. □

With respect to Theorem 5.2.1, the criterium given in (5.21) involves only f_{rep} and f_{attr} and not the third free model coefficient a, which can instead independently vary without affecting the H-stability of the system. Recalling that $d_{\text{rep}} = 0.3$ m and $d_{\text{attr}} = 10$ m, the permitted region of the parameter space is represented in Fig. 5.10. As in the previous

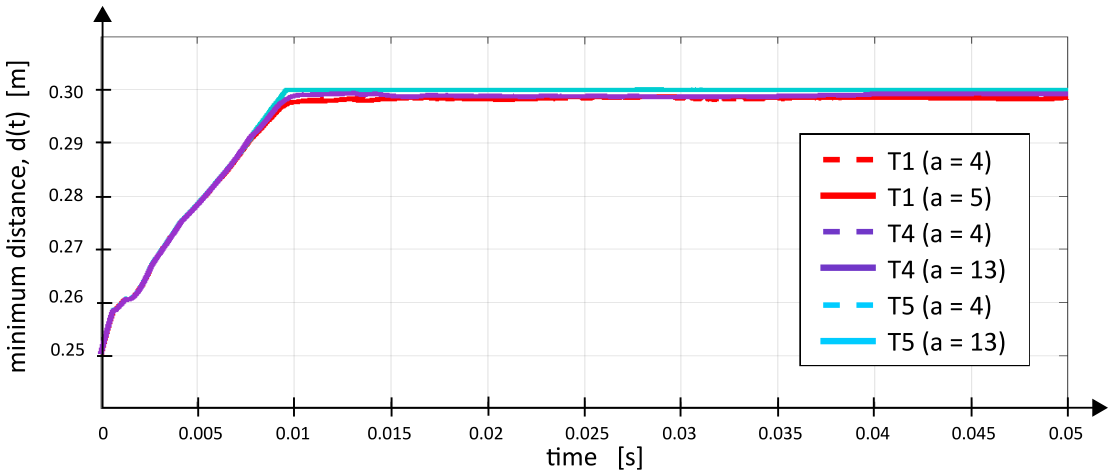

Figure 5.11 Topological neighborhood metric-based alignment mechanism. Time evolution of the minimal distance between pairs of bees, i.e., $d_{\min}(t)$, observed in selected combinations of parameters. We notice that, in all cases, $d_{\min}$ converges to $d_\infty = 0.3$ m, i.e., the swarm constantly organizes in a crystalline-like configuration. This is consistent to the fact that all sets of coefficients satisfy the criterium in Eq. (5.21) for the H-stability of the system. Interestingly the asymptotic spatial configuration of the insect is exactly the same obtained in the case of an Euclidean metric-based alignment velocity. This is indicative of the fact that the characteristic dimensions of the large-time pattern are solely determined by the repulsive component of bee dynamics, which is not affected by the variation of the hypothesis underlying the flight synchronization process.

Section, we then focus on the swarm behavior in selected parameter settings, labeled by Tk, where $k = 1,...,5$, and chosen to span the entire region of interest of the coefficient values. In particular, in the following numerical realizations, we maintain the domain configuration, as well as the initial conditions and the differentiated bee behavior (i.e., a leader insect which guides the rest of uninformed individuals), of the simulation proposed in the previous Section (see Fig. 5.4). The only modification is that the social velocity components are now determined by the interaction sets introduced in Eqs. (5.16)-(5.17)-(5.18) while the repulsive/attractive dynamics are defined in Eqs. (5.19)-(5.20). Also in this case, we neglect a random contribution in bee behavior, whereas the parameter values used in the simulations can be found in Table 5.1. The resulting swarm dynamics are classified according to Definition 5.2.2 as well.

As shown in Fig. 5.11, we observe that the swarm constantly reaches a stable crystalline configuration, regardless of the values given to the set of free parameters (provided that f_{rep} and f_{attr} satisfy the condition given in Eq. (5.21)). In particular, the characteristic

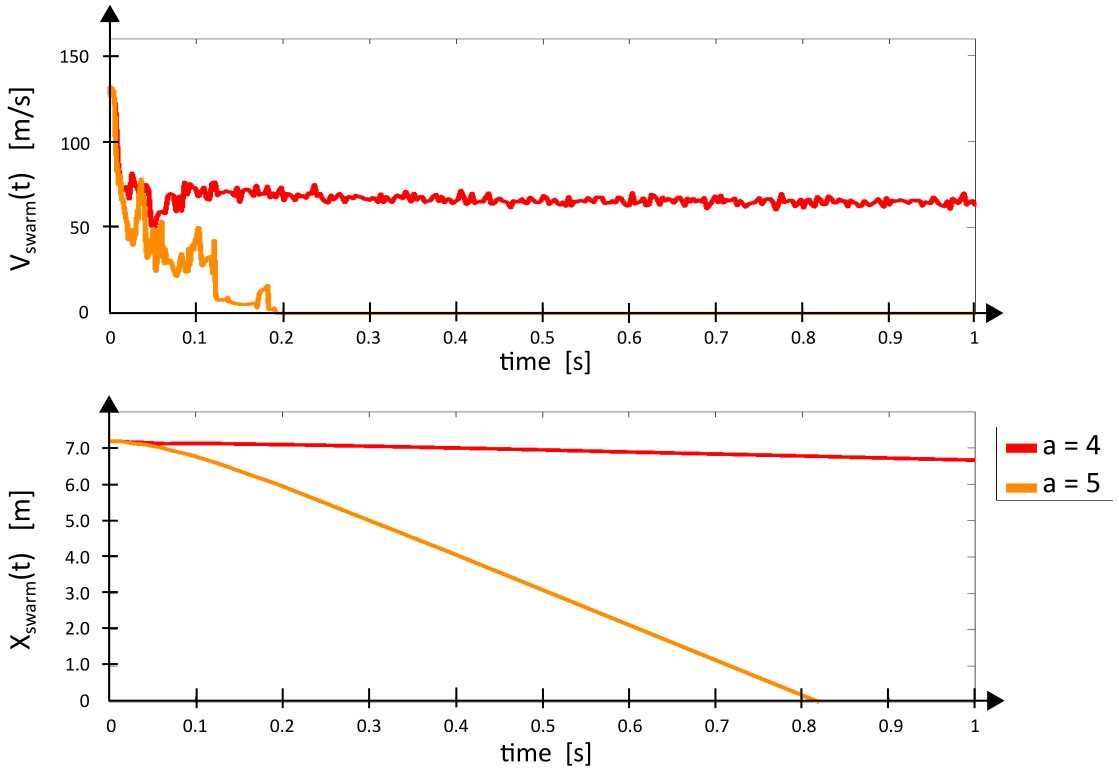

Figure 5.12 Topological neighborhood metric-based alignment mechanism. Characteristic time evolution of V_{swarm} (top panel) and X_{swarm} (bottom panel) observed in the representative parameter setting $T1$ in the case of swarming and productive motion (i.e., obtained with $a = 4$) or not (i.e., for $a = 5$). Exactly the same dynamics results in the other parameter combinations Tk, with $k = 2, \ldots, 5$.

stable dimensions of the particle system are, in all cases, $d_\infty = 0.3$ m and $D_\infty = 3.75$ m. These values, as well as the range of time needed for the patterning, are the same obtained in the previous Section, i.e., with the assumption of an Euclidean metric-based alignment mechanism. In this respect, we can speculate that the asymptotic spatial organization of the particle system is completely determined by the repulsive part of the pairwise interaction kernel (and by the relative coefficient d_{rep}, see also comments in [13]). The hypothesis underlying the flight synchronization process, as well as the resulting variation of the attractive velocity component, does not instead have an effect on the patterns of the large-time insect distribution. By comparing Figs. 5.7 and 5.11, it is also possible to notice that, in the first case, the specific set of parameter values have an effect on the temporal dynamics of stabilization, whereas in the second case, i.e., in the case of a topological neighborhood metric-based alignment mechanism, the evolution of d_{min} coincides for all the combination of coefficients taken into account.

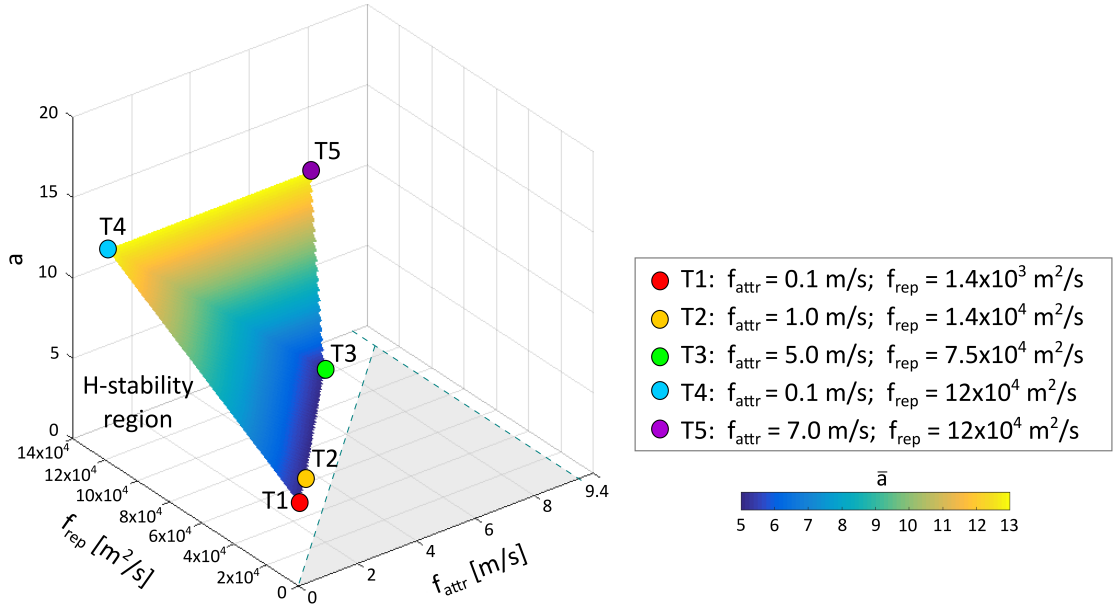

Figure 5.13 Topological neighborhood metric-based alignment mechanism. For any representative parameter setting Tk (with $k = 1, ..., 5$), the plot shows the threshold value of the communication rate a, i.e., $\bar{a}$, leading to a transition between an uncorrelated individual movement to a swarming behavior with productive motion. It is straightforward to observe that different ratios $f_{\text{rep}}/f_{\text{attr}}$ result in different $\bar{a}$. In particular, increments in the ratio $f_{\text{rep}}/f_{\text{attr}}$ result in increments in $\bar{a}$.

Fig. 5.12 shows the system migratory determinants in the case of the parameter setting $T1$: in particular, for representative purposes, we plot the evolution of X_{swarm} and V_{swarm} resulting from $a = 4$ (i.e., no swarming nor directional flight) and $a = 5$ (i.e., swarming and directional flight). We can observe that, also in the case of this second assumption on bee alignment, the productive motion (indicated by a drop of X_{swarm}) substantially starts after the stabilization of the bee configuration. Exactly the same dynamics have been replicated in the cases of the other coefficient combinations Tk, with $k = 2, ..., 5$.

In contrast to the assumption investigated in Section 5.2.1, we can however observe that the topological neighborhood metric-based synchronization hypothesis results in the fact that the migratory behavior of the swarm depends on the value of all the free model parameters (and not only to the one relative to the alignment velocity itself). As shown in Fig. 5.13, the threshold value of a, say $\bar{a}$, needed to have swarming and productive motion in fact depends on the ratio $f_{\text{rep}}/f_{\text{attr}}$. In particular, increments in the ratio $f_{\text{rep}}/f_{\text{attr}}$ result in increments in $\bar{a}$.

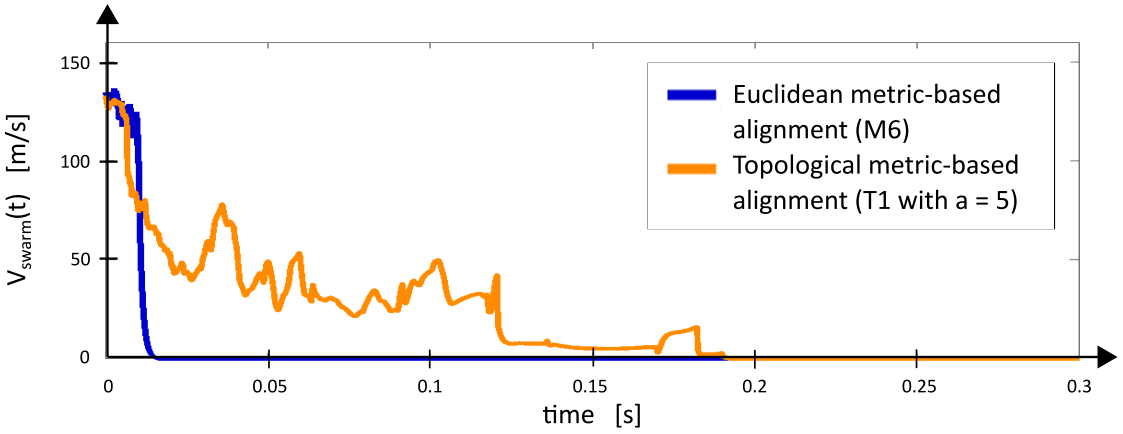

Figure 5.14 Comparison of the time evolution of V_{swarm} observed in a single representative parameter setting deriving either from the Euclidean or from the topological neighborhood metric-based alignment assumption. The former case is the coefficient combination $M6$, the latter the parameter setting $T1$ with $a = 5$. By comparing the two curves, it is possible to observe that the complete alignment of the bee population is significantly delayed in the case of the topological neighbourhood metric-based synchronization hypothesis, which involves a gradual diffusion of information within the insect cloud rather then a sudden and simultaneous flight alignment.

Further, it is interesting to notice that, regardless of the value of $f_{\text{rep}}/f_{\text{attr}}$, the phase transition of the insect collective migratory behavior dynamics (i.e., swarming vs. no swarming) is obtained by substantially low values of the communication rate a (i.e., $\bar{a} \leq 13$), i.e., significantly lower than the total amount of component individuals, see again Fig. 5.13. In this respect, we are observing a *diffusion of information* within the swarm: the knowledge of the direction towards the target destination in fact first passes from the leader to its closest a-th individuals and then gradually to the rest of the population. This is in contrast with respect to what happens in the previous set of simulations, where a productive collective motion required that $d_{\text{align}} \geq D_{\infty}$, i.e., that all bees simultaneously align to almost the rest of the groupmate (included the leader).

The different swarm phenomenologies resulting from the two alignment hypotheses reflect also on the characteristic time of the insect migratory dynamics. As shown in the representative plot in Fig. 5.14, the complete alignment of the bee population (i.e., given by $V_{\text{swarm}} = 0$) is significantly delayed in the case of a topological neighbourhood metric-based synchronization hypothesis. This observation is a further confirmation that, in the hypothesis investigated in this Section, the information of the direction of movement

gradually diffuses within the population, whereas in the other case, there is simultaneous flight synchronization, which involves almost all individuals at the same time.

5.3 Inclusion of random contributions

The numerical results proposed so far have been obtained by neglecting the random term in Eq. (4.5): we have indeed constantly assumed that all bees completely apply the given rules of motion. However, unconscious fluctuations may characterize individual behavior.

In this respect, for each insect i we add a fluctuation velocity component, given by a vector $\mathbf{v}_i^{\text{rand}}$, whose modulus and direction are, at any time t, random variables which uniformly fall within the ranges of values $[0, v_{\text{rand}}]$ (with $v_{\text{rand}} \leq v_{\max}$) and $[0, 360^\circ)$, respectively. The individual velocities now read as

$$\begin{aligned} \mathbf{v}_1(t) &= \mathbf{v}_1^{\text{targ}}(t) + \mathbf{v}_1^{\text{rep}}(t) + \mathbf{v}_1^{\text{attr}}(t) + \mathbf{v}_1^{\text{rand}}(t), \quad \text{with } s_1(t) = L \\ \mathbf{v}_i(t) &= \mathbf{v}_i^{\text{align}}(t) + \mathbf{v}_i^{\text{rep}}(t) + \mathbf{v}_i^{\text{attr}}(t) + \mathbf{v}_i^{\text{rand}}(t), \quad \text{with } s_i(t) = U, \quad \forall\, i = 2, 3, \ldots, N. \end{aligned}$$

As it is possible to see by comparing the plots in Fig. 5.15, which describe the swarm patterning and migratory determinants in the representative cases $M6$ (left panels) and $T1$ with $a = 5$ (right panels), the inclusion of random fluctuations in bee dynamics does not have an effect on the swarm organization in a stable crystalline pattern. However, when the maximal possible modulus of the random velocity component is large enough, i.e., $v_{\text{rand}} = v_{\max}$, the insect cloud undergoes uncorrelated (and therefore not productive) movement. In contrast, if $v_{\text{rand}} \ll v_{\max}$, the collective dynamics of the swarm are still characterized by fluctuations, which however do not have a dramatic effect on the asymptotic behavior of the system, in term of collective synchronized flight.

The obvious rationale underlying such a phenomenology is that, when $v_{\text{rand}} = v_{\max}$, the fluctuation term $\mathbf{v}_i^{\text{rand}}$ almost overcomes the other velocity contributions in Eq. (5.23)-(5.23), thereby preventing the normal behavior of the swarm. However, too large values of v_{rand} are not reasonable, since they only have to implement unconscious individual deviations from the exact application of the set rules of flight.

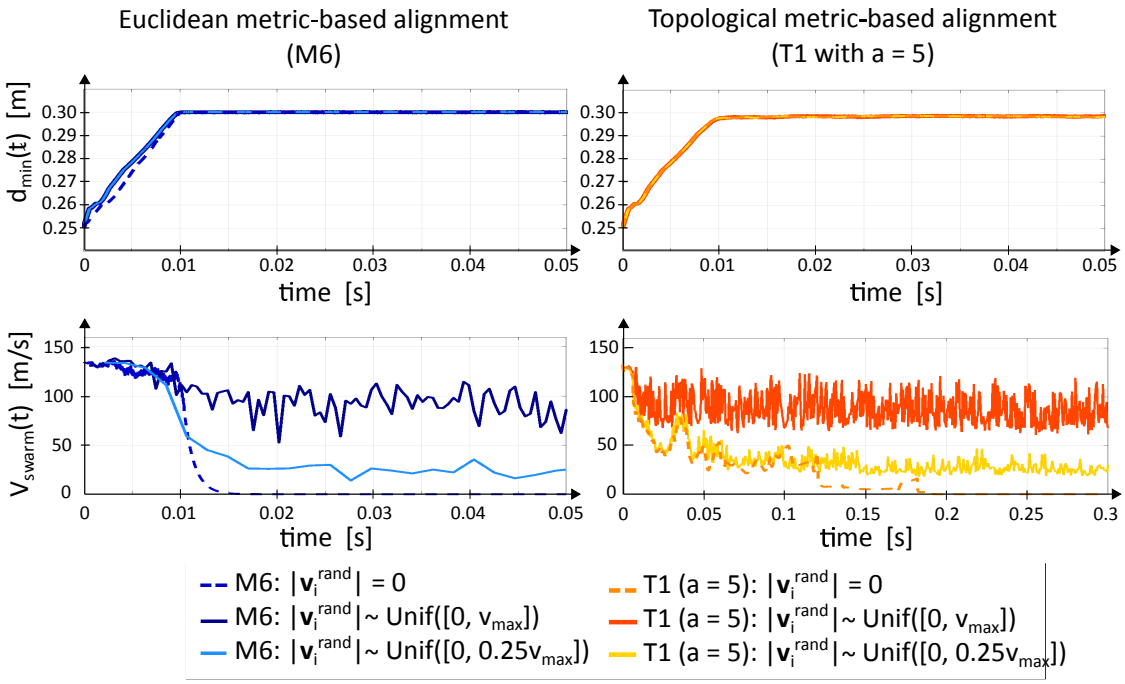

Figure 5.15 Comparison of the time evolution of $d_{\min}$ (top panels) and of V_{swarm} (bottom panels), observed in representative parameter settings (i.e., $M6$ for the Euclidean metric-based alignment assumption and $T1$ with $a = 5$ for the topological neighborhood metric-based alignment assumption), in the case of addition of the random velocity term $\mathbf{v}_i^{\text{rand}}$ in Eq. (4.5), for each bee $i = 1, ..., 100$. As it possible to see, the inclusion of fluctuations does not have an effect on the patterning of the bee swarm, but only on its flight dynamics.

5.4 Conclusions

In this Chapter, the above-presented general model for bee dynamics has been used to test some assumptions underlying insect social behavior. In particular, we have focused either on an Euclidean metric-based or on a topological neighborhood metric-based alignment mechanism, which impact also on the definition of the attraction/repulsion velocity components. In more details, we have analyzed, in each of the two cases, the model behavior in different regions of the parameter space.

In this respect, given the intrinsic multiparametric nature of the model components, we have taken advantage of some theoretical studies on the H-stability of particle interaction kernels, discussed in [13, 40], and here extended to the proposed velocity functions, following the calculations proposed in [14] in the case of cell systems. The concept of H-stability was introduced in statistical mechanics [84] and it is closely related to the

asymptotic configuration of discrete systems. More specifically, from the above-cited works, we can recall the following theoretical results: given a population of N agents, whose dynamics are determined by a pairwise interaction potential, say u, we have that: (i) if u is not H-stable (or *catastrophic*), then the minimal interparticle distance at the equilibrium collapses to 0 when the total amount of individuals N goes to infinity; (ii) if u is H-stable, then the minimal interparticle distance at the equilibrium is bounded by finite strictly positive values, regardless the number of individuals N. In this last case, if N goes to infinity, the system distribution explodes.

Since this Chapter has been focused on swarming phenomenology, which are characterized by a finite number of agents with a well-defined spacing maintained within the bee cloud during flight, it has been necessary to avoid catastrophic situations where the minimal interparticle distance at the equilibrium collapses to 0, i.e., to assure the H-stability of the attractive/repulsive kernels employed to describe insect behavior. Such an analytical approach, in conjunction with empirical observations, has been able also to restrict the range of value variations of the free model parameters, which have to assure a realistic crystalline configuration of the swarm.

Our results have first shown that, in the case of the Euclidean metric-based alignment process, the asymptotic distribution of bees within the cloud is independent from the specific set of parameter values (provided the condition for the H-stability of the interaction kernels). On the opposite, the collective migratory determinants dramatically and entirely rely on the extension of the synchronization region, which has to be in the range of the asymptotic dimensions of the bee cloud to have swarming and collective behavior.

We have then turn to analyze swarm phenomenology in the case of a topological neighborhood metric-based alignment mechanism. We have observed that the asymptotic configuration of the swarm remains unaltered with respect to the previous modeling assumption. This is indicative of the fact that the characteristic dimensions of the stable pattern are entirely determined by the repulsive part of the interaction kernel. The set of simulations proposed in Section 5.2.2 have also shown that the migratory dynamics of the bee population depend both on the ratio $f_{\text{rep}}/f_{\text{attr}}$ and on the communication rate a, i.e., on the values of the three free model parameters. However, in all the analyzed cases, the threshold number of individuals that each bee has to consider to have a productive swarming is substantially small (i.e., $\bar{a} \leq 13$), in contrast to the case of an Euclidean metric-based synchronization mechanism, where the alignment region had to include almost the entire cloud to observe an effective directional flight. A topological neighborhood metric-

based migratory assumption indeed results in a gradual diffusion of information within the bee population: this has been also confirmed by the greater time needed by the swarm to completely align with respect to the case of the Euclidean metric-based synchronization hypothesis. We have also discussed the role of possible random fluctuations in bee velocity.

It is finally interesting to notice that in our study we have not observed hybrid swarm phenomenologies (e.g., swarming without productive motion or *vice versa*), which are in principle possible and have been captured by other similar models [18].

Chapter 6

Analysis of the collective dynamics of a swarm guided by a group of leaders

In this Chapter we will further investigate the guidance mechanisms at the basis of bee swarming towards a new nest as well as different individual rules within the group. In this respect, we will here first introduce anisotropy in insect behavior by the definition of a more realistic visual region, i.e., not completely round. Then, we will include an experimentally observed bee differentiated behavior. In this respect, we will again distinguish between leader individuals and follower insects. However, we will here test different combinations of hypotheses relative (i) to the characteristic movement of the scout/informed bees and (ii) to the alignment strategy of the follower/uninformed individuals. In more details, each uninformed bee will be assumed to synchronize its movement to a given set of groupmates not only upon considerations on their mutual distance (as in the previous Chapter) but also taking into account their status and actual velocity.

Once the most reasonable assumptions resulting in a correct collective swarming of the insect population is found out, our second objective will be to demonstrate that the obtained behavioral rules are sufficient to reproduce realistic migratory dynamics in complex real-world scenarios, involving domains with structural elements and obstacles.

The rest of this Chapter is organized as follows. In Section 6.1, we will present the main model components. More specifically, we will first explain the characteristic representation of the virtual bees and their possible status/role within the population; then, we will introduce the relative velocity contributions. In particular, we will clarify the biological and experimental considerations each term is based on. Section 6.2 will provide a detailed

description of the parameter estimate employed in our theoretical framework. In Section 6.3, selected series of numerical realizations will analyze swarm dynamics under different combinations of the proposed behavioral hypotheses of the insect colony. A study on the influence of the fraction of scout individuals on the swarming process will be performed as well. After presenting in Section 6.3.2 the phenomenology of the bee cloud in more realistic situations, we will review in Section 6.4 the results obtained in this Chapter.

6.1 Modeling details

Bee characteristics and status transitions. The swarming honeybees are here modeled in a two-dimensional close domain $\Omega \subset \mathbb{R}^2$, with boundary $\partial\Omega$. We further assume that the new nest, i.e. the target destination of the bee cloud, is constituted by a subregion of the domain boundary, hereafter denoted by $\partial\Omega_{\text{nest}}$ ($\subset \partial\Omega$), refer to Fig. 6.1. According to the biological considerations presented in Chapter 3, for each bee i, s_i falls in the set

$$\mathcal{S} = \{\text{U ('uninformed'); S ('streaker'); P ('passive leader')}\}. \tag{6.1}$$

More specifically, scout individuals are set to have a streaker role when flying in the direction of the nest. Otherwise, they are defined as passive leaders. In this respect, we now introduce possible insect status transitions, which are summarized in Fig. 6.1.

Of course, an uninformed bee can not become informed, so it can not change role and just follows the rest of the swarm. Status transitions instead occur within the set of scout insects. In particular, let us first define for any point of the domain $\mathbf{x} \in \Omega$ the signed distance function $l_{\text{nest}}(\mathbf{x}) : \Omega \to \mathbb{R}_+ \cup \{0\}$, which is evaluated by solving the two-dimensional eikonal equation:

$$|\nabla l_{\text{nest}}(\mathbf{x})| = 1 \qquad \forall\, \mathbf{x} \in \Omega \tag{6.2}$$

with boundary conditions

$$\begin{cases} l_{\text{nest}}(\mathbf{x}) = 0, & \forall\, \mathbf{x} \in \partial\Omega_{\text{nest}}; \\ \dfrac{\partial l_{\text{nest}}(\mathbf{x})}{\partial \mathbf{n}} = 0, & \forall\, \mathbf{x} \in \partial\Omega \setminus \partial\Omega_{\text{nest}}, \end{cases} \tag{6.3}$$

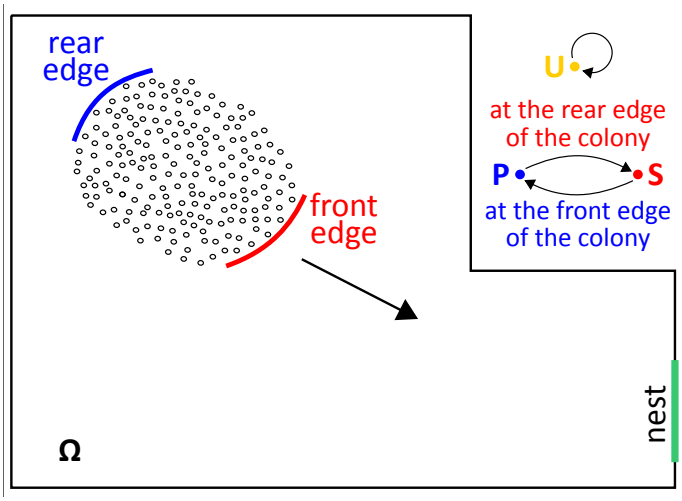

Figure 6.1 The bees within the swarm can have the following roles: U ("uninformed"), S ("streaker"), or P ("passive leader"). An uninformed bee does not change its status, i.e., it is not able to become a scout. Status transitions instead occur within the set of informed insects. More specifically, they are set to have a streaker role while flying towards the nest: in this respect, once reached the front edge of the cloud, they are assigned a passive leader role and turn direction of flight (in the case of hypothesis L1) or stop waiting for the passage of the rest of the insect cloud (in the case of hypothesis L2). Eventually, when a passive leader finds itself at the trailing edge of the swarm, it acquires again a streaker status and move towards the target destination as well.

where $\mathbf{n}$ is the unit vector locally normal to the domain boundary. It is useful to underline that, in other words, $l_{\text{nest}}(\mathbf{x})$ measures the length of the minimal path between any $\mathbf{x} \in \Omega$ and any point belonging to $\partial\Omega_{\text{nest}}$. Coherently with the previous experimental considerations, a streaker bee, say i, becomes a passive leader when it finds itself at the extreme frontal edge of the population, i.e., if, in mathematical terms,

$$l_{\text{nest}}(\mathbf{x}_i(t)) < \min_{\substack{k=1,\dots,N;k\neq i \\ \mathbf{x}_k(t)\in\Omega_i^{\text{vis}}(t)}} \{l_{\text{nest}}(\mathbf{x}_k(t))\},$$

being Ω_i^{vis} the visual region of individual i (see below). On the opposite, a passive leader, say again i, switches back to a streaker status if it finds itself at the trailing edge of the group of insects, i.e., if

$$l_{\text{nest}}(\mathbf{x}_i(t)) > \max_{\substack{k=1,\dots,N;k\neq i \\ \mathbf{x}_k(t)\in\Omega_i^{\text{vis}}(t)}} \{l_{\text{nest}}(\mathbf{x}_k(t))\}.$$

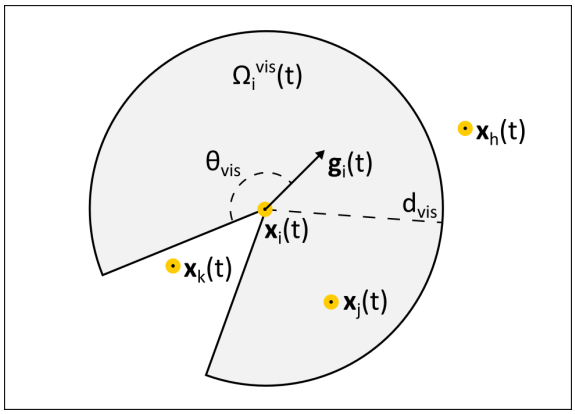

Figure 6.2 For each generic insect i, we define a visual region $\Omega_i^{\text{vis}}(t)$. It is a round section determined by the visual depth d_{vis} and the half visual angle θ_{vis}, which symmetrically extends from the gazing direction of bee i, defined by the unit vector $\mathbf{g}_i(t)$ (which, for the sake of simplicity, will be constantly aligned to the velocity $\mathbf{v}_i(t)$). The inclusion of an anisotropic visual field implies that each bee is not able to see and therefore to interact with the entire set of their groupmates (see, for instance, the individual k and h). For representative purposes, hereafter the virtual bees will be indicated by rigid disks centered at their actual position.

As most animal species, bees typically move and behave influenced by visual signals, captured by their large visual field, that covers almost the entire surrounding space. For the i-th insect (regardless of its status), we indeed denote by the unit vector $\mathbf{g}_i(t) \in B_1^2$ (denoting by B_1^2 the unit 2-D ball) its actual gazing direction and by

$$\Omega_i^{\text{vis}}(t) = \left\{ \mathbf{y} \in \Omega : |\mathbf{y} - \mathbf{x}_i(t)| \leq d_{\text{vis}}, \frac{\mathbf{y} - \mathbf{x}_i(t)}{|\mathbf{y} - \mathbf{x}_i(t)|} \cdot \mathbf{g}_i(t) \geq \cos\theta_{\text{vis}} \right\} \tag{6.4}$$

its visual region, being d_{vis} and θ_{vis} the visual extension and the half visual angle, respectively (see Fig. 11.1). For the sake of simplicity, we hereafter assume that the gaze of each bee is constantly aligned to its velocity, i.e.,

$$\mathbf{g}_i(t) = \frac{\mathbf{v}_i(t)}{|\mathbf{v}_i(t)|}, \qquad \text{for } i = 1, \ldots, N. \tag{6.5}$$

However, individual gazing direction may also evolve slightly independently from the direction of flight: therefore, a proper evolution equation for $\mathbf{g}_i$ may be included as well, as done for instance in [23].

Bee dynamics. Each insect behaves according to its role within the swarm, however its dynamics has to follow the general model (4.4). For the sake of simplicity, we set $v_{\max}^U = v_{\max}^S = v_{\max}^P = v_{\max}$, i.e., as in the previous Chapter we assume that the maximal speed does not depend on the bee status.

We now define three different velocities, each relative to an individual status. All of them are the sum of a given set of contributions, which can be in common for the entire population or characteristic of a single subgroup (and underlined in the following equations). In particular, for the generic i-th bee, we have

$$\begin{aligned}
\mathbf{v}_i(t) &= \mathbf{v}_i^{\text{rep}}(t) + \mathbf{v}_i^{\text{attr}}(t) + \mathbf{v}_i^{\text{boundary}}(t) + \mathbf{v}_i^{\text{rand}}(t) + \underline{\mathbf{v}_i^{\text{align}}(t)}, \ \text{if } i : s_i(t) = \text{U}; \\
\mathbf{v}_i(t) &= \mathbf{v}_i^{\text{rep}}(t) + \mathbf{v}_i^{\text{attr}}(t) + \mathbf{v}_i^{\text{boundary}}(t) + \mathbf{v}_i^{\text{rand}}(t) + \underline{\mathbf{v}_i^{\text{streak}}(t)}, \ \text{if } i : s_i(t) = \text{S}; \\
\mathbf{v}_i(t) &= \mathbf{v}_i^{\text{rep}}(t) + \mathbf{v}_i^{\text{attr}}(t) + \mathbf{v}_i^{\text{boundary}}(t) + \mathbf{v}_i^{\text{rand}}(t) + \underline{\mathbf{v}_i^{\text{passive}}(t)}, \ \text{if } i : s_i(t) = \text{P}.
\end{aligned} \tag{6.6}$$

We now comment each term in Eq. (6.6), starting from those active for all individuals.

As introduced in Chapter 4, for the generic i-th insect, regardless of its status, both the repulsive and attractive behaviors are described by proper kernels $\mathbf{H}_{ij}^{\text{rep}}, \mathbf{H}_{ij}^{\text{attr}} : \mathbb{R}^2 \times \mathbb{R}^2 \longmapsto \mathbb{R}^2$, which define its pairwise interaction instances with the generic j-th individual here belonging to one of the following interaction sets:

$$\begin{aligned}
\mathcal{N}_i^{\text{rep}}(t) &= \{j = 1,...,N, j \neq i : \mathbf{x}_j(t) \in \Omega_i^{\text{vis}}(t), 0 < |\mathbf{r}_{ij}(t)| \leq d_{\text{rep}}\}; \\
\mathcal{N}_i^{\text{attr}}(t) &= \{j = 1,...,N, j \neq i : \mathbf{x}_j(t) \in \Omega_i^{\text{vis}}(t), d_{\text{rep}} < |\mathbf{r}_{ij}(t)| \leq d_{\text{attr}}\},
\end{aligned} \tag{6.7}$$

where we recall $\mathbf{r}_{ij}(t) := \mathbf{x}_j(t) - \mathbf{x}_i(t)$. Exactly as in the previous chapter, d_{rep} is a measure of the comfort space that each insect tries to preserve, whereas d_{attr} is assumed to be equal to d_{vis}, i.e., the bees tend to keep a connection with the groupmates within their visual region, see Fig. 11.2.

In principle, as already mentioned in the previous Chapter, there are many possible forms for the above-introduced interaction kernels. In this respect, such interaction kernels are chosen exactly as in Eqs. (5.19) and (5.20) of Section 5.2.2 (see comments therein). However, we remark that the introduction of anisotropy in the definition of the perception region directly affects the characterization of the interaction sets in (6.7). The overall repulsive/attractive velocity terms thus slightly differ from the ones proposed in the previous Chapter.

The pair of coefficients f_{rep} and f_{attr} have a clear mathematical meaning but not a direct and measurable experimental counterpart. In this respect, a detailed parameter study is

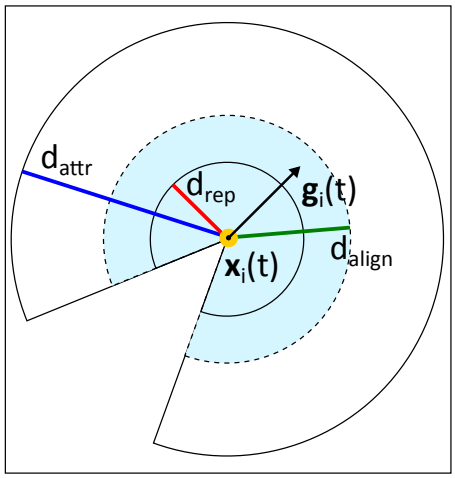

Figure 6.3 Representation of the spatial extension of three interaction regions. The repulsive and attractive sets of the i-th bee, i.e., $\mathcal{N}_i^{\text{rep}}$ and $\mathcal{N}_i^{\text{attr}}$, are in fact given by the insects that i sees and whose distance falls in the ranges $(0, d_{\text{rep}}]$ and $(d_{\text{rep}}, d_{\text{attr}}]$, respectively. Finally, alternative assumptions are set for the flight synchronization mechanism of uninformed bees. However, in all cases, the insects taken into account by the i-th follower individual have to locate within a distance of $d_{\text{align}} \in (d_{\text{rep}}, d_{\text{attr}})$.

needed to provide their estimate which is not the same as in the previous Chapter due to the model differences, as we will see in the next Section. It is finally useful to underline that, according to the kernels h^{rep} and h^{attr}, and to the corresponding interaction sets $\mathcal{N}^{\text{rep}}$ and $\mathcal{N}^{\text{attr}}$, two individuals do not interact (i) when they do not see each other and (ii) when they are exactly at the comfort distance d_{rep}.

We then include a velocity term that implements the intention of bees to remain sufficiently distant from the domain boundary (which may represent, e.g., architectural structures or natural obstacles). In accordance to the case of pedestrians [23], such a migratory contribution enters the picture when the i-th individual (regardless of its status) is close enough, i.e., at a maximal distance hereafter defined with the coefficient d_{boundary}, to a boundary:

$$\mathbf{v}_i^{\text{boundary}}(t) = \begin{cases} a_{\text{boundary}} \exp\left(\dfrac{d_{\text{boundary}} - l_{\text{boundary}}(\mathbf{x}_i(t))}{b_{\text{boundary}}}\right) \mathbf{n}_{\text{boundary}}(\mathbf{x}_i(t)), \\ \text{if } l_{\text{boundary}}(\mathbf{x}_i(t)) < d_{\text{boundary}}; \\ \mathbf{0}, \qquad \text{otherwise}, \end{cases} \tag{6.8}$$

where

$$\mathbf{n}_{\text{boundary}}(\mathbf{x}_i(t)) = \frac{\nabla l_{\text{boundary}}(\mathbf{x}_i(t))}{|\nabla l_{\text{boundary}}(\mathbf{x}_i(t))|} \tag{6.9}$$

is the unit vector directed from the nearest point of the domain boundary to the actual position of the insect i. $l_{\text{boundary}}(\mathbf{x}_i(t)) : \Omega \to \mathbb{R}_+ \cup \{0\}$ is in fact the distance function resulting from the following eikonal equation and relative boundary conditions:

$$\begin{cases} |\nabla l_{\text{boundary}}(\mathbf{x})| = 1 & \forall\, \mathbf{x} \in \Omega; \\ l_{\text{boundary}}(\mathbf{x}) = 0, & \forall\, \mathbf{x} \in \partial\Omega \setminus \partial\Omega_{\text{nest}}; \\ \dfrac{\partial l_{\text{boundary}}(\mathbf{x})}{\partial \mathbf{n}} = 0, & \forall\, \mathbf{x} \in \partial\Omega_{\text{nest}}. \end{cases} \tag{6.10}$$

We here remark that, despite the term defined in Eq. (6.8), proper boundary conditions are needed. More specifically, we hereafter assume that when a bee touches a part of the domain not occupied by the nest, it stops, whereas it is taken out from the simulation when reaches a point of the target nest.

For each insect i, a fluctuation velocity term is added as well. It is given by a vector $\mathbf{v}_i^{\text{rand}}$, whose modulus and direction are, at any time t, random variables which uniformly fall within the ranges of values $[0, v_{\text{mean}}/10]$ and $[0, 360^\circ)$, respectively (see below for the meaning of v_{mean}).

We now turn to describe the velocity components characteristic of the different bee subgroups. First, $\mathbf{v}_i^{\text{align}}$ is an alignment term typical of the following individuals which, being uninformed of the position of the new nest, are only able to synchronize their flight with selected sets of mates. In this respect, for the i-th follower insect we define

$$\mathbf{v}_i^{\text{align}}(t) = v_{\text{mean}} \frac{< \mathbf{v}_j(t) >_{j \in \mathcal{N}_i^{\text{align}}(t)}}{| < \mathbf{v}_j(t) >_{j \in \mathcal{N}_i^{\text{align}}(t)} |}, \tag{6.11}$$

where v_{mean} denotes the characteristic speed of uninformed bees and

$$< \mathbf{v}_j(t) >_{j \in \mathcal{N}_i^{\text{align}}(t)} = \frac{1}{\#\mathcal{N}_i^{\text{align}}(t)} \sum_{j \in \mathcal{N}_i^{\text{align}}(t)} \mathbf{v}_j(t) \tag{6.12}$$

is the mean of the velocities of the groupmates falling within the alignment set $\mathcal{N}_i^{\text{align}}(t)$, denoting by # its cardinality. In this respect, we propose four alternative definitions of $\mathcal{N}_i^{\text{align}}$, in accordance with the different experimental hypotheses:

HP A1 - the i-th uninformed bee synchronizes its flight with the follower and the streaker individuals that are sufficiently fast and close to its position. This results in

$$\begin{aligned}\mathcal{N}_i^{\text{align}}(t) &= \{j=1,\dots,N, j\neq i : s_j(t)\in\{\text{U, S}\}, \mathbf{x}_j(t)\in\Omega_i^{\text{vis}},\\ &\quad 0<|\mathbf{r}_{ij}(t)|\leq d_{\text{align}}, |\mathbf{v}_j(t)|>|\mathbf{v}_i(t)|\},\end{aligned} \tag{6.13}$$

where again $\mathbf{r}_{ij}(t) := \mathbf{x}_j(t) - \mathbf{x}_i(t)$;

HP A2 - the i-th uninformed bee aligns to the faster groupmates, regardless of their status, provided that they are close enough, i.e.,

$$\begin{aligned}\mathcal{N}_i^{\text{align}}(t) &= \{j=1,\dots,N, j\neq i : \mathbf{x}_j(t)\in\Omega_i^{\text{vis}},\\ &\quad 0<|\mathbf{r}_{ij}(t)|\leq d_{\text{align}}, |\mathbf{v}_j(t)|>|\mathbf{v}_i(t)|\};\end{aligned} \tag{6.14}$$

HP A3 - the i-th uninformed bee synchronizes its flight to all insects falling within a given neighborhood, regardless of their status and speed. In mathematical terms:

$$\begin{aligned}\mathcal{N}_i^{\text{align}}(t) &= \{j=1,\dots,N, j\neq i : \mathbf{x}_j(t)\in\Omega_i^{\text{vis}},\\ &\quad 0<|\mathbf{r}_{ij}(t)|\leq d_{\text{align}}\},\end{aligned} \tag{6.15}$$

HP A4 - the i-th uninformed bee synchronizes its flight with the follower and the streaker individuals that fall within a given region, regardless of their velocity:

$$\begin{aligned}\mathcal{N}_i^{\text{align}}(t) &= \{j=1,\dots,N, j\neq i : s_j(t)\in\{\text{U,S}\}, \mathbf{x}_j(t)\in\Omega_i^{\text{vis}},\\ &\quad 0<|\mathbf{r}_{ij}(t)|\leq d_{\text{align}}\}.\end{aligned} \tag{6.16}$$

In all cases, d_{align} defines the extension of the alignment region. As discussed in the following, $d_{\text{align}} \in (d_{\text{rep}}, d_{\text{attr}})$, i.e., the flight synchronization set of an individual intersects those relative to its pairwise interactions with the groupmates. This assumption implies that each uninformed bee can simultaneously align to and avoid or be attracted by another individual, see Fig. 11.2. Further, we remark that, in the case of hypotheses A1 and A4, the passive leaders are not taken into account by the follower bees, as assumed in the biological literature [85, 87]. However, it is useful to underline that the explanation of such a phenomenon is far to be understood. For instance, it is hypothesized that the passive

leaders make themselves invisible to their groupmates by flying either close to the ground or backlight with respect to the sun or hidden in the middle the rest of the cloud (see again [85, 87]). In this respect, given the absence of detailed experimental evidence and in order to avoid further model overcomplications, we here opt to focus only on the typology of the flight of the informed insects (i.e., "back-and-forth" vs. "go-and-stop") and not on the zones of the swarm where such characteristic movements are performed. This issue would require further empirical investigations and, from a mathematical point of view, the introduction of three-dimensional settings. However, planar domains to describe bee swarming, including the dynamics of the leader individuals, are consistently employed across the theoretical literature (refer, for instance, to [18, 39]).

In Eq. $(6.6)_2$, $\mathbf{v}_i^{\text{streak}}$ describes the characteristic motion of the scout bees with a streaker status, i.e., when they fly at high speed in the direction of the nest thereby behaving as guidance leaders for the rest of the swarm. In particular, for the i-th streaker insect (i.e., $i : s_i(t) = \text{S}$), we set:

$$\mathbf{v}_i^{\text{streak}}(t) = -v_{\max} \frac{\nabla l_{\text{nest}}(\mathbf{x}_i(t))}{|\nabla l_{\text{nest}}(\mathbf{x}_i(t))|}, \tag{6.17}$$

where ∇l_{nest} has been introduced in (6.2), respectively. Equation (6.17) implies that each streaker individual performs a flight that, at each time instant t, is aligned to the direction minimizing the distance between its position and the target nest, i.e., it moves along the *optimal trajectory*, consistently to the single leader of the previous Chapter. In this respect, we here remark that the use of eikonal equations is usually employed in methods related to the computation of optimal paths. More specifically, Eq. (6.17) has the advantage that it can be used regardless the complexity of the domain, with straightforward extension to the case of non-planar geometries. Further comments on this aspect can be found in [23], where different approaches for evaluating individual minimal trajectories to a given target are discussed as well.

We then propose two alternative hypotheses for the characteristic behavior of scout bees when they take a passive leader role:

HP L1 - on one hand, they are assumed to slowly fly back towards the rear edge of the swarm, in order to slightly affect the movement of the rest of the groupmates. In this respect,

for the i-th passive leader bee, we set

$$\mathbf{v}_i^{\text{passive}}(t) = v_{\text{mean}} \frac{\dfrac{\mathbf{x}_{\bar{k}}(t)-\mathbf{x}_i(t)}{|\mathbf{x}_{\bar{k}}(t)-\mathbf{x}_i(t)|} + \dfrac{\nabla l_{\text{nest}}(\mathbf{x}_i(t))}{|\nabla l_{\text{nest}}(\mathbf{x}_i(t))|}}{\left|\dfrac{\mathbf{x}_{\bar{k}}(t)-\mathbf{x}_i(t)}{|\mathbf{x}_{\bar{k}}(t)-\mathbf{x}_i(t)|} + \dfrac{\nabla l_{\text{nest}}(\mathbf{x}_i(t))}{|\nabla l_{\text{nest}}(\mathbf{x}_i(t))|}\right|}, \tag{6.18}$$

where $\bar{k}$ is such that

$$l_{\text{nest}}(\mathbf{x}_{\bar{k}}(t)) = \max_{\substack{k:s_k(t)=\text{U} \\ \mathbf{x}_k(t)\in\Omega_i^{\text{vis}}(t)}} l_{\text{nest}}(\mathbf{x}_k(t)),$$

i.e., $\bar{k}$ is the uninformed insect farthest from the target nest;

HP L2 - on the other hand, we hypothesize that the passive leaders stop and wait for the passage of the rest of the population. For the i-th passive leader, we indeed set

$$\mathbf{v}_i^{\text{passive}}(t) = \mathbf{0}. \tag{6.19}$$

6.2 Parameter estimate

The half visual angle θ_{vis}, which symmetrically extends from the individual gazing direction, is taken equal to 156.5°, according to the biological measures presented in [91]. We here remark that a visual field determined by such an angle θ_{vis} (i.e., $< 180°$) introduces anisotropy in the behavior of bees although, with respect to most animal species, they are characterized by a substantially limited blind area behind them. As far as we know, in the experimental literature there is instead no study that explicitly defines the depth of the bee visual field. We therefore opt to set d_{vis} = 20 m, which is a value that allows each insect to perceive the presence of all groupmates when the swarm is sufficiently compact and not dispersed. The proposed estimate takes also into account the domain characteristic dimensions, such as the distance of the nest from the initial position of the insect population: in this respect, d_{vis} is set small enough to avoid that the target destination falls within the visual field of the uniformed individuals at the beginning of the observation time.

In our model two characteristic bee speed values are taken into account. The maximal admissible velocity $v_{\max} = v_{\max}^U = v_{\max}^S = v_{\max}^P$ is common to all subgroup of the population

and set equal to 9.4 m/s in accordance with [87]. The mean speed of the uninformed insects, defined in Eq. (6.11), is instead fixed equal to 6.7 m/s, again coherently with the experimental literature [49]. Here, we underline that $v_{\max}$ is also used in the case of the fast fly of the streaker bees towards the nest, whereas v_{mean} for the slower backward movement of the passive leader towards the trailing edge of the swarm. The difference between the speed of streakers and of the uninformed individuals has been empirically demonstrated.

All bees, regardless of their status, are characterized by repulsive/attractive interactions. According to the measure reported in [87], the insects tend to preserve a minimal mutual distance, here denoted by d_{rep}, equal to 0.3 m. The extension of the alignment region d_{align} is taken equal to 2 m. Since this value can not be empirically measured, its estimate is obtained referring to the modelling literature. The ratio $d_{\text{rep}}/d_{\text{align}}$ used in this work falls in fact in the middle of the range of analogous quantities tested by Couzin and colleagues [28]. A $d_{\text{attr}} = d_{\text{vis}}$ is instead set since we assume that each insect aims to maintain a connection with all individuals within its visual region.

As already commented, from a mathematical point of view, f_{rep} (with units m^2/s) gives the slope of the hyperbolic repulsive kernel h^{rep}, whereas f_{attr} (with units m/s) establishes the maximum of the parabolic-type attraction behavior of bees, described by function h^{attr}. Both positive parameters indeed do not have a clear and direct experimental counterpart and therefore their estimate is not straightforward as also commented in Chapter 5. In particular, due to the model extensions added in Section 6.1 we can not take advantage of the previous estimate. However, a numerical study, supported by selected empirical evidences, facilitated in this respect. In particular, we first took into account the following considerations: (i) upon attrative/repulsive stimuli only (in the absence of directional, alignment, and random dynamics), the computational swarm has to stabilize in a realistic crystalline configuration, characterized by optimal interparticle spacing $\approx d_{\text{rep}}$ (i.e., we have to avoid unrealistical situations such as the collapse or the explosion of the insect cloud); (ii) the specific flight of the informed bees has not to be affected by other velocity contributions, in the case of both assumptions L1 and L2.

To account for observation (i), we run a series of numerical realizations varying the interaction parameters f_{rep} and f_{attr} in the case of a swarm formed by $N = 500$ bees (480 of them with a follower role and the remaining 20 with an initial streaker status), which are assumed to be subjected only to repulsive/attractive stimuli, i.e.,

$$\mathbf{v}_i(t) = \mathbf{v}_i^{\text{rep}}(t) + \mathbf{v}_i^{\text{attr}}(t), \tag{6.20}$$

for all $i = 1, ..., N$, where the interaction velocity components are again defined as in the previous Section, Eqs. (5.19) and (5.20). Within a rectangular domain $[0,200] \times [0,200]$ m^2 Ω, the swarm is initially arranged in an almost round area centered at (100 m, 100 m) of radius equal to $r_0 = 4$ m, where the positions of the insects are randomly assigned. In this respect, we account for a reasonable density of ≈ 8 bees/m^2 [87]; also the percentage of informed individuals, i.e., 4 % of the entire population, is in agreement with the experimental literature [88, 90, 98]. The initial gazing direction $\mathbf{g}_i(0)$ of each generic i-th bee is randomly generated as well. The obtained dynamics are then classified according to the following asymptotic quantities:

$$d_{\min}(t_f) = \min_{\substack{i,j=1,...,N \\ i \neq j}} |\mathbf{x}_i(t_f) - \mathbf{x}_j(t_f)|; \tag{6.21}$$

$$d_{\max}(t_f) = \max_{\substack{i,j=1,...,N \\ i \neq j}} |\mathbf{x}_i(t_f) - \mathbf{x}_j(t_f)|, \tag{6.22}$$

being t_f an observation time sufficiently large to allow the insect cloud to reach a stable equilibrium configuration. These measures already introduced in Theorems 5.2.1 and 5.2.3 have clear empirical meanings: $d_{\min}(t)$ is in fact the minimal interparticle distance, whereas $d_{\max}(t)$ defines the extension of the overall swarm. As shown by the representative cases reported in Fig. 6.4, almost all pairs of coefficients (f_{rep}, f_{attr}) such that $f_{rep}/f_{attr} \geq 10^6$ resulted in realistic swarm pattern, as $d_{\min}$ is very close to the experimentally measured bee comfort space d_{rep}. In these cases, also the swarm overall diameter $d_{\max}$ is consistent with the empirical observations relative to the spatial density of bees [87]. On the opposite, if $f_{rep}/f_{attr} < 10^6$ the insects are observed to stabilize unrealistically close one to another, as $d_{\min} \ll d_{rep}$. Such simulation outcomes are indeed able to give a first restriction of the possible variations of the interaction coefficients f_{rep} and f_{attr}. Interestingly, the resulting permitted interaction parameters fall within the H-stability region[1] of the space of interaction parameters (f_{rep}, f_{attr}) that would characterize pairs of attractive/repulsive interaction kernels analogous to h^{rep} and h^{attr}, with the same coefficients d_{rep} and d_{attr}, if we neglected the asymmetry introduced by the anisotropic visual region of bees (cf. Hypothesis 3 in [13] is not satisfied in our case). In fact, referring to the series of works by Carrillo and colleagues [12–14, 16–18] (in particular, [18] deals with particle-based models of swarming), and to the calculations proposed in Section 5.2 of the previous

[1] As discussed in the previous chapter, from statistical mechanics [84], a system of mutual interacting particles is said H-stable if, for any arbitrarily large number of agents, the microscopic agents will not collapse onto themselves and a typical distance between individuals will be well defined.

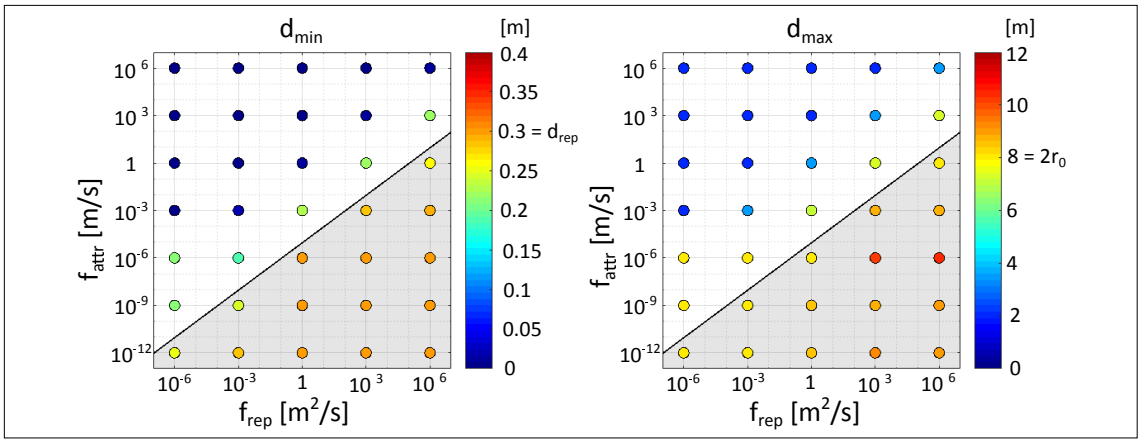

Figure 6.4 Dependence of the stable configuration of the bee cloud, subjected only to attractive and repulsive dynamics, upon variations in the values of the interaction parameters f_{rep} and f_{attr}. The quantities $d_{\min}$ and $d_{\max}$ represent the minimal interagent distance and the overall diameter of the swarm at a observation time t_{f} sufficiently large to have a stabilization of the system, as defined in Eqs. (6.21) and (6.22), respectively. The grey area in each panel indicates the H-stability region that one would have in the case of the same interaction kernels by assuming a isotropic visual region of bees.

Chapter, we have that the H-stability region for the swarm of our interest in the case of fully isotropic hypotheses (i.e., if the bees had a round visual field) would be given by the following parametric relation:

$$\frac{f_{\text{rep}}}{f_{\text{attr}}} > \frac{2(d_{\text{attr}} - d_{\text{rep}})}{5(d_{\text{rep}})^2}\left(3(d_{\text{rep}})^2 + 4d_{\text{attr}}d_{\text{rep}} + 3(d_{\text{attr}})^2\right) = 1.0719164 \cdot 10^5, \qquad (6.23)$$

which is indicated by the grey-shadowed area in Fig. 6.4 that contains the couples of permitted parameters found by the above numerical investigation. However, despite the consistence between these analytical results and the obtained computational outcomes, it is useful to underline that a theoretical analysis of the H-stability properties of an agent-based system in the case of asymmetric attractive/reulsive kernels is far to be provided and therefore would require further investigations.

Having reduced the range of values of the interaction parameters, we then use the above-cited observation (ii) to have a further estimate. In this respect, we now vary the coefficients f_{rep} and f_{attr} in the case of a simulation setting involving a swarm formed again by 480 follower individuals and 20 streaker bees. Given the same domain Ω and initial conditions described above, the insect population is assumed to behave according to the

following rules:

$$\begin{aligned}
\mathbf{v}_i(t) &= \mathbf{v}_i^{\text{rep}}(t) + \mathbf{v}_i^{\text{attr}}(t), \text{ if } i : s_i(t) = \text{U}; \\
\mathbf{v}_i(t) &= \mathbf{v}_i^{\text{rep}}(t) + \mathbf{v}_i^{\text{attr}}(t) + \mathbf{v}_i^{\text{streak}}(t), \text{ if } i : s_i(t) = \text{S}; \\
\mathbf{v}_i(t) &= \mathbf{v}_i^{\text{rep}}(t) + \mathbf{v}_i^{\text{attr}}(t) + \mathbf{v}_i^{\text{passive}}(t), \text{ if } i : s_i(t) = \text{P},
\end{aligned} \tag{6.24}$$

for $i = 1, ..., 500$, being the velocity contributions defined exactly as in Section 6.1 (in particular $\mathbf{v}_i^{\text{passive}}$ was set to take the form either of Eq. (6.18) or of Eq. (6.19)). With respect to the complete model, we indeed neglect alignment mechanisms and random contributions. Our choice is justified by the fact that the aim of the study was to find the values of the attraction/repulsion parameters that do not affect the characteristic motion of the informed bees, under the assumptions L1 and L2. As summarized in Figs. 6.5 and 6.6, we observe that, in both cases, too large values of f_{attr} disrupt the hypothesized flight of the informed bees, regardless of the value given to f_{rep}. In more details, the group of following bees constantly stabilize into a crystalline configuration but, for $f_{\text{attr}} > 10^{-3}$, the following dynamics arose:

- in the case of assumption L1, the scout individuals are not able to reach any edge of the fixed cloud (see the bottom-right panel of Fig. 6.5);
- in the case of assumption L2, the informed insects are not able to rest at the leading front of the population (where they have to remain since the follower bees are not allowed to have a directional movement and therefore to pass the scouts), as reproduced in the bottom-right panel of Fig. 6.6.

The underlying rationale involves two competing mechanisms: on one hand, a too large attraction strength f_{attr} makes the group of follower individuals almost a rigid disk which is difficult to be flown across; on the other hand, it causes the scout bees to perform an abnormal movement.

Within the remaining set of permitted interaction parameter values, we finally opt to fix $f_{\text{rep}} = 1$ m^2/s, i.e., we opt for a classical equilateral hyperbolic repulsive kernel as done, for instance, by Kolokolnikov and Chen in the already cited work [19] dealing with predator-prey swarming dynamics. An $f_{\text{attr}} = 10^{-6}$ m/s is consequently set to avoid further increments in the difference between the order of magnitude of the two parameters.

As seen, a repulsive velocity component from the domain boundary, given by a negative exponential function, has been set for each bee. In this respect, the insects perceive and

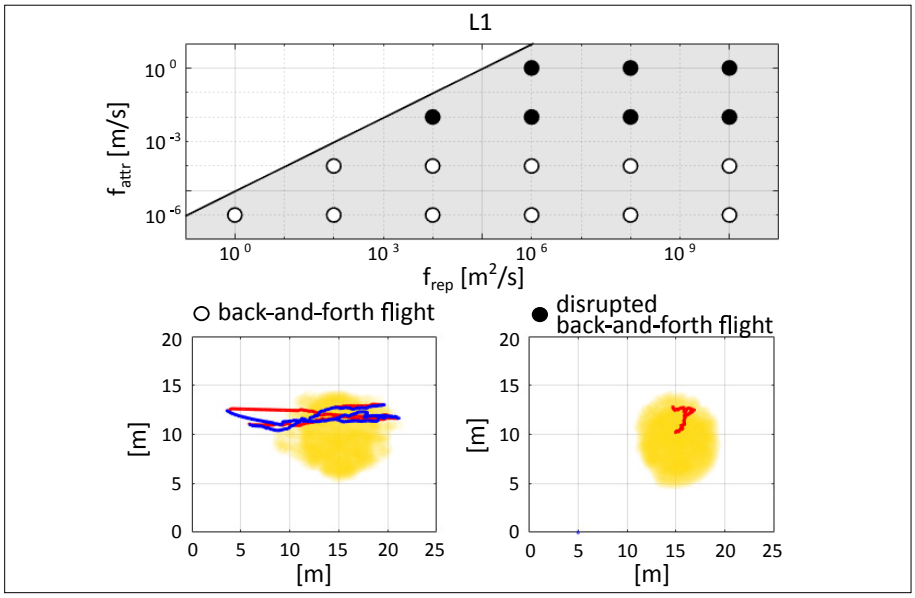

Figure 6.5 Dependence of the dynamics of the informed bees upon variations in the values of the interaction parameters f_{rep} and f_{attr}, in the case of assumption L1. As it is possible to observe the hypothesized "back-and-forth" flight can be obtained only for $f_{\text{attr}} < 10^{-3}$, regardless of the values of coefficient f_{rep} (provided that the pair (f_{rep}, f_{attr}) leads to crystalline equilibrium configurations upon attractive/repulsive interactions only). Too large values of f_{attr} in fact result in a disrupted behavior of the informed insects, which remain stuck within the bee cloud (represented by the yellow shadow), as reproduced in the corresponding representative bottom panel.

react to the presence of the boundaries from a distance of d_{boundary}, whereas a_{boundary} and b_{boundary} determine the exact form of $\mathbf{v}_i^{\text{boundary}}$. In the absence of pertinent experimental measurements, a reasonable estimate of such triplet of coefficients is obtained with a series of preliminary simulations, i.e., in order to avoid unrealistic dynamics such as swarm collapse at the domain boundary or deflection from the optimal flight trajectory at too large distances from the domain edge. In particular, the found values of a_{boundary} and b_{boundary} are analogous to their counterpart employed in a particle model reproducing pedestrian behavior [23]. For the sake of completeness, we illustrate in Fig. 6.7 some pathological system evolutions in the case of rejected sets of values of d_{boundary}, a_{boundary} and b_{boundary}.

Finally, the modulus of the random velocity vectors falls within the range $[0, v_{\text{mean}}/10]$: in particular, we set such an upper threshold to avoid unrealistically large fluctuations in bee flight, taking also advantage of the study and relative observations performed in Section 5.3 of the previous Chapter.

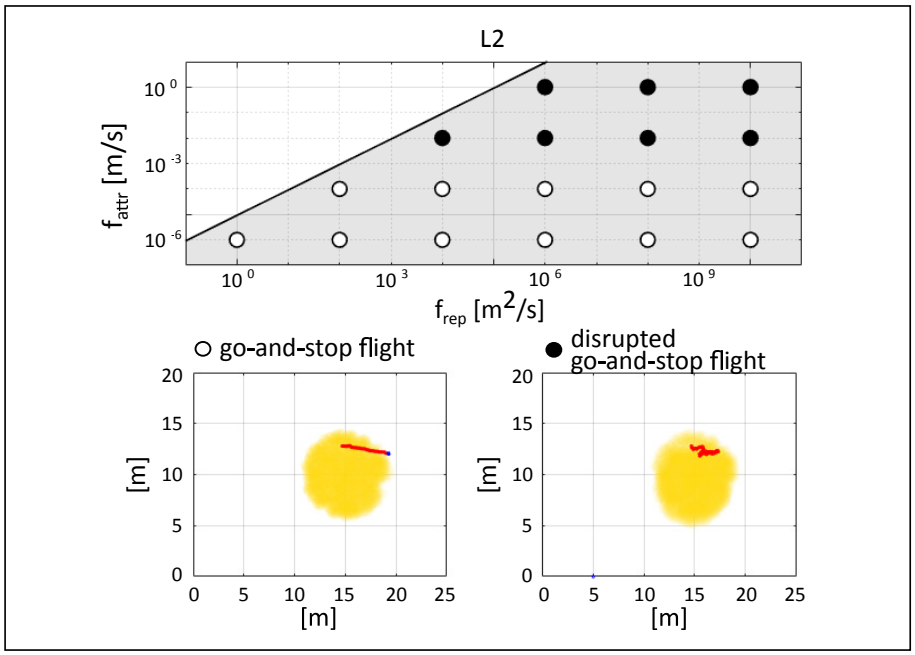

Figure 6.6 Dependence of the dynamics of the informed bees upon variations in the values of the interaction parameters f_{rep} and f_{attr}, in the case of assumption L2. As it is possible to observe the hypothesized "go-and-stop" flight can be obtained only for $f_{\text{attr}} < 10^{-3}$, regardless of the values of coefficient f_{rep} (provided that the pair (f_{rep}, f_{attr}) leads to crystalline equilibrium configurations upon attractive/repulsive interactions only). Too large values of f_{attr} in fact result in a disrupted behavior of the informed insects, which are not able to stop at the leading edge of the bee cloud (represented by the yellow shadow) being dragged within the population, as reproduced in the corresponding representative bottom panel.

The entire model parameter setting used in the following simulations is summarized in Table 6.1.

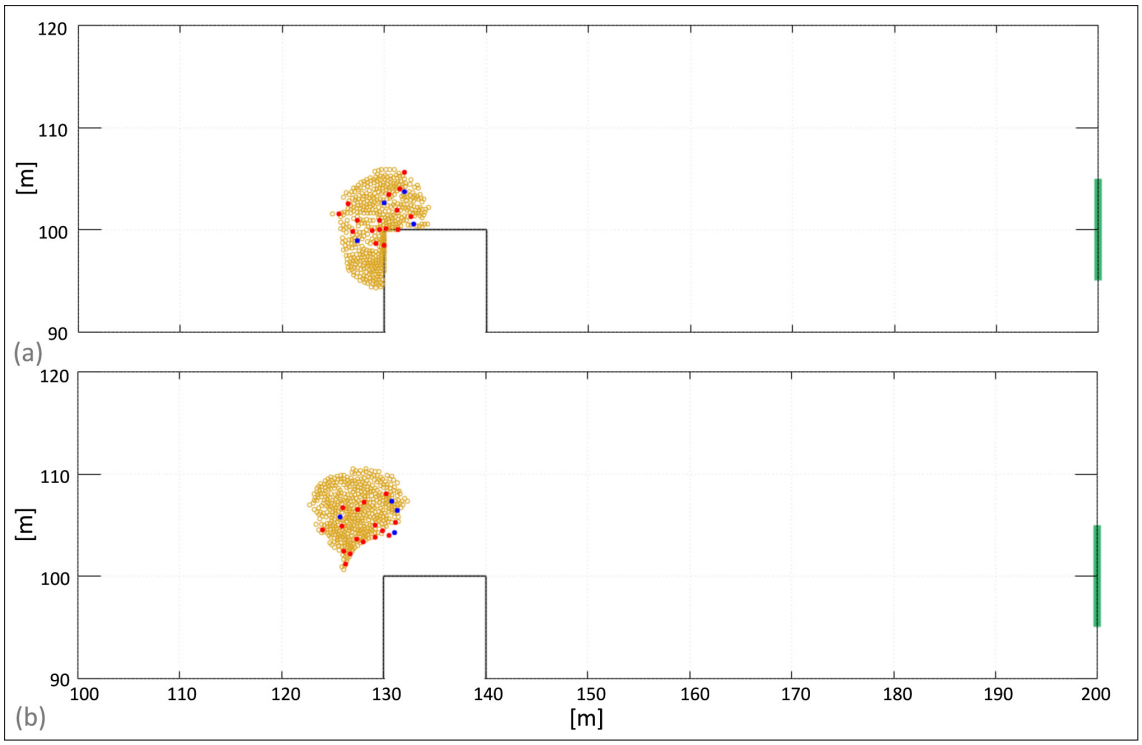

Figure 6.7 Unrealistic bee swarming in the cases of representative rejected sets of parameters relative to the velocity component $\mathbf{v}^{\text{boundary}}$. (a) The bee swarm collapses on the domain structural element being unable to react to its presence. This phenomenology can be obtained, for instance, with a too low value of d_{boundary} and a too high value of b_{boundary}. (b) The insect population deforms at an implausibly high distance from the obstacle. This system behavior is instead the result of too high values of d_{boundary} and a_{boundary}.

6.3 Numerical results

The numerical results proposed in this Section will be divided in two parts. In the first Section 6.3.1, we will test different combinations of the alternative assumptions relative to the alignment mechanism of the uninformed bees and to the behavior of the passive leaders. By considering swarm dynamics within a simple rectangular domain, we will look at the rules of motion that result in a realistic migration of the insect cloud, which has to fly compactly and productively towards the nest. The effect of variations in the percentage of informed bees will be analyzed as well. Section 6.3.2 will be instead devoted to reproduce the collective phenomenology of the bee population in more complex environments, which involve domains with different obstacles.

Table 6.1 Model parameters.

Par.	**Description**	**Value [Unit]**	**Reference**
d_{vis}	depth of visual field	20 [m]	biological evidences
θ_{vis}	half visual angle	156.5 [deg]	[91]
v_{mean}	mean velocity of uninformed bees	6.7 [m/s]	[49]
v_{max}	bee maximal admissible speed	9.4 [m/s]	[87]
d_{rep}	extension of the avoidance region	0.3 [m]	[87]
d_{align}	extension of the alignment region	2 [m]	coherent with [27]
d_{attr}	extension of the attractive region	20 [m]	biological evidences
f_{rep}	avoidance coefficient	1 [m^2/s]	parametric analysis
f_{attr}	attraction coefficient	10^{-6} [m/s]	parametric analysis
d_{boundary}	extension of boundary repulsion	4.0 [m]	parametric analysis
a_{boundary}	coeff. of the boundary repulsion	0.18 [m/s]	parametric analysis
b_{boundary}	coeff. of the boundary repulsion	1.0 [m]	parametric analysis

6.3.1 Swarming in a large open-space domain

In this first set of simulations, we use an open-space (without structural elements) rectangular $[0,200] \times [0,200]$ m^2 domain Ω (exactly the same domain has been chosen for the simulations supporting the estimate of parameters f_{rep} and f_{attr} in the previous Section) where the target destination is constituted by the boundary segment $y \in [95,105]$ on the right side of the domain, see Fig. 11.4. The measure of $\partial\Omega_{\text{nest}}$ is larger than the dimension of a real nest, since we here intend to describe the behavior of the swarm while approaching the new home and not the subsequent entrance mechanisms, that are driven by other processes (e.g., pheromone cues). The insect population is formed by $N = 500$ individuals (we recall that we are dealing with a planar section of a larger three-dimensional swarm). In particular, 480 of them are uninformed followers, whereas the remaining ones are scouts with an initial streaker role, i.e., $s_i(0) = \text{S}$ for $i \in \{481,...,500\}$. We here recall that uninformed bees are not allowed to change status, whereas the informed insects can switch between the streaker and the passive leader role. The initial conditions are left unchanged from the previous Section, see Fig. 11.4.

The objective of the swarm is to reach the target destination. In this respect, the numerical realizations are stopped as soon as the last insect touches a point of $\partial\Omega_{\text{nest}}$, i.e., at a time denoted with t_{F}. The dynamics of the bee population resulting from different combinations of the individual behavioral hypotheses outlined in Section 6.1 are classified according to the following criteria:

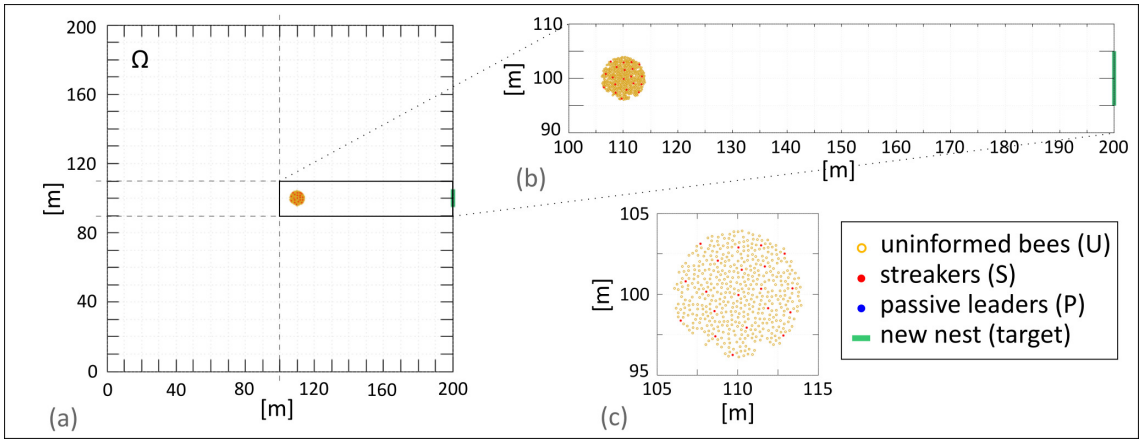

Figure 6.8 The sets of simulations proposed in Section 6.3.1 are employed in a rectangular $[0,200] \times [0,200]$ m^2 domain Ω, where the target destination is constituted by the boundary segment $\partial\Omega_{\text{nest}} = 200 \times [95,105]$ (indicated by the green line). The swarm is initially arranged in an almost round area centered at (110 m, 100 m) of radius equal to $r_0 = 4$ m, where the positions of the insects are randomly assigned. In particular, we account for $N = 500$ bees, with 480 follower individuals and 20 scouts. All the informed bees are initially assigned a streaker status. For representative purposes, the virtual insects will be hereafter indicated by rigid disks centered at their actual position. More specifically, we will use yellow circles for uninformed individuals, red circles for streaker scouts and blue circles for passive leader scouts.

Definition 6.3.1. The swarm undergoes a *directionally productive motion* towards the nest if

$$E_{\text{swarm}} = \lim_{t\to\infty} l_{\text{nest}}(\mathbf{x}_{\text{swarm}}(t)) = 0, \tag{6.25}$$

where $\mathbf{x}_{\text{swarm}}(t) = \dfrac{\sum_{i=1}^{N} \mathbf{x}_i(t)}{N}$ is the center of mass of the bee cloud and l_{nest} is the distance function introduced in Eq. (6.2).

The swarm undergoes a *coherent and collective flight* if

$$C_{\text{swarm}} = \max_{t>0} \frac{a_{\text{swarm}}(t)}{a_{\text{R}}} < 2, \tag{6.26}$$

where $a_{\text{swarm}}(t)$ is a measure of the space extension[2] of the bee cloud at time t and a_{R} is equal to $\pi(r_0)^2$, i.e., the area of the round region initially containing all individuals.

[2]The spatial extension of the swarm is evaluated by the Matlab (the MathWorks®) function `boundary`. More specifically, this function returns the area enclosed by the single conforming 2-D boundary containing of a given set of discrete particles. For further details, we refer to Matlab manuals and tutorials.

The swarm undergoes a *collective and productive flight* towards the nest if both conditions (11.13) – (6.26) are satisfied.

The quantity defined in Eq. (6.26) is able to give an indication of the presence of dispersed insects, i.e., of bees unable to correctly synchronize their movement with the rest of the group. In fact, our simulation results have consistently shown that if, at a given time t, the surface of the insect cloud is twice the reference initial area a_{R} (or even more), then there is at least a follower bee that actually has no groupmate within its alignment set which means that it has lost.

Figs. 11.5 – 6.11 summarize the results obtained by the different combinations of the individual behavioral hypotheses. In particular, for each pair of assumptions, we have run 10 independent numerical realizations, given the presence of randomness both in the initial position of the bees and in their dynamics due to the velocity term $\mathbf{v}^{\mathrm{rand}}$. We can observe that in all cases the distance $l_{\mathrm{nest}}(\mathbf{x}_{\mathrm{swarm}}(t))$ between the swarm center of mass and the nest decreases almost linearly (see also the inset graph in Fig. 11.5 (a)). In particular, it becomes null in a finite time (< 14 seconds), as E_{swarm} is zero. However, as shown in the plot of C_{swarm} in Fig. 11.5 (b), only under hypotheses (A3, L1), (A3, L2) and (A4, L2), the flight of the insect population is completely synchronized and therefore collective in all realizations. In the other cases, as also shown in the representative snapshots in Figs. 11.6 and 6.11, at least one uninformed bee does not correctly align to the rest of the swarm, flying away from the groupmates. In these situations, the scout bees have to take time to reach/wait for the dispersed individual(s) and to guide it (them) towards the nest: the experimentally-observed compactness of the insect cloud is therefore not maintained. From the graph in Fig. 11.5 (b), it can be further noticed that bee dispersion is more significant in the case of assumptions (A2, L1) and (A2, L2), i.e., when the uninformed bees align to the faster groupmates, regardless of their status.

Taking all the results together, we can state that in our model alignment mechanisms involving a control over groupmate velocity do not certainly imply directionally productive and collective swarm dynamics. An efficient and coordinate flight is instead reproduced if the follower individuals synchronize their movement (i) to all insects sufficiently close to their position, regardless of their status and of the behavior of the passive leaders, or (ii) only to close enough uninformed and streaker groupmates, provided the fact that the passive leaders stop upon reaching the front of the cloud. In particular, it is somehow worth to remark that, in the case of hypotheses A1 and A4, passive leader bees are not considered for

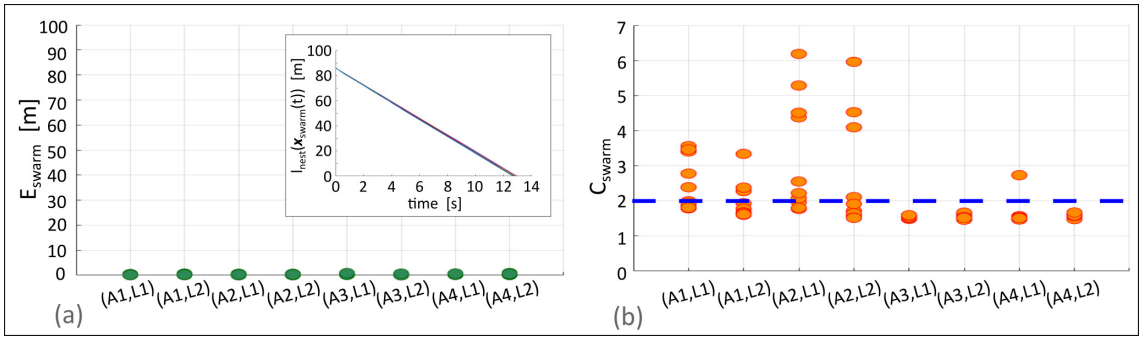

Figure 6.9 (a) Plot of E_{swarm}, defined in Eq. (11.13), in the case of 10 independent numerical realizations for each combination of bee behavioral assumptions. It is worth to notice that, in all cases, the swarm undergoes a productive movement, in terms of center of mass displacement. For the sake of completeness, in the inset graph, we represent the evolution in time of the distance of the center of mass of the insect cloud from the nest. (b) Plot of C_{swarm}, defined in Eq. (6.26), in the case of 10 independent realizations for each combination of bee behavioral assumptions. A consistent (i.e., in all realizations) absence of bee dispersion is only obtained in the case of hypotheses (A3, L1), (A3, L2) and (A4, L2).

the alignment mechanism: however, they determine the flight of the follower groupmates by affecting the other velocity components (e.g., collision avoidance and attraction).

We now turn to describe and compare in more details selected characteristics of swarm dynamics under the plausible combinations of behavioral assumptions. In this respect, Fig. 6.12 shows the time-evolution of the amount of bees belonging to each subpopulation in the different cases. As it is possible to observe, the number of follower individuals remains obviously constant whereas, transitions between streaker and passive leader states continuously occur. In particular, under the coupled hypotheses (A3, L1), the amount of streaker insects remains substantially higher than the number of passive leaders during the entire migration (the former falling within the range 14-20, the latter within the range 0-6). On the opposite, in the case of assumptions (A3, L2) and (A4, L2) (i.e., when the passive leaders are assumed to stop and wait for the rest of the colony), the fluctuations in the cardinality of two subgroups of scout bees are more significant: for instance, the amount of streakers can drop and be almost equal to the number of passive leaders.

Fig. 6.13 finally compares the trajectories of representative scout bees under the different assumptions resulting in realistic swarm dynamics. In particular, under the coupled hypotheses (A3, L1), it is straightforward to notice the short-time backward movement of the informed individual during its passive leader status. It is also interesting

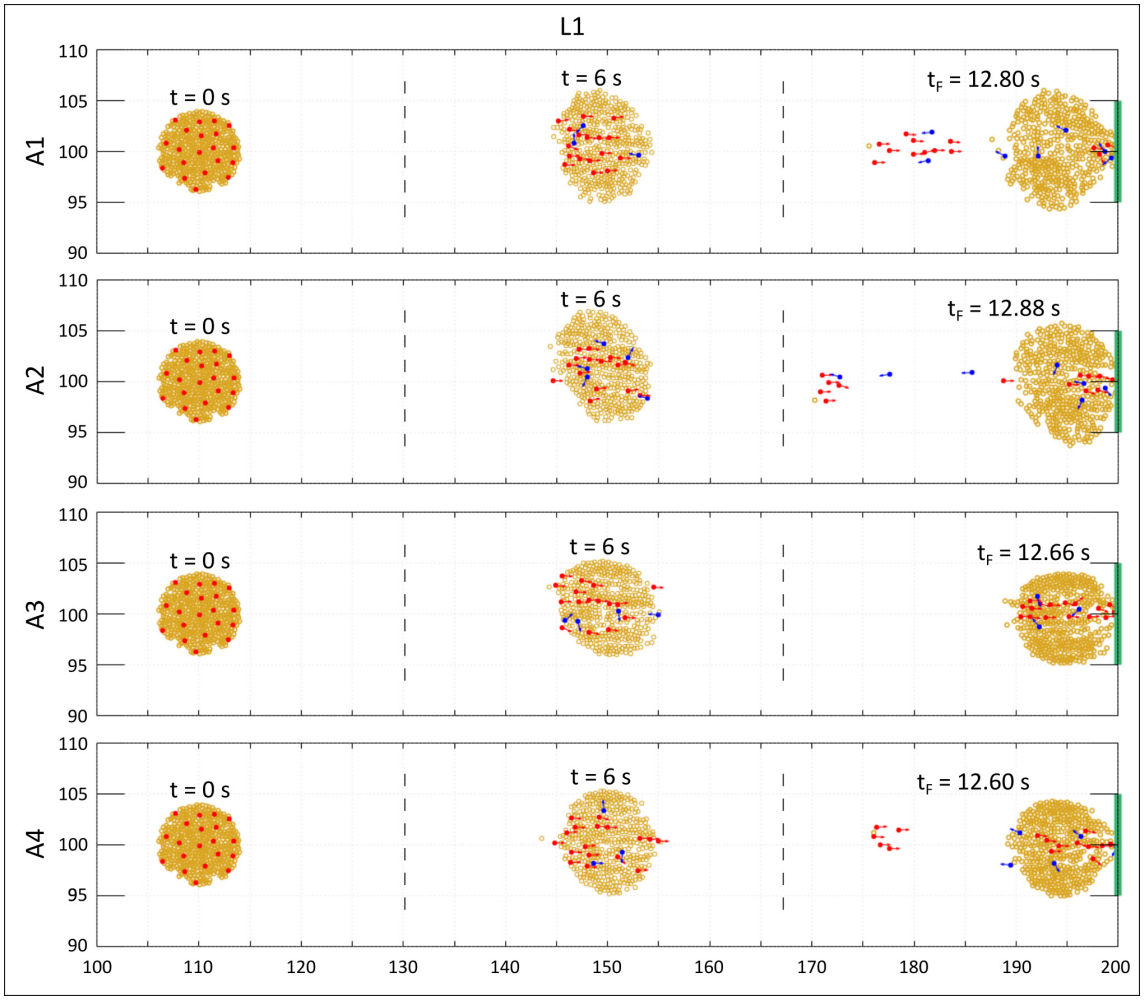

Figure 6.10 Representative evolutions of the bee population in the case of combinations between the hypothesis L1 (relative to the behavior of the passive leader scouts) and the alternative assumptions on the alignment mechanism of the follower insects. It is possible to notice that, in all cases, the swarm reaches the target destination, but only for the pair (A3, L1) without bee dispersion. We recall that yellow disks represent follower bees, red circles represent streakers, and blue disks represent passive leaders. For each scout individual, we finally indicate by a colored arrow its velocity.

to observe that under the assumptions (A3, L2) and (A4, L2), the scout bees, when passive leaders, do not completely stop but rather still move as a consequence of the velocity components which are still active (i.e., those relative to attractive/repulsive interactions and to random fluctuations).

Variations in the percentage of scout bees. As seen, the collective migration of bee swarms is guided by few informed individuals, that are able to diffuse information on the nest

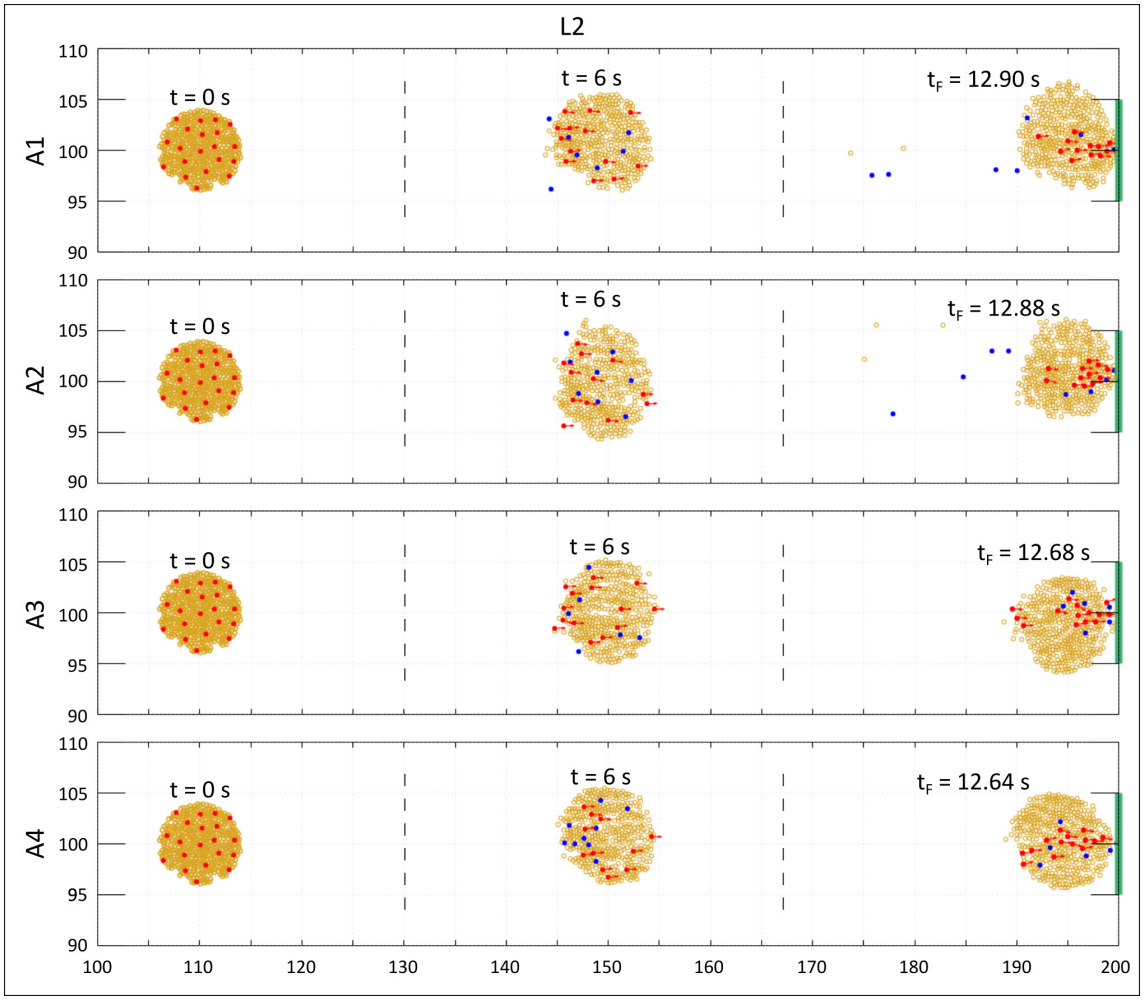

Figure 6.11 Representative evolutions of the bee population in the case of combinations between the hypothesis L2 (relative to the behavior of the passive leader scouts) and the alternative assumptions on the alignment mechanism of the follower insects. It is possible to notice that, in all cases, the swarm reaches the target destination, bee dispersion is not observed for the pairs (A3, L2) and (A4, L2). We recall that yellow disks represent follower bees, red circles represent streakers, and blue disks represent passive leaders. For each scout individual, we finally indicate by a colored arrow its velocity.

location within the rest of the population. An interesting question is indeed relative to the consistency of the flight directional efficiency upon variations in the ratio between the number of individuals having the different roles within the colony.

In this respect, we now study the dynamics of insect clouds characterized by different numbers of scouts and of overall components. In particular, we employ the same domain of the previous Section and the rules of motion defined in Section 6.1: however, only the

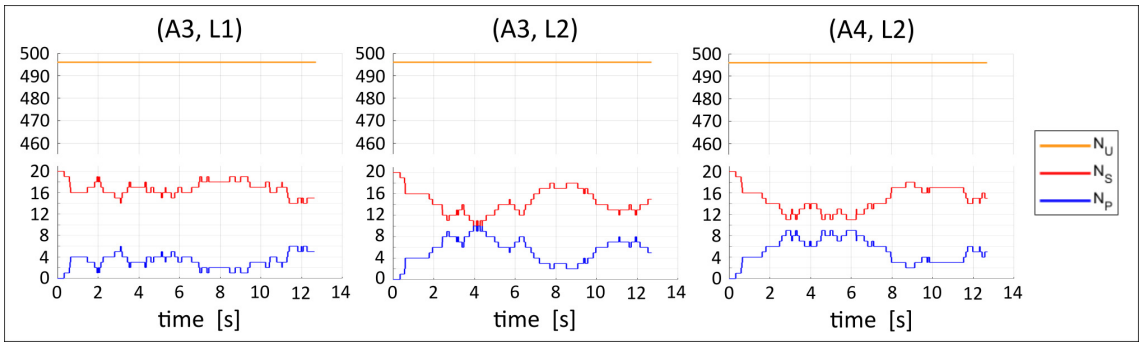

Figure 6.12 Evolution in time of the number of bees belonging to each subpopulation in the case of hypothesis combinations resulting in directionally productive and collective swarming. For clarity purposes, we plot the outcomes of a single numerical realization for each setting, since we do not observe large variances in the case of multiple independent simulations.

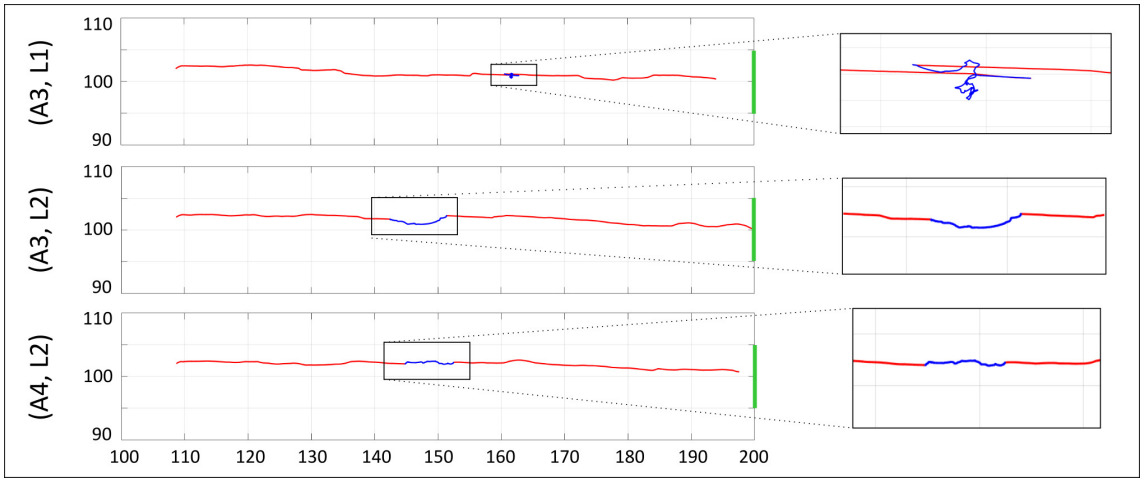

Figure 6.13 Representative trajectories of scout bees during swarming, in the case of the three combinations of behavioral assumptions resulting in a directionally productive and collective insect flight.

combinations of assumptions that have resulted in a plausible system phenomenology are hereafter used, i.e., the pairs (A3, L1), (A3, L2), and (A4, L2). As initial data, the bees are again randomly disposed in round regions, whose radius is chosen, in each case, to maintain the density of 8 bees/m^2. All scout individuals have a streaker status whereas the initial bee gazing direction is randomly assigned.

As it is possible to observe in Fig. 6.14, for a given group size, i.e., for a fixed N, the directionally productive component of swarm movement increases (i.e., E_{swarm} decreases) as the percentage of informed individuals increases. Furthermore, still from the same plot,

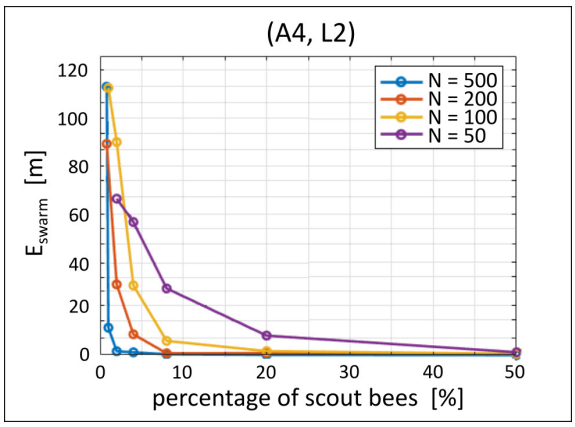

Figure 6.14 Relationships between the directional efficiency of swarm flight (in terms of E_{swarm}, defined in Eq. (11.13)) and the percentage of informed bees, in the case of different sizes of the colony (i.e., of overall number of components N). To avoid redundancy, we plot the outcomes obtained from a single realization in the case of coupled hypotheses (A4, L2): however, these results have been obtained also with assumptions (A3, L1) and (A4, L1) and are robust in the case of independent simulations.

we can notice that the higher the overall number of bees is, the smaller the proportion of informed individuals necessary is in order to have an efficient migration towards the nest. In particular, substantially large swarms require a very small set of scout bees to reach the target destination.

These results are observed for all the tested combinations of behavioral assumptions (even if for clarity we represented only the case relative to the pair (A4, L2), being completely robust also in the case of independent simulations in the different settings (in each case, the standard deviation deriving from 10 simulations is $< 1\%$ and therefore not represented in the graphs). We also remark that in the cases of full productive swarming (i.e., when $E_{\text{swarm}} \approx 0$) no bee dispersion occurs (i.e., $C_{\text{swarm}} < 2$), in agreement with the outcomes presented in the previous subsection.

As it will be commented in more details in the conclusive part of the Chapter, analogous quite surprising results have been obtained in the works by Couzin et al. [27] and by Fetecau and Guo [44], where similar microscopic/discrete models have been employed to describe collective swarming.

6.3.2 Swarming in more realistic situations

Finally, we turn to asses the applicability of our model in real-world situations by means of representative numerical results involving more complex environments.

In particular, referring to Figs. 6.15 and 6.16, we deal with domains characterized either by a structural obstacle or by a bottleneck, placed in between the initial position of the swarm and the target destination. Such environmental elements may represent architectural buildings or trees that the insect cloud has to avoid during its migration. Hereafter, the bee population is still assumed to be composed of $N = 500$ individuals, which are initially subdivided into 480 uninformed insects and 20 streakers. As usual, the initial configuration of the swarm consists of a circle of radius $r_0 = 4$ m with bee position and gazing direction randomly assigned. Again we test the coupled hypothesis (A3, L1), (A3, L2), and (A4, L2). The center of the nest is located at the same y-coordinate of the initial center of mass of the insect cloud.

As it is possible to observe in Figs. 6.15 and 6.16, in both situations, the swarm has to slightly deflect its direction of movement and to deform to pass the structural elements and reach the target destination. In particular, in the case of the square obstacle, the bees located at the bottom part of the population are pressed towards the center of the swarm by the repulsive velocity $\mathbf{v}^{\text{boundary}}$. We indeed have an increasing density of insects in the center of the cloud. However, the productive direction of flight is still maintained. Once passed the structural element, the compressed area of the swarm slightly relaxes and an almost homogeneous density of bees is recovered.

Referring to Fig. 6.16, when approaching the bottleneck, the swarm is instead substantially stretched horizontally and compressed vertically, i.e., it switches from a round shape to a ellipsoidal geometry, with shorter axis along the y-direction of the domain. Interestingly, after passing the bottleneck, there is only a slight relaxation of the insect cloud, which does not acquire again a fully-round configuration. The underlying rationale is that, even when the colony has an elongated shape, the component bees are at a sufficient (but not excessive) distance one from another and therefore there is no reason to spend energy to further reorganize.

In both domain configurations, the swarm finally redirect again its coordinate flight to reach the target destination.

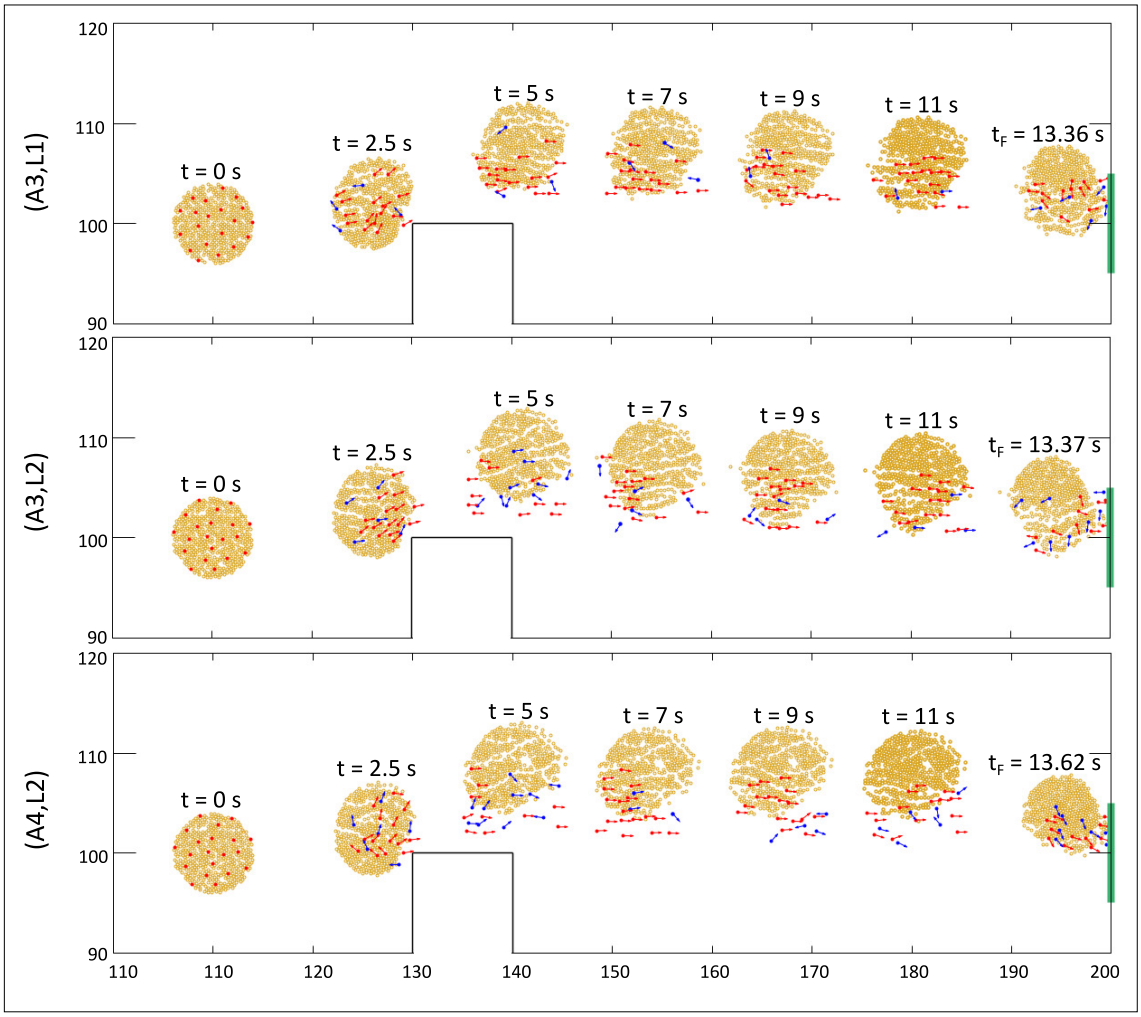

Figure 6.15 Bee swarming in the case of more complex environments. Representative evolutions of the bee population placed within a domain characterized by a square obstacle between its initial position and the new nest, whose center is located at the same y-coordinate of the initial center of mass of the insect cloud, in the case of the sets of plausible behavioral assumptions (A3, L1), (A3, L2), and (A4, L2). The insect population is assumed to be composed of $N = 500$ individuals, which are initially subdivided into 480 uninformed insects and 20 streakers. The initial configuration of the swarm consists of a circle of radius $r_0 = 4$ m with bee position and gazing direction randomly assigned. It is possible to observe that the swarm autonomously deflects its motion and undergoes morphological reorganization in order to pass the structural element and compactly reach the target destination. We recall that yellow disks represent follower bees, red circles represent streakers, and blue disks represent passive leaders. For each scout individual, we finally indicate by a colored arrow its velocity.

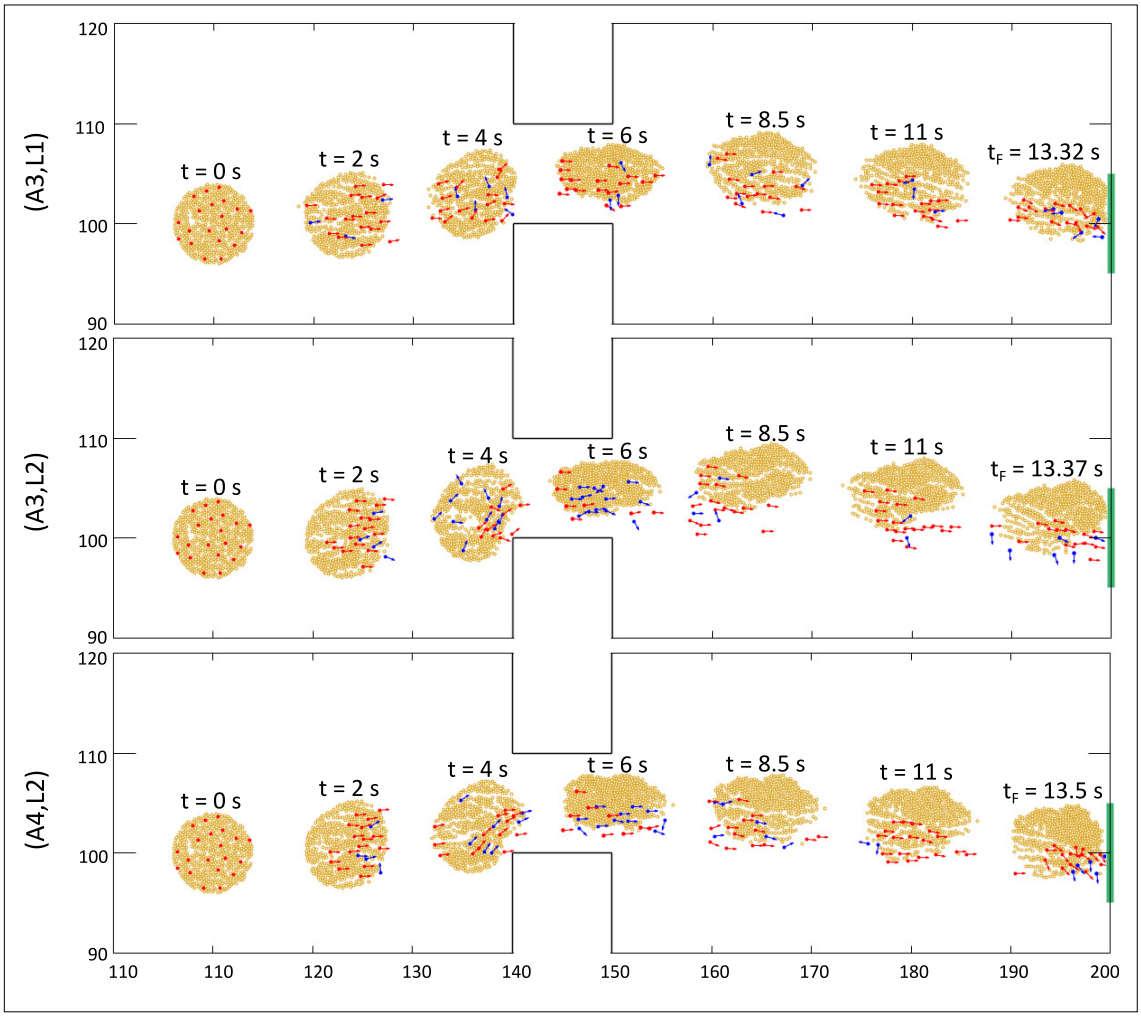

Figure 6.16 Bee swarming in the case of more complex environments. Representative evolutions of the bee population placed within a domain with a bottleneck between its initial position and the new nest, whose center is located at the same y-coordinate of the initial center of mass of the insect cloud, in the case of the sets of plausible behavioral assumptions (A3, L1), (A3, L2), and (A4, L2). The insect population is assumed to be composed of $N = 500$ individuals, which are initially subdivided into 480 uninformed insects and 20 streakers. The initial configuration of the swarm consists of a circle of radius $r_0 = 4$ m with bee position and gazing direction randomly assigned. It is possible to observe that the swarm squeezes to pass through the structural element. We recall that yellow disks represent follower bees, red circles represent streakers, and blue disks represent passive leaders. For each scout individual, we finally indicate by a colored arrow its velocity.

The above-described phenomenologies are observed under the three tested coupled hypotheses, with slight differences in the morphological transitions of the swarm. However, we remark that, in all settings, there is no bee dispersion.

The results presented in this Section allow us to conclude that the behavioral rules of bees (A3, L1), (A3, L2), and (A4, L2) give a realistic swarming not only in open-space simple domains but also in more complex scenarios. In particular, our model, under such plausible hypotheses, is able to capture autonomous morphological reorganizations and changes of flight direction of the insect cloud, necessary to preserve its compactness and to reach the target destination.

6.4 Conclusions

The aim of this Chapter has been indeed to test alternative assumptions both on the flight synchronization mechanism of uninformed individuals and the characteristic dynamics of the scout insects in order to find out those resulting in realistic swarming phenomenologies. To do this, we employed the discrete modeling framework introduced in Chapter 4. Taking advantage of the study of the alignment process carried out in the previous Chapter, here we have explored different possible definitions of the alignment set (the specificity of individuals involved). On the other hand, we have developed the modeling description of the leader dynamics. Their movement is defined according to the alternation of two behavioral status, i.e. streaker and passive leader. Specifically, they fly at the maximum velocity from the back to the front of the swarm (streaker status). Once they reach the front of the bee cloud, they switch to a passive leader status. For the latter, we have implemented both the hypotheses proposed by Seeley, [87]: under the first hypothesis they slowly come back to the rear edge of the swarm; under the second one, they stop and wait the passage of the rest of the migrating population. The three subgroups of bees have then in common some general rules of motility, such as the tendency to remain within the population while keeping a comfort distance from the other components as well as from the domain boundary.

The resulting model has been used to test combinations of alternative assumptions underlying the synchronization mechanisms of uninformed bees and the individual behavior of passive leader bees. In particular, our results have shown that a productive collective flight of the swarm is only possible if the uniformed individuals synchronize their movement (i) to all insects sufficiently close to their position regardless of their status and velocity and of the dynamics of the passive leaders (i.e., coupled assumptions (A3, L1) and (A3, L2)) or (ii) only to close enough follower and streaker groupmates, provided the fact that the passive leaders stop upon reaching the front of the swarm (i.e.,

coupled assumptions (A4, L2)). Other sets of hypotheses have produced the unrealistic phenomenon of bee dispersion, i.e., at least one follower individual is not able to synchronize its movement with the rest of the swarm during the entire flight, thereby flying away and affecting the migration of the informed bees and eventually of the entire population.

Once the most plausible behavioral assumptions have been identified, we have turned to analyze the effect of variations in the number of scout bees. Interestingly, we have found that larger swarms require fewer scout individuals to compactly reach the target destination. This quite surprising outcome is in agreement with the results obtained by similar models [27, 44]. However, it is useful to remark that from experimental observations it is known that, regardless the size of the population, the fraction of informed insect typically falls in the range 3%-5%. In this respect, we can speculate that, although in principle the percentage of scout bees could decrease, their amount may be established also by other social dynamics of the swarm not involving migration issues. For instance, a sufficiently high number of scout bees could be necessary to explore the environment to find a new home in a substantially short time.

With the last set of simulations, we have finally provided the fact that our model, with the selected combinations of bee behavioral assumptions, is able to capture swarm dynamics in more complex scenarios, that may require morphological rearrangements of the insect cloud to pass structural elements and significant changes of flight directions.

Chapter 7

Analysis of the collective dynamics of a swarm subjected to conflicting flight information

In the previous Chapter, both hypotheses proposed by M. Lindauer (*back-and-forth flight* and *go-and-stop flight*) have been mathematically investigated in combination with distinct assumptions for the set of individuals involved in the synchronisation process of uniformed bees. The numerical results have allowed us to exclude that follower individuals consider only fast-flying bees and to identify three combinations of assumptions related to scout behaviour and alignment mechanism that results in an efficient and coherent swarming. Specifically, both M. Lindauer hypotheses result in a compact and productive swarm dynamics when we assume that the follower insects align to all groupmates falling within a given neighbourhood; on the opposite, only the go-and-stop hypothesis results realistic under the assumption that followers do not consider the presence of the scouts in their way back to the rear edge of the swarm.

The goal of this Chapter will be to further investigate these three plausible combinations of behavioral assumptions accounting for the empirical evidences provided by T. Latty and coworkers in [71], who studied if and how the migration of real swarms is affected by the presence of a fast-flying traffic line of honeybees pointing towards a different destination. Specifically, they made different artificial swarms, constituted by the queen bee and about 6000 workers per swarm, located in a tree-less field. The swarms were divided in two treatment groups: test swarms and control swarms. To reach the nestbox, test swarms had

to fly through a traffic area of fast flying bee foragers headed in a wrong direction, while control swarms were allowed to migrate towards the new nest in absence of bee foragers. To set up the traffic area affecting the dynamics of test swarms, eight honeybee colonies were placed in a row not far from the swarm mount, while a large lucerne field was located on the other side of the minimum path that would lead the swarm to the nest box. As a result, compact and productive navigation of swarms were essentially disrupted whenever they were exposed to a traffic area of fast moving bees headed in a wrong direction. It revealed that the presence of honeybee foragers (whose mean velocity is in the range of streakers mean speed) confused the transmission of flight information provided by the scout bees and leads to noticeable effects of disrupted guidance, as dispersion of the group and, in most cases, failing to approach the selected nest site.

In this respect, in Section 7.1, we propose an extended version of the model presented in the previous Chapter to describe the dynamics of both the informed and non-informed individuals that collectively fly towards a new nest, and of the group of honeybee foragers who individually move to provide food to their hives. In Section 7.2, we test the above-cited hypotheses on honeybee behaviour by performing proper numerical simulations specifically designed to reproduce the experimental scenarios considered in [71]. The possible coherence between the experimental and the modeling outcomes would reveal which are, according to the proposed model, the most reliable assumptions underlying the swarm dynamics, thereby pointing out the consistency of the proposed approach. Finally, some conclusive considerations are reported in Section 7.3.

7.1 Modeling details

Bee characteristics. The dynamics of the migrating swarm and of the group of fast-moving foraging bees is here described in the overall plane $\Omega = \mathbb{R}^2$. The nest site selected by scout bees, i.e., the target of the migrating colony, is represented by a dimensionless point $\mathbf{x}_{\text{nest}} \in \mathbb{R}^2$. Moreover, we denote by $\mathbf{x}_h^{\text{hive}} \in \mathbb{R}^2$, with $h = 1, \ldots, 8$, and $\Omega^{\text{food}} \subset \mathbb{R}^2$, the centers of the eight hives and the food source, respectively, that have been used by T. Latty and coworkers to produce the highway of fast flying bees.

In order to model both the migrating swarm and the bee foragers involved in the experiments described in [71], the set of possible values of the status variable s_i is defined as

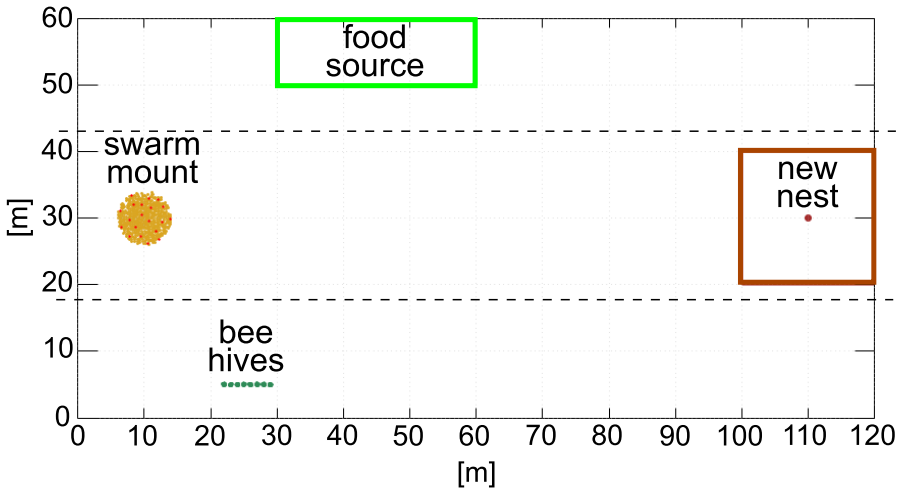

Figure 7.1 Representative initial condition reproducing the experimental setting. Yellow and red dots respectively denote the uninformed individuals and the scout bees with a streaker role. Dashed lines define the domain portion represented in Figure 7.4.

follows

$$s_i(t) = \begin{cases} \text{'U'}, & \text{if } i \text{ is a uninformed bee;} \\ \text{'S'}, & \text{if } i \text{ is a scout with a streaker role;} \\ \text{'P'}, & \text{if } i \text{ is a scout with a passive role;} \\ \text{'F'}, & \text{if } i \text{ is a bee forager,} \end{cases} \tag{7.1}$$

where the first three values characterize the individuals constituting the migrating colony (according to the modeling description presented in Chapter 6), and the last one denotes honeybee foragers. Like the uninformed bees, also the foraging individuals never change their role. In fact, according to the biological observations in [71, 87], bee foragers do not join the migrating swarms. The streaker-passive leader status transition as well as the introduction of the gazing direction, and, consequentially, the definition of the individual perception region Ω^{vis} are kept the same as in the previous Chapter. Further, we remark that the distance function $l_{\text{nest}}(\mathbf{x}) : \Omega \to \mathbb{R}_+ \cup \{0\}$ involved in the latter modeling description here reduces to the Euclidean distance from the nest, being the domain Ω coincident with the two-dimensional space $\mathbb{R}^2$, i.e. $l_{\text{nest}}(\mathbf{x}) = |\mathbf{x} - \mathbf{x}_{\text{nest}}|$, for all $\mathbf{x} \in \mathbb{R}^2$. In this respect, the conditions regulating the scout status transitions read as follows. A streaker bee maintains its status until it reaches the leading edge of the swarm, then as soon as its position satisfies

the condition

$$|\mathbf{x}_i(t) - \mathbf{x}_{\text{nest}}| < \min_{\substack{k \neq i \,:\, s_k(t) \neq \text{F} \\ \mathbf{x}_k(t) \in \Omega_i^{\text{vis}}(t)}} |\mathbf{x}_k(t) - \mathbf{x}_{\text{nest}}|, \tag{7.2}$$

it becomes a passive leader. On the other hand, when a passive leader approaches the trailing edge of the bee cloud, i.e., in mathematical terms

$$|\mathbf{x}_i(t) - \mathbf{x}_{\text{nest}}| > \max_{\substack{k \neq i \,:\, s_k(t) \neq \text{F} \\ \mathbf{x}_k(t) \in \Omega_i^{\text{vis}}(t)}} |\mathbf{x}_k(t) - \mathbf{x}_{\text{nest}}|, \tag{7.3}$$

it turns again to have a streaker role.

Bee dynamics. In order to reproduce the biological experiment by Latty and coworkers, we add here the conflicting directional information provided by the fast traffic line of forager bees to the mathematical framework proposed in the previous Chapter. Referring again to the system of ODEs (4.4), the velocity of each individual is defined by the superposition of the following velocity contributions

$$\begin{aligned}
\mathbf{v}_i(t) &= \mathbf{v}_i^{\text{rep}}(t) + \mathbf{v}_i^{\text{attr}}(t) + \mathbf{v}_i^{\text{rand}}(t) + \underline{\mathbf{v}_i^{\text{align}}(t)}, \;\; \text{if } i : s_i(t) = \text{U}; \\
\mathbf{v}_i(t) &= \mathbf{v}_i^{\text{rep}}(t) + \mathbf{v}_i^{\text{attr}}(t) + \mathbf{v}_i^{\text{rand}}(t) + \underline{\mathbf{v}_i^{\text{streak}}(t)}, \;\; \text{if } i : s_i(t) = \text{S}; \\
\mathbf{v}_i(t) &= \mathbf{v}_i^{\text{rep}}(t) + \mathbf{v}_i^{\text{attr}}(t) + \mathbf{v}_i^{\text{rand}}(t) + \underline{\mathbf{v}_i^{\text{passive}}(t)}, \;\; \text{if } i : s_i(t) = \text{P}; \\
\mathbf{v}_i(t) &= \mathbf{v}_i^{\text{rep}}(t) + \mathbf{v}_i^{\text{attr}}(t) + \mathbf{v}_i^{\text{rand}}(t) + \underline{\mathbf{v}_i^{\text{forager}}(t)}, \;\; \text{if } i : s_i(t) = \text{F}.
\end{aligned} \tag{7.4}$$

Equations $(7.4)_1$, $(7.4)_2$ and $(7.4)_3$ describe the dynamics characteristic of the swarming honeybees: we find the same contributions in Eq. (6.6). However, here we neglect the repulsion from the domain boundary since, according to the experimental setting, we reproduce the empirical tests in the open-space $\mathbb{R}^2$.

The interaction velocity contributions $\mathbf{v}_i^{\text{rep}}$ and $\mathbf{v}_i^{\text{attr}}$ are left unaltered from Section 6.1. The impact of the random velocity term $\mathbf{v}_i^{\text{rand}}$ is here specified according to the speed of each population subgroup. This choice finds its reason in the fact that here, in accordance to the experimental measurement in [71], we set different values for $v_{\max}$ depending on the individual status variable, i.e., in particular $v_{\max}^U = v_{\max}^P < v_{\max}^S = v_{\max}^F$. Specifically, the modulus and the direction of this velocity component are here assumed to be random variables which uniformly vary within the ranges of values $[0, v_{\max}^{s_i(t)}/10]$ and $[0, 360^\circ)$, respectively.

In order to complete the description of the model, we now discuss the last velocity terms, identifying the individual strategy of each insect involved in the simulated experiment.

The directional velocity component of uninformed individuals $\mathbf{v}_i^{\text{align}}$ is left unchanged with respect to Eq. (6.11). Specifically, accounting for the empirical suggestions and the numerical results reported in Chapter 6 and reference therein, we consider two possible definitions of the alignment set of a given uninformed individual:

HP N1 - the i-th uninformed bee aligns its flight to all insects falling within a given neighbourhood, regardless of their status, i.e.,

$$\mathcal{N}_i^{\text{align}}(t) = \{j \neq i \,:\, \mathbf{x}_j(t) \in \Omega_i^{\text{vis}}, 0 < |\mathbf{r}_{ij}(t)| \leq d_{\text{align}}\}; \tag{7.5}$$

HP N2 - the i-th uninformed bee synchronises its flight to all surrounding individuals that fall within a given region, except passive leaders, i.e.,

$$\mathcal{N}_i^{\text{align}}(t) = \{j \neq i \,:\, \mathbf{x}_j(t) \in \Omega_i^{\text{vis}}, 0 < |\mathbf{r}_{ij}(t)| \leq d_{\text{align}}, s_j(t) \in \{\text{U,S,F}\}\}, \tag{7.6}$$

being $\mathbf{r}_{ij}(t) := \mathbf{x}_j(t) - \mathbf{x}_i(t)$ and d_{align} the depth of the alignment region. In this respect, comparing (7.5) and (7.6) to (6.15) and (6.16), we observe that the alignment assumptions N1 and N2 coincide with A3 and A4 in the previous chapter except for the fact that here both the alignment hypotheses N1 and N2 involve the forager bees.

The characteristic dynamics of the informed individuals as well as the behavioral assumptions on the passive leader movement is here maintained the same as those in Chapter 6, see Eq. (6.17), (6.18) and (6.19). In this respect, the latter can be simply formulated in terms of the Euclidean distance instead of the distance funcion l_{nest}, as already commented in the text. Specifically, scout bees with a streaker role are assumed to fly at high speed pointing towards the target nest, i.e., in mathematical terms it reads as

$$\mathbf{v}_i^{\text{streak}}(t) = v_{\max}^S \frac{\mathbf{x}_{\text{nest}} - \mathbf{x}_i(t)}{|\mathbf{x}_{\text{nest}} - \mathbf{x}_i(t)|}. \tag{7.7}$$

On the other hand, for the passive leaders, we consider the two possible behaviours proposed by T.D. Seeley in [87].

HP L1 - Passive leaders slowly fly back towards the rear edge of the swarm, in order to slightly influence the movement of the uninformed swarming bees. In this respect,

for the i-th passive leader bee, we define

$$\mathbf{v}_i^{\text{passive}}(t) = v_{\max}^P \frac{\dfrac{\mathbf{x}_{\bar{k}}(t)-\mathbf{x}_i(t)}{|\mathbf{x}_{\bar{k}}(t)-\mathbf{x}_i(t)|} - \dfrac{\mathbf{x}_{\text{nest}}(t)-\mathbf{x}_i(t)}{|\mathbf{x}_{\text{nest}}(t)-\mathbf{x}_i(t)|}}{\left|\dfrac{\mathbf{x}_{\bar{k}}(t)-\mathbf{x}_i(t)}{|\mathbf{x}_{\bar{k}}(t)-\mathbf{x}_i(t)|} - \dfrac{\mathbf{x}_{\text{nest}}(t)-\mathbf{x}_i(t)}{|\mathbf{x}_{\text{nest}}(t)-\mathbf{x}_i(t)|}\right|}, \tag{7.8}$$

where $\bar{k}$ denotes the uninformed insect farthest from the new nest according to the following relation

$$|\mathbf{x}_{\text{nest}} - \mathbf{x}_{\bar{k}}(t)| = \max_{\substack{k:s_k(t)=\text{U} \\ \mathbf{x}_k(t)\in\Omega_i^{\text{vis}}(t)}} |\mathbf{x}_{\text{nest}} - \mathbf{x}_k(t)|. \tag{7.9}$$

HP L2 - Passive leaders stop and wait to be passed by the rest of the groupmates. For the i-th passive leader, we indeed set

$$\mathbf{v}_i^{\text{passive}}(t) = \mathbf{0}. \tag{7.10}$$

Finally, bee foragers individually move back and forth between their original hive and a food source. In particular, it has been experimentally observed that bees pointing to a desirable source of food fly at a speed comparable to that of the fast-flying streakers, so we can assume $v_{\max}^F = v_{\max}^S$. We then state that, at regularly spaced instant times, a bee forager i leaves a randomly selected hive, identified by the number $h_i \in \{1,\dots,8\}$, and begins to fly fast towards a point in the lucerne field, said $\mathbf{x}_i^{\text{food}} \in \Omega^{\text{food}}$, which is randomly selected as well. Once reached the food source, foragers change their desired travel direction to come back home. In this respect, given the initial condition $\mathbf{x}_i(0) = \mathbf{x}_{h_i}^{\text{hive}}$, $s_i = \text{F}$, the velocity contribution $\mathbf{v}_i^{\text{forager}}$ is given in mathematical terms by

$$\mathbf{v}_i^{\text{forager}}(t) = \begin{cases} v_{\max}^F \dfrac{\mathbf{x}_i^{\text{food}}-\mathbf{x}_i(t)}{|\mathbf{x}_i^{\text{food}}-\mathbf{x}_i(t)|}, & 0 \le t \le \tilde{t} \\ \\ v_{\max}^F \dfrac{\mathbf{x}_{h_i}^{\text{hive}}-\mathbf{x}_i(t)}{|\mathbf{x}_{h_i}^{\text{hive}}-\mathbf{x}_i(t)|}, & \tilde{t} < t \le \bar{T}, \end{cases} \tag{7.11}$$

where $\mathbf{x}_{h_i}^{\text{hive}}$ is the hive from which bee i flies away. Further, $\tilde{t}$ and $\bar{T}$ respectively are the time instants when the bee i reaches the food field, i.e. $\mathbf{x}_i(\tilde{t}) = \mathbf{x}_i^{\text{food}}$, and the bee i gets back home, i.e. $\mathbf{x}_i(\bar{T}) = \mathbf{x}_{h_i}^{\text{hive}}$. The frequency of the foragers' liftoff is set according to the experimental amount of bee traffic n_F recorded in [71], i.e., the number of bees leaving the

hives over 1 min. Finally, it is worth to stress that we neglect the dynamics of bee foragers within the hives, since it does not affect the behaviour of the migrating swarm.

7.2 Numerical results

The aim of the simulations proposed in this Section is to point out the sets of assumptions relative to the behaviour of the passive leaders and the alignment mechanism of the uninformed bees that are able to reproduce the empirical results presented by T. Latty and coworkers in [71]. In this perspective, we design two simulation settings that reproduce the dynamics either of "control swarms", which fly towards a target nest in the absence of other bees, or of "test swarms" exposed to a flux of fast-moving bees. In both scenarios, we will test the three different combinations of the proposed hypotheses (N1, L1), (N1, L2), and (N2, L2). As a remark, we here discard the set of assumptions (N2, L1), since proper numerical results presented in Section 6.3 of the previous Chapter demonstrated that it is not able to reproduce the coordinated and productive migration of a swarm even in the absence of other bees.

Simulation details. In all simulations, we consider a migrating colony of 500 individuals. As commented above, we are indeed dealing with a planar section of the larger control/test swarm. The initial swarm configuration is left unchanged from Chapter 6. Specifically, as shown in Figure 7.1, these bees are initially randomly distributed within a round area of radius 4 m centered at $(10\text{ m}, 30\text{ m})$, leading to a realistic density of about 8 bees/m^2 [87]. The initial gazing direction $\mathbf{g}_i(0)$ of each individual is randomly generated. In agreement with the experimental literature [90], we assume that 4% of the migrating individuals are informed of the location of the new nest, while the remaining 480 bees are uninformed. In particular, all scouts initially have a streaker role, i.e., $s_i(0) = S$, then they are able to undergo status transitions according to the evolution of the system, as defined in Equations (7.2)-(7.3). We here recall that uninformed bees are conversely not able to change status. The nestbox constituting the target of the migrating colony is located 100 m far from the initial position of the swarm, i.e., at $\mathbf{x}_{\text{nest}} = (110\text{ m}, 30\text{ m})$. The eight hives from where bee foragers start flying to provide food for their colony, are respectively located at $\mathbf{x}_1^{\text{hive}} = (22\text{ m}, 5\text{ m})$, $\mathbf{x}_2^{\text{hive}} = (22.5\text{ m}, 5\text{ m})$, $\mathbf{x}_3^{\text{hive}} = (23\text{ m}, 5\text{ m})$, $\mathbf{x}_4^{\text{hive}} = (23.5\text{ m}, 5\text{ m})$, $\mathbf{x}_5^{\text{hive}} = (24\text{ m}, 5\text{ m})$, $\mathbf{x}_6^{\text{hive}} = (24.5\text{ m}, 5\text{ m})$, $\mathbf{x}_7^{\text{hive}} = (25\text{ m}, 5\text{ m})$ and $\mathbf{x}_8^{\text{hive}} = (25.5\text{ m}, 5\text{ m})$, according to the experimental scenario. Finally, the food source is represented by the rectangle area $\Omega^{\text{food}} = [30, 60] \times [50, 60]\text{ m}^2$. According to

the experimental scenario, the hives and the food site are located on the opposite sides of the straight path connecting the initial position of the swarm and the nest site, see again Figure 7.1.

Table 7.1 Model parameters.

Par.	**Description**	**Value [Unit]**	**Reference**
θ_{vis}	half visual angle	156.5 [deg]	[91]
d_{vis}	depth of visual field	20 [m]	biological data
v_{mean}	mean velocity of uninf. bees	3 [m/s]	[71]
v^U_{max}	maximal speed of uninformed bees	3 [m/s]	[71]
v^S_{max}	maximal speed of streakers	9.4 [m/s]	[6, 71, 87]
v^P_{max}	maximal speed of passive scouts	3 [m/s]	[85, 87]
v^F_{max}	maximal speed of foragers	9.4 [m/s]	[71]
n_F	bee traffic	$25-85$ [bees/min]	[71]
d_{rep}	extension of the avoidance region	0.3 [m]	[87]
d_{align}	extension of the alignment region	2 [m]	[27, 28]
d_{attr}	extension of the attraction region	20 [m]	biological data
f_{rep}	avoidance coefficient	1 [m^2/s]	see Ch. 6
f_{attr}	attraction coefficient	10^{-6} [m/s]	see Ch. 6

The entire model parameter setting used in all numerical simulations is summarized in Table 7.1. These values have been set by taking advantage of the empirical measurements reported in the literature of the field and of the parameter estimation performed in Section 6.2 of the previous Chapter. The bee visual region already introduced in Equation (6.4) is characterized by setting the half visual angle $\theta_{\text{vis}} = 156.5^\circ$ and the visual depth $d_{\text{vis}} = 20$ m. The former is a measure provided in [91]. The latter estimate allows each insect to potentially see all groupmates (provided that the swarm is not completely dispersed) and it is small enough to avoid that the target destination initially falls within the visual field of uninformed individuals. The maximal flight speeds introduced in Equation (4.4) are estimated according to the empirical measurements reported in [71] and reference therein. Specifically, the flight of uninformed individuals in the swarm do not exceed $v^U_{\text{max}} = 3$ m/s [71], while scouts in the streaker role are able to fly up to $v^S_{\text{max}} = 9.4$ m/s [6, 71, 87]. The maximal speed of passive leaders is assumed to be equal to that of uninformed individuals, i.e., $v^P_{\text{max}} = v^U_{\text{max}}$, according to the biological hypothesis that scouts in a passive role become almost invisible to the followers, see [85, 87]. As a remark, the measurements performed in [71] allow us to estimate the maximal speed of honeybee foragers equal to that of scouts in the streaker role, i.e., $v^F_{\text{max}} = v^S_{\text{max}} = 9.4$ m/s. Plausible values for the outbound bee

traffic n_F fall in the range $[25, 85]$ bees/min, so that the resulting ratio between the number of scouts and n_F is consistent with the quantities recorded in [71].

The model parameters that characterize honeybee mutual interactions (affecting all individuals regardless their status) and the alignment mechanism (regulating the behaviour of uniformed insects only) are set exactly as in Chapter 6. Specifically, the minimal comfort distance between individuals d_{rep} is fixed at 0.3 m, according to the measurements reported in [87]. The extension of the alignment region d_{align} is assumed to be equal to 2 m, accounting for the values of the ratio $d_{\text{rep}}/d_{\text{align}}$ tested by Couzin and colleagues in [28, 27]. We further set $d_{\text{attr}} = d_{\text{vis}}$, assuming that each bee tends to maintain a minimal connection with any other individual it sees. The technical coefficients f_{rep} and f_{attr} are finally settled at 1 m^2/s and 10^{-6} m/s, respectively, following the parametric estimation proposed in Chapter 6. In particular, in Section 6.2, we ran a series of numerical realizations looking for pairs of parameters that (i) result in a crystalline equilibrium configuration of the swarm without superposition of individuals, when the evolution of the system is regulated by attractive/repulsive stimuli only; and (ii) allow the specific flight of scouts through the swarm under either hypotheses L1 and L2, when the evolution is regulated by the complete dynamics. On one hand, the numerical results reported in Section 6.2 show that requirement (i) is satisfied if the parametric relation $f_{\text{rep}}/f_{\text{attr}} \geq 10^6$ holds. To account for requirement (ii), we have to verify that the interaction parameter values used in Chapter 6 are still admissible even though we here opt for a different value of v_{mean} and of the maximal speed of uniformed bees. In fact, in order to mathematically reproduce the experiments performed by T. Latty and coworkers, we here set v_{mean} and v_{max}^U rispectively equal to the empirically estimated value reported in [71], i.e., both equal to 3 m/s, rather than $v_{\text{mean}} = 6.7$ m/s and $v_{\text{max}}^U = 9.4$ m/s as in Chapter 6. In this respect, we analyze the motion of the scout bees through the cloud of uninformed individuals by running two series of computational tests involving a modified control swarm whose dynamics is regulated only by the repulsive/attractive interactions and the characteristic motion of scouts, L1 and L2, respectively. Specifically, with respect to the complete model in Equations (4.4)-(7.4), we neglect the alignment mechanisms and the random contributions. Figure 7.2 shows the trajectories of a representative informed bee observed in the two cases: under hypothesis L1 (left panel), the informed bee is actually able to streak and fly back repeatedly through the swarm; under hypothesis L2 (right panel), once the scout bee reaches the leading edge of the swarm, it stops waiting the passage of the rest of the colony. However, the cloud of uninformed individuals (and, in turn, the entire swarm) substantially maintains its initial position due to the absence of the alignment process. These numerical results clearly

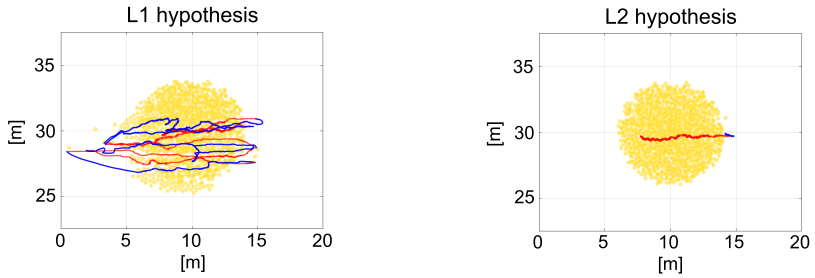

Figure 7.2 Trajectory of a representative bee scout upon either the back-and-forth hypotheses L1 (left panel) and the go-and-stop hypotheses L2 (right panel). The trajectory is red when the scout has a streaker role, and it is blue when it has a passive role. The yellow shadow represents the entire bee cloud.

demonstrate that the proposed variation in the model parameters do not disrupt the specific behaviour of informed bees, i.e., the proposed set of parameters satisfies requirement (ii) too.

Control and test swarms. We then turn to test the considered combinations of alternative hypotheses on the behaviour of leader scouts and on the alignment mechanism of uninformed bees, i.e., (N1, L1), (N1, L2), and (N2, L2), looking for those able to reproduce the dynamics of both the control swarms and the test swarms described in [71]. By considering the complete model defined in Equations (4.4)-(7.4), we run six series of simulations for each couple of assumptions. First, we deal with the *control cases*: by setting $n_F = 0$ bees/min, we show that, in absence of conflicting information, all proposed set of hypotheses reproduce the coordinated and productive flight of honeybees towards their new nest. Then, we look at the evolution of swarms exposed to five different levels of bee traffic (*test cases*): specifically, n_F is respectively set equal to $25; 40; 55; 70; 85$ bees/min.

In order to identify the sets of assumptions able to reproduce the experimental outcomes presented by T. Latty and co-workers, let us recall that in [71] they classify their empirical results accounting for the fraction of the bees belonging to the swarm that actually enters the nestbox. By considering that honeybees begin to coordinate their entrance in the nest at about 10 m from the target [87], we record the number of insects that simultaneously fall within the neighborhood $\Omega^{\text{nest}} := [100, 120] \times [20, 40]$ m^2 around $\mathbf{x}_{\text{nest}}$, see Figure 7.1. The dynamics of the bee population resulting from the considered set of assumptions are then classified according to the following criterion.

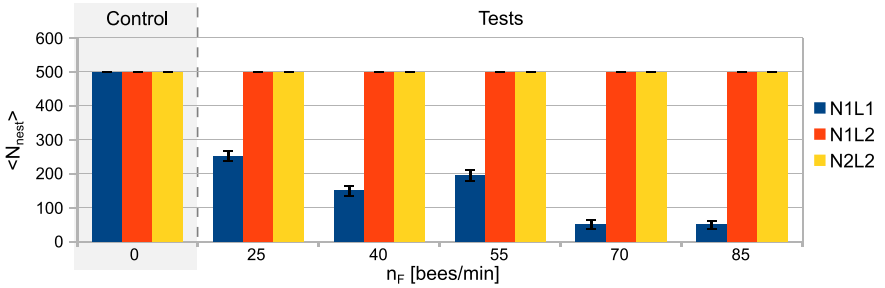

Figure 7.3 Representation of the mean number of bees that reach the nest, i.e., the mean of N_{nest} defined in Equation (7.12), arising from 10 independent numerical realizations for each combination of the bee behavioural assumptions and for each level of the traffic bees n_F. The error bars represent the variance obtained for each case.

Definition 7.2.1. The coordinated and productive flight of a swarm toward the nest is *disrupted* if

$$N_{\text{nest}} = \max_{t\in[0,T]} \left\{ \#\left\{ j \,:\, s_j(t) \neq \text{'F'},\ \mathbf{x}_j(t) \in \Omega^{\text{nest}} \right\} \right\} \leq 450, \tag{7.12}$$

where # denotes the cardinality of a set and T is the period of observation of the realization. Otherwise, the swarm *successfully reaches* the target nest.

All numerical tests are stopped at $T = 1$ min. By noticing that in control cases the simulated swarm need about 35 sec to cover the straight path and reach the nest (see Figure 7.4), it is clear that this choice of T allows to properly classify as *disrupted* the dynamics of swarms that would arrive at the target nest after large deflections from the straight path. Moreover, for each combination of assumptions and for each considered amount of bee traffic (included the control case), we run 10 independent simulations to account for the randomness present both in the initial distribution of the swarm and in honeybee dynamics. The numerical results are then summarized in Figs. 7.3-7.5.

In particular, Figure 7.3 reports the mean value and the relative variance of N_{nest} characterizing each case. These computational outcomes first highlight that all control cases are characterized by $N_{\text{nest}} = 500$ (i.e., $< N_{\text{nest}} >= 500$, with zero variance), thereby pointing out that the considered set of assumptions on bee behaviour equivalently reflect the empirical outcomes obtained by T. Latty and co-workers in the absence of conflicting directional information. In fact, as shown in the representative snapshots in Figure 7.4, in all cases the honeybee swarm remains cohesive during all the dynamics and compactly reach the target nest without large deviations from the straight path. This further confirms that the

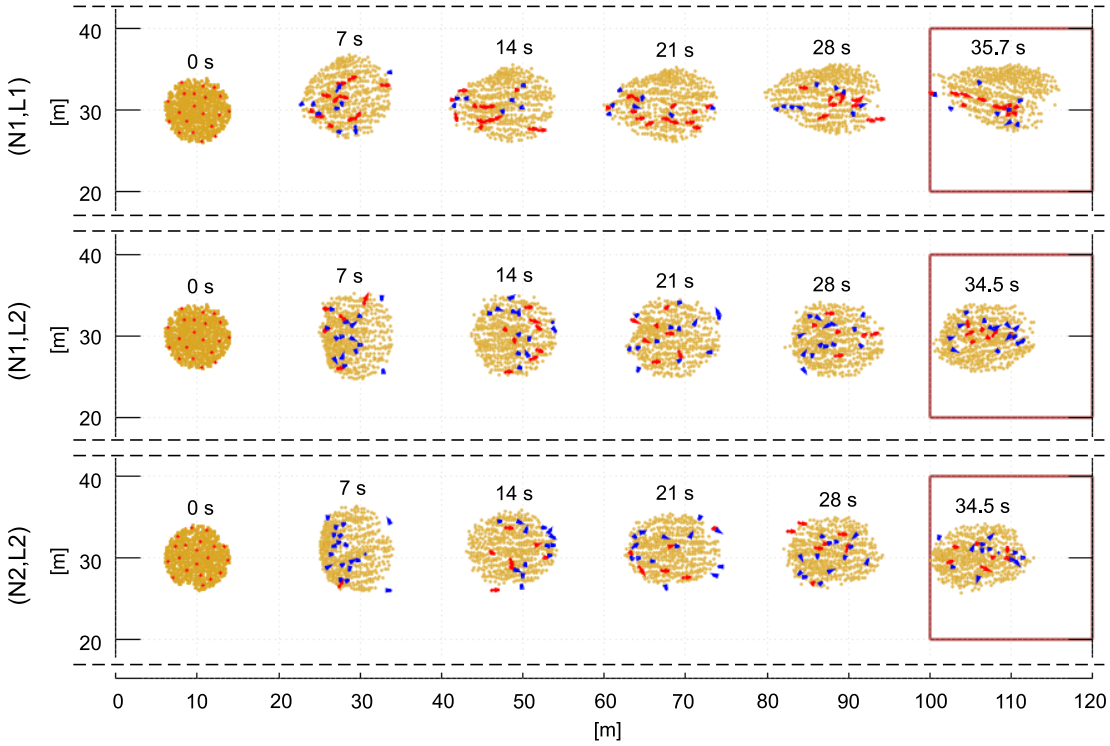

Figure 7.4 Control cases. Representative evolutions of the bee swarms in the absence of fast-moving bee foragers upon the three hypotheses combinations (N1, L1), (N1, L2) and (N2, L2). For each case, we here show only the portion of interest of the entire empirical scenario represented in Figure 7.1. Yellow dots denote uninformed individuals, red dots scout bees with a streaker role, and blue dots passive leaders.

proposed variation in the speed of uninformed bees w.r.t. Chapter 6, does not disrupt the coordinated flight of honeybees, but only gets the swarm migration slightly slower.

Figure 7.3 further highlights that upon the coupled sets of assumptions (N1, L2) and (N2, L2), the swarm productive navigation obtained in test cases is never disrupted by the presence of conflicting directional information. In fact, regardless the level of the traffic bees n_F, the mean number of insects that reach the target upon the coupled set of assumptions (N1, L2) and (N2, L2) is still $< N_{\text{nest}} >= 500$, with zero variance. In other words, the coordinated flight of the bee cloud is not affected by crossing the traffic area of fast moving foraging bees thereby reaching undisturbed the nest, i.e. exactly as in the control cases. This suggests that the presence of passive leaders waiting to be passed by the rest of swarm, i.e. assumption L2, prevents followers from synchronizing their movement to fast moving forager bees and disrupting the coordinated flight of the migrating colony.

However, these *in silico* outcomes do not reflect the experimental findings presented in [71], and therefore lead us to discard both the assumptions (N1, L2) and (N2, L2).

On the contrary, honeybee dynamics obtained under the set of assumptions (N1, L1) are consistent with the empirical outcomes presented in [71], as we have $< N_{\text{nest}} > \ll 450$, with negligible variance, for any tested value of the bee traffic, see again Figure 7.3. In particular, only 24% of the numerical tests we performed under the set of assumptions (N1, L1) results in a coordinated and productive flight of the swarm. This is consistent with the work of T. Latty and coworkers, which observed that only one of their six test swarms (i.e., 16%) reaches the nest. Despite the discrepancy in these values, this is in fact a good starting point with respect to the above discarded set of assumptions.

Furthermore, the swarm dynamics resulting under the coupled assumptions (N1, L1) present clear signs of disturbance of the scout guidance, including splitting, deviated path, and reclustering, in agreement with the experimental outcomes described by T. Latty and coworkers in [71]. In this respect, representative snapshots of three selected *in silico* experiments are provided in Figure 7.5. In the first row of Fig. 7.5, once the swarm has passed the highway of bee foragers, some uninformed individuals at the rear of the migrating group stop following the scouts and separate from the colony. According to hypothesis L1, the scouts begin to follow these confused bees trying to keep compact the swarm but, at the same time, they leave the rest of the uniformed individuals without a guide. These latter then mutually align and wander in a randomly selected direction. In the second row of Figure 7.5, as soon as the swarm bumps into the forager highway, the uniformed bees begin to disperse, clearly confused by the presence of conflicting directional information. In this case, scout bees are able to recluster the colony but not to restore the productive migration of the swarm toward the nest, which therefore undergoes large deviations from the optimal path. Finally, in the bottom row of Figure 7.5, the migrating bee population initially seems to pass safely the traffic area where forager bees go back and forth between their hives and the food source. The effect of the exposition of the swarm to conflicting information in fact arises at about $20-30$ sec with the separation of the uninformed bees from the scouts individuals. However, the scout individuals result able both to regroup the entire colony and to re-establish the swarm guidance conducting all migrating bees to the nestbox. This is actually one of the few realizations in which, as observed in a experimental test in [71], the simulated swarm reaches the nest in spite of the interaction with bee foragers headed in a wrong direction.

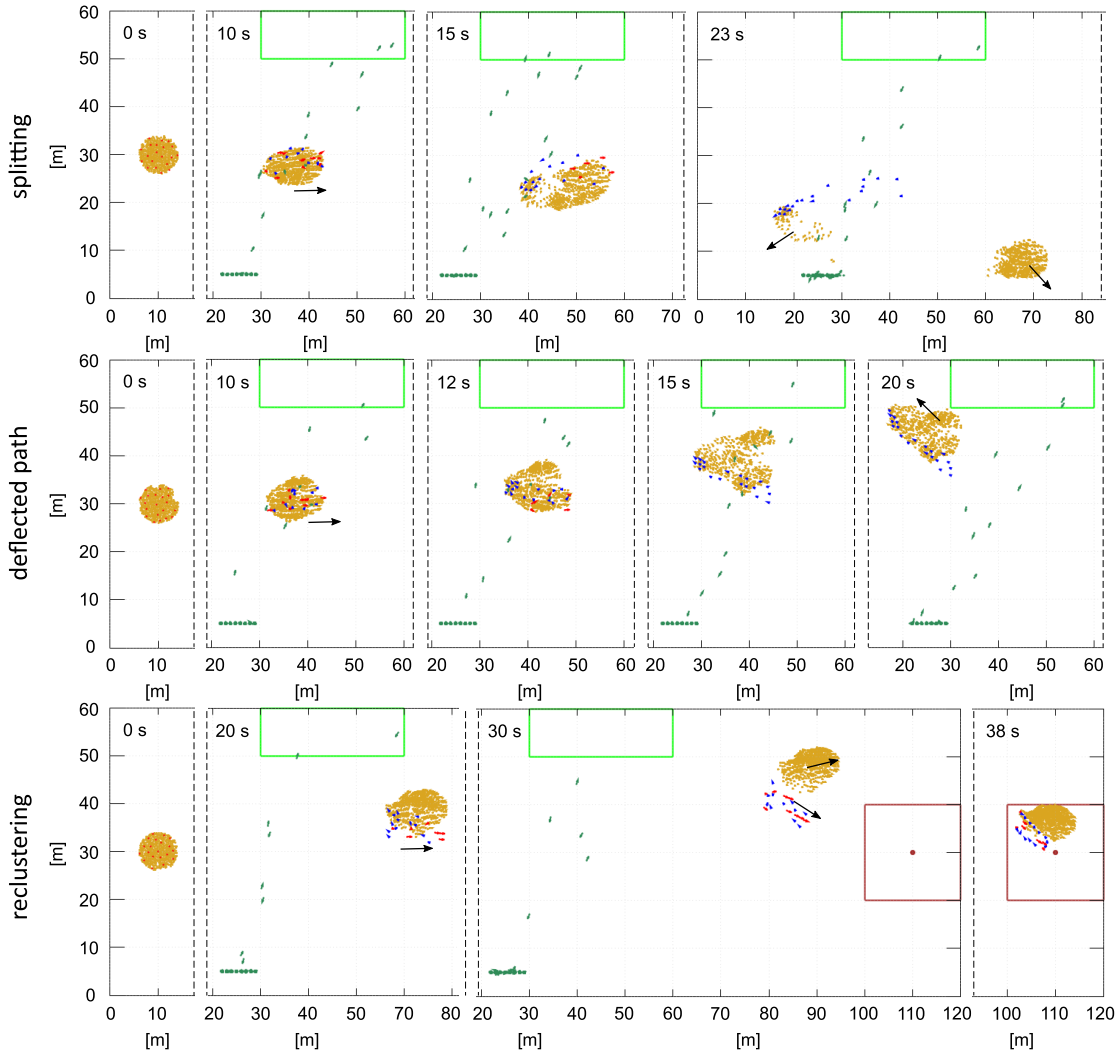

Figure 7.5 Test cases. Representative realizations of the dynamics of a swarm exposed to conflicting flight information, upon the behavioural set of assumptions (N1, L1). Yellow dots denote uninformed individuals, red dots scout bees with a streaker role, blue dots passive leaders, and greed dots forager bees.

7.3 Conclusions

The aim of this Chapter has been to clarify the mechanisms underlying both the swarming process and the effect of conflicting directional information on the honeybee guidance. In this perspective, we have proposed an extended version of the model presented in the previous Chapter to test selected assumptions on bee behaviour, and to find out the rules of motions that reproduce *in silico* the experiments presented by T. Latty and coworkers in [71].

The numerical realizations described in the previous Section have shown that both assumptions (N1, L2) and (N2, L2) are not able to successfully reproduce the experimental findings. In these cases the bee cloud is in fact able to achieve the nest, by substantially moving along the shortest straight path, even if it has to cross the traffic area of the forager bees to reach the target. Conversely, scenarios comparable to the experimental findings have emerged under the coupled hypotheses (N1, L1). In this case, in fact, the introduction of the conflicting directionality of the fast-flying foragers had a strong impact on the coordinated migration of honeybees and resulted in clear signs of disturbance of the scout guidance, including splitting, deviated path, and reclustering. For these reasons, we have been led to discard both the assumptions (N1, L2) and (N2, L2) in favor of (N1, L1). In other words, this study suggested that the leading plausible assumptions behind the swarming process, according to the proposed model, are the following: the uninformed bees could acquire the travel route synchronising their movement to all the insects sufficiently close to their position regardless of their status, provided that the passive leaders slowly come back from the front to the rear edge of the bee cloud.

In more details, under the behavioural assumptions (N1, L1) none of the simulated swarms presenting signs of disrupted guidance, steered in direction of the lucerne field, nor towards the eight colonies, but they rather seemed to randomly redirect their flight consistently with empirical evidences. This effect could be attributed to the fact that the foragers alternatively moves back and forth, i.e., the bee highway does not include one single preferential movement direction, but two opposite ones (i.e., from the colonies to the field and viceversa). Therefore, it could be interesting to investigate in future works the effect of a one-directional traffic flow on a flying swarm and, in this respect, to address new sets of simulations to the question of how many misleading bees are necessary to completely redirecting the swarm towards a different direction.

In literature, several studies have analysed the mechanisms underlying the decision-making process in presence of multiple conflicting movement information within groups of both humans and animals, see, for instance, [27, 42, 100]. These studies highlight that individuals generally tend to collectively select the direction adopted by the majority of the informed individuals, thus following the largest group. Furthermore, the quorum rule allows the naive individuals to neglect potentially incorrect information. Conversely, in the experiments by T. Latty and coworkers, as well as in the model outcomes so far presented, a small fraction of forager bees has caused the disruption of the swarm flight. Honeybee swarms therefore appear more sensitive to conflicting information with respect to the other groups studied in literature. As suggested in [71], this observation could be related to the specific nature of the misleading information. In fact, in this experimental scenario the disturbing traffic line of the foragers represent an external source of flight information for the swarming bees while both in [27] and [42] divergent directional information compete within the same group. Furthermore, we remark that the specific streaker guidance mechanism itself could provide a minimum conflicting information when the leaders come back to the rear edge of the swarm in order to streak again. These considerations could explain the strong effect of the foraging bees on the swarming process.

Chapter 8

Future developments of the proposed approach

The proposed model has investigated and tested different social behaviors underlying the collective dynamics of a bee swarm. However, our approach can be improved in several directions. First, it would be useful to have a better comparison with experimental data. This would improve the quality of the work from two points of view: it could be possible to derive a more precise parameter estimate and we could have a quantitative validation of the predictive theoretical results.

Further, a three-dimensional extension of the computational setting would be a natural development. In fact, it would allow to better describe the dynamics of the informed bees which, when passive leaders, are also supposed to hide themselves along the top or the bottom region of the swarm in order to not significantly affect the flight of the groupmates, as hypothesized in the empirical literature [85, 87].

Another model improvement can be represented by the inclusion of a proper evolution equation for the gazing direction, i.e., indeed considered a further degree of freedom. For instance, it could take into account the head rotation of each insect with respect to its direction of motion, due for example to environmental stimuli (e.g., sounds or light signals) and/or due to unconscious fluctuations.

Finally, from a purely speculative point of view, our approach can be extended to larger swarms, formed by thousands of individuals. In this respect, it would be interesting to test if the results obtained by varying the alignment mechanisms (and the relative parameters), as well as the leader movement rules, would apply also in the case of significantly increased

numbers of bees. It is useful to remark, however, that the proportion between informed/non-informed individuals set in the models proposed in this Thesis (i.e., 1/99 in Chapter 5 and 20/500 in Chapters 6 and 7) is in the range of values empirically measured (i.e., 300 to 400 leaders in a swarm of 10000 insects [87]). Obviously, a model extension involving a huge number of particles would cause computational issues, i.e., mainly related to the optimization of computing time. In this respect, a possible solution is represented by the use of serial and parallel computing. High performance serial computing can be achieved by using the same programming techniques employed in particle fluid-dynamic simulations. Otherwise, parallel computing is possible, for example, using Message Passing paradigm (MPI) or shared memory parallelization. In the first case, the computational domain would be divided in subdomains that in turn would be assigned to a single processor. At each time step, each processor should communicate the bees who leave its portion of domain and enter the sub-domain of a neighboring node. In case of a shared memory parallelization (e.g., on GPU devices), the computational domain and the data structure storing population data would be shared among different threads, each of them updating the state of a sub-set of individuals.

Chapter 9

A scan of the theoretical literature on bee swarming dynamics

As explained in the Abstract and Chapter 2, the models presented in this Thesis belong to the class of microscopic/discrete approaches dealing with collective dynamics of animal populations. Of this group of methods, some are devoted to reproduce selected features of bee swarming. It is indeed important to discuss their differences and similarities with respect to our approach.

We first remark that most of the discrete models presented in the literature are based on the already-introduced set of first principle of swarming [18], accounting for attraction/cohesion, avoidance, and flight alignment.

Entering in more details, in [44], Fetecau and Guo implement a second-order model, where attraction and repulsion stimuli are described by a Morse potential, whereas the alignment process of a given bee involves its two-fold faster neighbors (with an effect that decreases with the mutual distance between the pair of interacting insects, according to a quite complex, hyperbolic tangent-based, rule). Bee dynamics also account for a random component, which is active only when the interaction of an individual with the rest of the swam is low enough. The authors introduce a visual field for each bee, given by a planar sector which is constantly aligned to the direction of motion and formed by two regions: a central cone where the other individuals are set to be directly seen, and therefore assigned a unit weight, and a peripheral area where the other individuals are set to be partially seen, and therefore assigned a lower weight. In our model, a peripheral vision is not considered, since it is known from biology that the compound eyes of bees cover most of the front and

of the sides of their head, assuring an almost homogeneous vision. Fetecau and Guo finally differentiate a subpopulation of leader bees, that do not interact with their groupmates and are assigned an oscillatory motion. They in fact move faster towards the target destination according to two alternative hypothesis: (i) they streak with a constant acceleration or (ii) they fly with a constant speed. In both cases, when such informed individuals reach the leading edge of the cloud, they come back to the rear of the population being substantially invisible to the follower agents. The model by Fetecau and Guo is therefore based on behavioral rules similar to the pairs (A1, L1) and (A2, L1) employed in our Chapter 6. Interestingly, in both works, such hypotheses result in a directionally efficient swarming: however, we have discarded the two combinations of assumptions as a consequence of the lack of a consistent compactness of the insect cloud.

Attraction, repulsion, and alignment are also at the basis of the first order model presented in [58]. Entering in more details, the cohesion velocity contribution is modeled as a vector pointing from the position of the generic bee to the center of mass of the set of neighboring insects which fall within its visual distance. In this respect, we have here preferred to implement pairwise interaction kernels, since it is difficult to establish whether a bee exactly knows the position of the barycenter of the rest of the groupmates. The alignment rule employed by [58] instead relies on an Euclidean metric-based assumption, namely each bee is set to synchronize its movement with all the seen groupmates (regardless of their speed). This is quite similar to the assumption tested in Section 5.2.1 of Chapter 5, even if in our case the region of attraction and alignment do not coincide. As in the case of the work by Fetecau and Guo, also in [58], a set of leader bees is defined and assigned a back-and-forward motion within the swarm, in order to diffuse the information on the correct flight direction to the overall population.

In [39], the authors describe both the decision-making process used by the house-hunting honeybees to find a new nest site and their guidance role within the rest of the swarm. Focusing on the latter, we can notice that Diwold and colleagues employ a cohesion term that makes each bee attracted by the barycenter of a set of fast enough individuals, which are also involved in a topological metric-based alignment mechanism. Such an assumption on flight synchronization is similar to the hypothesis tested in Section 5.2.2 of Chapter 5, although we have there implemented different interaction velocity components. The resulting model is then applied to compare the swarming of two different species of honeybees, namely *Apis Mellifera* and *Apis Florea*. In particular, *A. Mellifera* is a cavity-nesting species whereas *A. Florea* is an open-nesting one. This means that the *Apis Mellifera* has to find a roomy and comfortable homesite, protected from cold winds

and from predators. Conversely, *A. Florea* usually nests on a shaded branch, having less constraints in finding a suitable location.

A more general (i.e., not strictly related to bee dynamics) model is proposed in [27]. The authors here focus on two aspects: how information is transferred within groups of animals and how they can find an agreement when informed individuals suggest different moving directions to rest of the population. Such an approach still relies on the classical social principle of attraction/repulsion and alignment. As previously commented, one of their main results deals with the relationships between the percentage of informed individuals and the flight efficacy of population of different sizes. The same research group also proposes a model that focuses on the pattern characteristic of animal groups, [28]. In particular, their approach includes a Morse potential and two additional terms: accounting for self-propulsion and friction. The balance between the different contributions establishes the capability of the system to reach an asymptotic collective speed.

The dichotomy between topological vs. Euclidean metric-based interactions between animals belonging to the same population, which has been here addressed in Chapter 5, is the topic of a very interesting article by Ballerini and coworkers, who deal with flocking events of *European Starling* swarms under external perturbations (e.g., predator attacks) [3]. More specifically, these authors experimentally demonstrate, by an analysis of a large amount of photographic data, that each individual interacts with a fixed number of groupmates (6-7) and not with all neighbors falling within a given region. In other words, the collective and coordinated migration of bird colonies is the result of topological interactions, as also confirmed by the computational results proposed in the same work, which are obtained with an agent-based model. The observations by Ballerini and colleagues well fit with the arguments proposed in Chapter 5. In this respect, it would be interesting to perform their empirical study in the case of bee colonies, in order to point out if topological arguments are involved in bee swarming as well. In particular, it would be relevant (but very difficult) to address two points: (i) if topological-based interactions underly only attractive/repulsive insect behavior or also flight synchronization mechanisms and (ii) if external conditions and/or the objective of migration affect the type of interindividual interactions (e.g., a predator attack may stimulate topological metric-based interactions, whereas exploring or feeding tasks may require Euclidean metric-based interactions).

By reviewing the different works commented so far, we can conclude that the main features of a swarming phenomenology can be captured by minimal, i.e., two- or three-component, models. In fact, reasonable configurations of swarms (where the agents

stabilize at given and finite mutual distances) can be obtained only by taking into account repulsive/attractive pairwise dynamics. The inclusion of alignment mechanisms is instead needed to get effective directional flights. Such simple approaches have also the advantage of being suitable for interesting analytical analysis and insights, e.g., on the properties of the steady states of the system as done by different groups [16, 17, 45].

The addition of more sophisticated model ingredients, i.e., bee status differentiations and relative transitions and flight rules, is therefore not essential to reproduce basic collective dynamics of insect swarms. However, such model components have been here introduced in order to be as close as possible to experimental evidences and to find out reasonable assumptions at the basis of the still unknown bee swarming behavior, i.e., to give our theoretical approach an *experimentally predictive value*.

Part II

A particle-based model analyzing collective dynamics in both homogeneous and heterogeneous animal groups

Chapter 10

Introduction

In the Second Part of the Thesis we propose a slightly different *particle-based* approach able to describe the collective dynamics of a generic group of animals, i.e. not necessarily bees. As a relevant feature, this approach distinguishes between individual speed and direction of motion. The former is in fact typically established by the purpose of the movement and/or by physiological limitations, the latter results instead from the competition between different behavioral stimuli, mainly coming from the environment (e.g., attraction, repulsion and velocity alignment). In particular, each of these inputs is here simply defined by an orientation and a weight, which is correlated to an individual preference. A constraint on the sum of the weights is finally given to avoid simultaneous minimization/maximization of all individual behavioral traits. The description of animal dynamics therefore does not necessarily require the introduction of complex algorithmic rules or artificial laws of motion. The proposed mathematical framework has the clear advantage to be based on a minimal set of parameters (i.e., one per directional contribution), which first allows to avoid computationally expensive sensitivity analysis. The interpretation of the results is substantially facilitated as well, thanks to the fact that the few model coefficients have a direct empirical meaning. In this respect, the description of animal dynamics does not necessarily require the introduction of artificial laws or functions (such as adhesion/repulsion kernels), that usually, e.g. as in the models presented in Part I, involve strictly technical parameters.

The rest of this Part is organized as follows. Chapter 11 shows that our model is able to reproduce and classify collective movement and patterning of an animal population emerging from different individual behavioral preferences. It is then enriched to include

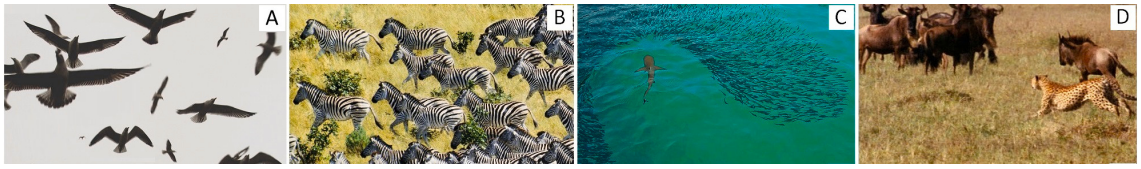

Figure 10.1 Different collective dynamics of animal populations. (A) A small swarm of seagulls undergoes chaotic group flight. (B) A large zebra herd coordinately migrates, as all component individuals have a common direction of movement. (C) A school of fish is dispersed by a shark, with the consequent formation of empty space around the predator. (D) A group of bison individually runs away from an attacking cheetah. All the images are courtesy of the Department of Life Sciences and Systems Biology, Universita' degli Studi di Torino (Italy), and have been modified by the authors of this paper.

more sophisticated scenarios and situations, such as the presence of a predator which impacts on group dynamics. It also includes a coupled analytical/numerical study of the equilibrium configurations of our animal system when subjected only to attractive and repulsive interactions. An extensive comparison between our model and the pertinent literature is finally provided in Chapter 12, in order to highlight similarities and differences with respect to analogous approaches. In this respect, the proposed model combines and modifies concepts and ingredients already present in the literature, however giving rise to some quite distinct numerical and analytical results.

Chapter 11

A different modeling approach distinguishing individual speed and orientation

11.1 Mathematical model

A generic group of animals is described by a particle system within the d-dimensional space $\mathbb{R}^d$. In this perspective, the i-th agent (with $i = 1, ..., N$, N being the total number of individuals) is represented by a material point with position $\mathbf{x}_i(t)$. Individual dynamics are then described by the following first-order model

$$\frac{d\mathbf{x}_i(t)}{dt} = v_i(t)\frac{\boldsymbol{\omega}_i(t)}{|\boldsymbol{\omega}_i(t)|}, \tag{11.1}$$

which can be derived from a generic second-order Newtonian approach under the assumption of overdamped force-velocity response (a consistent hypothesis for living entities, see Section 4.2 of Chapter 4 for comments). Eq. (11.1) effectively decouples the magnitude of the velocity of the i-th animal, given by the scalar $v_i(t) \in \mathbb{R}_+$ (possibly, $v_i(t) \in [0, v_{\max}]$ to account for physiological limitations), from its direction, given by the unit vector $\dfrac{\boldsymbol{\omega}_i(t)}{|\boldsymbol{\omega}_i(t)|} \in B_1^d \subset \mathbb{R}^d$ (where B_1^d denotes the d-dimensional ball with unitary radius). As a relevant feature of the proposed model, these two quantities are assumed to be independent, since they have distinct physical meanings. For instance, the individual speed $v_i(t)$ can be determined by the intrinsic status of the agent (e.g., calm or in a hurry) as well as by the

purpose of its movement and by physiological/physical limitations. On the other hand, the velocity orientation of the particle, $\dfrac{\boldsymbol{\omega}_i(t)}{|\boldsymbol{\omega}_i(t)|}$, can be formally correlated to the competition between different behavioral stimuli (triggered, for example, by environmental signals, own preference or interactions with the surrounding agents). In this respect, the vector $\boldsymbol{\omega}_i(t)$ can be determined by a weighted sum of proper contributions, i.e.,

$$\boldsymbol{\omega}_i(t) = \sum_{j\in\mathcal{J}_i} \alpha_i^j(t)\mathbf{w}_i^j(t), \tag{11.2}$$

where $\mathcal{J}_i$ is the set of behavioral inputs that influence the dynamics of i while the unit vectors $\mathbf{w}_i^j \in B_1^d \subset \mathbb{R}^d$ define the corresponding orientations. Finally, the coefficients $\alpha_i^j(t)$ are weights that describe the relative importance of each stimulus with respect to the others; they may also evolve in time due to variations of internal or external conditions, e.g., visibility. In particular, to have comparable effects on agent dynamics and to avoid simultaneous maximization/minimazion of all behavioral traits, we assume that

$$\begin{cases} \alpha_i^j(t) \in [0,1]; & j \in \mathcal{J}_i; \\ \sum_{j\in\mathcal{J}_i} \alpha_i^j(t) = 1; & \forall t \geq 0, \end{cases} \tag{11.3}$$

for all $i = 1,...,N$. In this respect, relation (11.2) is a linear combination of the directional cues that affect the movement of the i-th agent.

Given the generical mathematical structure, we now recall that the majority of animal groups undergoes *collective* motion mainly guided by interindividual *social* interactions. In particular, three fundamental behavioral rules are classically identified, as explained in [66, 79, 83, 92] and in the First Part of this Thesis in the case of swarming honeybee populations. First, a *short-range repulsion* describes the tendency of each animal to maintain a minimum comfort space within the group: it is here implemented by a directional unit vector that allows the i-th agent to move away from close enough neighbors:

$$\mathbf{w}_i^{\text{rep}}(t) = \frac{\displaystyle\sum_{j\in\mathcal{N}_i^{\text{rep}}(t)} (\mathbf{x}_i(t) - \mathbf{x}_j(t))}{\left|\displaystyle\sum_{j\in\mathcal{N}_i^{\text{rep}}(t)} (\mathbf{x}_i(t) - \mathbf{x}_j(t))\right|}, \tag{11.4}$$

where

$$\mathcal{N}_i^{\text{rep}}(t) = \left\{ j = 1,\dots,N, j \neq i : 0 < |\mathbf{x}_j(t) - \mathbf{x}_i(t)| \leq d_{\text{rep}} \right\}, \tag{11.5}$$

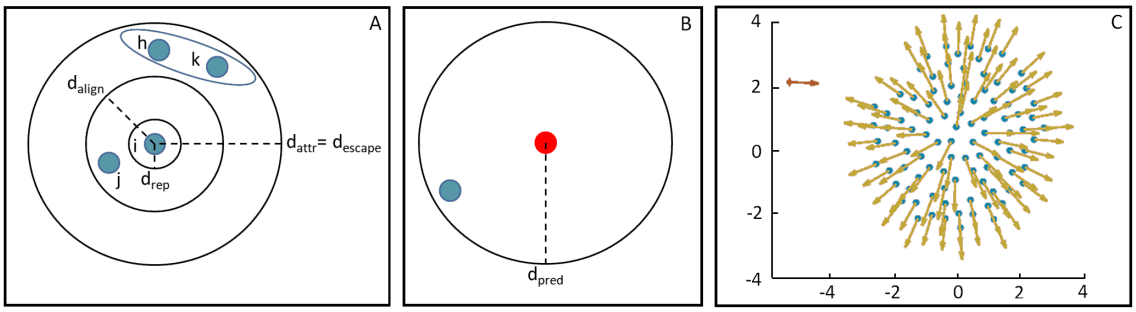

Figure 11.1 (A) Schematic representation of the interaction regions of the generic i-th member of the animal group. In particular, we recall that d_{rep}, d_{align}, d_{attr}, and d_{escape} measure the extensions of the repulsion, the alignment, the attraction and the escape areas, respectively. In this respect, we have that $\mathcal{N}_i^{\text{rep}} = \emptyset$, $\mathcal{N}_i^{\text{align}} = \{j\}$, and $\mathcal{N}_i^{\text{attr}} = \{h,k\}$ (as identified by the ellipsoid). (B) Schematic representation of the hunter predation zone, whose extension is defined by d_{pred}. As explained in the text, to obtain the corresponding dimensionless values, lengths are scaled with d_{rep}. (C) The animal group is initially arranged in a round configuration with random individual positions (indicated by the blue dots) and velocities (indicated by the arrows). In the case of the heterogenous system, a predator (the red diamond) is located at a significant distance from the cluster of individuals, however with at least a prey within its hunting region.

d_{rep} being the extension of the avoidance region.

A *middle-range alignment* mechanism then reproduces the aim of each agent to synchronize its movement, in term of orientation, with the groupmates falling within a given surrounding area of radius d_{align}, i.e.,

$$\mathbf{w}_i^{\text{align}}(t) = \frac{\mathrm{M}(\boldsymbol{\omega}_j(t)/|\boldsymbol{\omega}_i(t)|)_{j\in\mathcal{N}_i^{\text{align}}(t)}}{|\mathrm{M}(\boldsymbol{\omega}_j(t)/|\boldsymbol{\omega}_i(t)|)_{j\in\mathcal{N}_i^{\text{align}}(t)}|}. \tag{11.6}$$

In Eq. (11.6), $\mathrm{M}(\boldsymbol{\omega}_j(t)/|\boldsymbol{\omega}_i(t)|)_{j\in\mathcal{N}_i^{\text{align}}(t)}$ denotes in fact the mean of the actual velocity directions evaluated over the set of particles

$$\mathcal{N}_i^{\text{align}}(t) = \left\{ j = 1,\ldots,N, j \neq i : d_{\text{rep}} < |\mathbf{x}_j(t) - \mathbf{x}_i(t)| \leq d_{\text{align}} \right\}. \tag{11.7}$$

A *long-range attraction* finally enters the picture if the i-th animal falls too far apart from the rest of the group and tries to reach again its mates: in mathematical terms, we have

indeed

$$\mathbf{w}_i^{\text{attr}}(t) = \frac{\displaystyle\sum_{j\in\mathcal{N}_i^{\text{attr}}(t)} (\mathbf{x}_j(t) - \mathbf{x}_i(t))}{\left|\displaystyle\sum_{j\in\mathcal{N}_i^{\text{attr}}(t)} (\mathbf{x}_j(t) - \mathbf{x}_i(t))\right|}, \tag{11.8}$$

with

$$\mathcal{N}_i^{\text{attr}}(t) = \left\{ j = 1,\dots,N, j \neq i : d_{\text{align}} < |\mathbf{x}_j(t) - \mathbf{x}_i(t)| \leq d_{\text{attr}} \right\}. \tag{11.9}$$

The extension of the attraction region, d_{attr}, can be also interpreted as the visual distance of the animal of interest as done for instance in the modeling descriptions presented in Part I. A schematic representation of the different interparticle interaction areas is proposed in Fig. 11.1 (A).

Putting the introduced velocity components in Eq. (11.2), $\boldsymbol{\omega}_i$ results specified as

$$\boldsymbol{\omega}_i(t) = \alpha_i^{\text{rep}}(t)\mathbf{w}_i^{\text{rep}}(t) + \alpha_i^{\text{align}}(t)\mathbf{w}_i^{\text{align}}(t) + \alpha_i^{\text{attr}}(t)\mathbf{w}_i^{\text{attr}}(t), \tag{11.10}$$

being $\mathcal{J}_i = \{\text{rep, align, attr}\}$ and $\alpha_i^{\text{rep}}(t) + \alpha_i^{\text{align}}(t) + \alpha_i^{\text{attr}}(t) = 1$ for any $i = 1,...,N$. As written, the proposed approach includes a minimal set of parameters: individual speeds and extensions of interparticle interaction regions, that can be easily quantified for a given animal species, as well as the intensities of the behavioral inputs, that need at least a hierarchical estimate but have clear biological meaning. No other strictly technical coefficients need to be introduced.

We finally propose a proper dimensionless form of the model, in order to facilitate its application to any group of animals, regardless of their characteristic measures. For this purpose, we scale lengths with the repulsion radius d_{rep}, velocities with the characteristic speed of the agents of interest, say v, and times with d_{rep}/v. Trivial calculations allow then to rewrite Eqs. (11.1) as

$$\frac{d\overline{\mathbf{x}}_i(\bar{t})}{d\bar{t}} = \overline{v}_i(\bar{t})\frac{\overline{\boldsymbol{\omega}}_i(\bar{t})}{|\overline{\boldsymbol{\omega}}_i(\bar{t})|} = \overline{v}_i(\bar{t})\frac{\alpha_i^{\text{rep}}(\bar{t})\overline{\mathbf{w}}_i^{\text{rep}}(\bar{t}) + \alpha_i^{\text{align}}(\bar{t})\overline{\mathbf{w}}_i^{\text{align}}(\bar{t}) + \alpha_i^{\text{attr}}(\bar{t})\overline{\mathbf{w}}_i^{\text{attr}}(\bar{t})}{|\alpha_i^{\text{rep}}(\bar{t})\overline{\mathbf{w}}_i^{\text{rep}}(\bar{t}) + \alpha_i^{\text{align}}(\bar{t})\overline{\mathbf{w}}_i^{\text{align}}(\bar{t}) + \alpha_i^{\text{attr}}(\bar{t})\overline{\mathbf{w}}_i^{\text{attr}}(\bar{t})|}, \tag{11.11}$$

where the dimensionless variables are overlined. In particular, the extensions of the interaction regions scale as $\overline{d}_{\text{rep}} = 1$, $\overline{d}_{\text{align}} = d_{\text{align}}/d_{\text{rep}}$, and $\overline{d}_{\text{attr}} = d_{\text{attr}}/d_{\text{rep}}$, so that $\overline{d}_{\text{align}}$ and $\overline{d}_{\text{attr}}$ measure the relative extension of the corresponding areas with respect to the radius of the avoidance neighborhood.

11.2 Simulation details and results

The proposed model is employed in a planar setting, i.e., $d = 2$. In all forthcoming simulations, the animal population of interest is formed by $N = 100$ individuals. In particular, as shown in Fig. 11.1 (C), they are initially arranged in an almost round configuration with diameter equal to 6 (in non-dimensional terms) and randomly assigned positions. The initial velocity direction of each generic i-th agent, i.e., $\overline{\boldsymbol{\omega}}_i(\bar{t} = 0)$ is randomly established as well. Given that the proposed scaling results in a unitary dimensionless repulsion radius $\overline{d}_{\text{rep}} = 1$, we set the linear extension of the alignment and the attraction regions equal to $\overline{d}_{\text{align}} = 8$ and $\overline{d}_{\text{attr}} = 30$, respectively. The ratios between the depth of the different interacting areas are consistent with the biologically plausible ranges explored by Couzin and coworkers in [28] and also employed by Wood and Ackland in [104]. In this respect, as commented also in the conclusive section, the application of the model to a specific animal species would lead to a more proper parameter setting. We furthermore assume that all individuals have a constant and common speed equal to the characteristic value v: this implies a non-dimensional quantity $\overline{v}_i(\bar{t}) = 1$, for any i and $\bar{t}$. The weights αs are finally hypothesized to be independent from both time and animal individuality, i.e., $\alpha_i^{(\cdot)}(\bar{t}) = \alpha^{(\cdot)}$ for any i and $\bar{t}$, being $(\cdot) \in \{\text{rep, align, attr}\}$. In particular, the resulting set of permitted triplets (i.e., those satisfying constraint (11.3)) identifies the simplex $\mathcal{S}$, identified by the triangle in Fig. 11.2 (A).

We now analyse how individual behavioral preferences affect group dynamics. In more details, our strategy is to vary the values of the α-coefficients and to *numerically* explore the large-time states of the animal system. In this perspective, we introduce the following classification for the simulation outcomes:

Definition 11.2.1. (i) The animal group has a time-asymptotic crystalline/non collapsed configuration if the following condition is satisfied:

$$\overline{d}_{\min} = \lim_{\bar{t}\to\infty} \min_{\substack{(i,j)\in\{1,\dots,N\}\times\{1,\dots,N\} \\ i\neq j}} |\overline{\mathbf{x}}_i(\bar{t}) - \overline{\mathbf{x}}_j(\bar{t})| \in (\overline{d}_{\text{rep}} - \varepsilon; \overline{d}_{\text{rep}} + \varepsilon). \tag{11.12}$$

(ii) The animal group has a time-asymptotic synchronized movement if the following condition is satisfied:

$$\sigma = \lim_{\bar{t}\to\infty} N^{-\frac{1}{2}} \sqrt{\sum_{i=1}^{N} \left| \frac{\overline{\boldsymbol{\omega}}_i(\bar{t})}{|\overline{\boldsymbol{\omega}}_i(\bar{t})|} - \mathrm{M}\left(\frac{\overline{\boldsymbol{\omega}}_j(\bar{t})}{|\overline{\boldsymbol{\omega}}_j(\bar{t})|} \right)_{\substack{j=1,\dots,N \\ j\neq i}} \right|^2} < \sigma_{\mathrm{c}}, \tag{11.13}$$

where the overlines identify, as usual, dimensionless measures. Further, the notation $\mathrm{M}(\cdot)_{\substack{j=1,\dots,N \\ j\neq i}}$ indicates the mean of the velocity directions over the entire animal group.

These quantities are particularly suitable to describe the phenomenology of a set of interacting particles, in term of both patterning and motion. In particular, condition (11.12) assures that there is no large-time individual overlap. In fact, if the asymptotic minimal interagent distance falls within the range $(\overline{d}_{\mathrm{rep}}-\varepsilon;\overline{d}_{\mathrm{rep}}+\varepsilon)$, $\varepsilon=0.05$ being introduced to account for numerical errors in a multiparticle system, then all pairs of animals have an equal or a larger spacing, i.e., they do not collapse. Condition (11.13) instead assures that all individuals have almost the same direction of movement. In fact, preliminary simulations have shown that standard deviations σ of the distribution of the agent orientations smaller than the critical value $\sigma_{\mathrm{c}}=2$ imply a fully aligned animal movement. Similar classifications have been used in the literature to differentiate the evolutions of a wide range of multiagent populations, see for instance the case of swarming birds in [18] and references therein.

Our numerical study allows indeed to subdivide the permitted parameter space $\mathcal{S}$ in four *disjointed* regions, according to Definition 11.2.1. In particular, the subregion $\mathcal{S}_1$ is characterized by triplets of coefficients resulting in the asymptotic collapse of the cluster of particles, which also maintain an uncorrelated movement. The group of animals is instead observed to have a large-time synchronized collective motion, however coupled with an asymptotic collapse, when the intensities of the behavioral stimuli fall within $\mathcal{S}_2$. On the other hand, $\alpha^{(\cdot)}$-triplets belonging to the subregion $\mathcal{S}_3$ allow to avoid unrealistic animal overlapping but the agent locomotion remains completely individual (i.e., no common direction emerges). $\mathcal{S}_4$ is finally characterized by the triplets of $\alpha^{(\cdot)}$s that result in an asymptotic collective crystallization *and* alignment, i.e., all agents finally move in the same direction keeping a comfort spacing.

To further support the above dissertation, for each subregion $\mathcal{S}_i$ $(i=1,\dots,4)$ of the permitted parameter space we show in Fig. 11.2 (B) a representative asymptotic configuration of the system and in Fig. 11.6 (A) the mean (with the corresponding standard deviation) of the quantities introduced in Definition 11.2.1, evaluated over a set of 10 numerical realizations resulting from randomly chosen $\alpha^{(\cdot)}$-triplets.

By reviewing the simulation results summarized in Fig. 11.2 (A), we can also notice that below a given value of the alignment parameter α^{align} (i.e., ≈ 0.2), a synchronized movement of the animal group is not obtained regardless the intensity of the other stimuli. On the opposite, a directionally collective movement is captured for any pair $(\alpha^{\mathrm{rep}},\alpha^{\mathrm{attr}})$

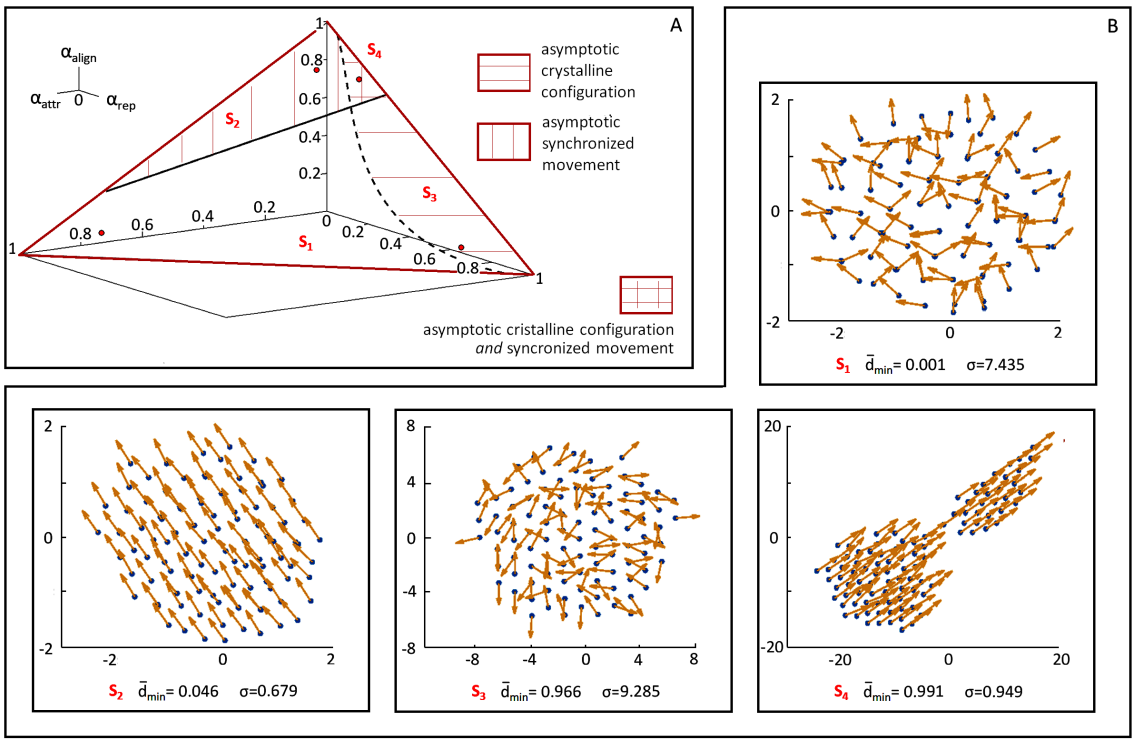

Figure 11.2 (A) The set of permitted values of the weights $\alpha^{(\cdot)}$s (i.e., those satisfying constraint (11.3)) defines the simplex $\mathcal{S}$, identified by the red triangle. It can be in turn divided in four disjointed regions, i.e., $\mathcal{S}_i$ ($i = 1,...,4$), identifying different behavior of the animal group, as captured by numerical realizations classified according to Definition 11.2.1. The red dots indicate the four triplets of $\alpha^{(\cdot)}$s (one for each subregion) whose resulting large-time, i.e., at $\bar{t} = 100$, system pattern and dynamics are taken as representative, and shown in the (B) panels. In particular, coefficients $\overline{d}_{\min}$ and σ are introduced in Definition (11.2.1).

if α^{align} is larger than ≈ 0.6. Analogously, a lower threshold of the weight α^{rep} (i.e., ≈ 0.1) is necessary (but not sufficient) to avoid particle collapse, which is instead impossible for any parameter setting involving $\alpha^{\text{rep}} > 0.95$. It is also interesting to notice that a complete balance between the three weights (i.e., $\alpha^{\text{rep}} = \alpha^{\text{align}} = \alpha^{\text{attr}}$) does not result in a system crystallization nor in a synchronized movement. Region $\mathcal{S}_4$ is rather characterized by a significant hierarchy of the intensity of the behavioral stimuli, with the alignment coefficient that substantially overcomes the repulsive one, which is in turn one order of magnitude larger than attraction parameter. In this respect, it is finally useful to remark that (so far) we have not included the presence of elements that may cause dispersion of single animals. Therefore, a small attraction stimulus is sufficient to avoid group scattering.

Comparable classifications of groups dynamics, done in the case of similar models, are obtained varying the extension of the interaction regions [28, 104] or the parameters defining the magnitude and the shape of the individual velocity components [18, 50].

11.3 Asymptotic configurations of the particle system

In this Section, we discuss some theoretical results concerning the stationary states of the agent based system. In particular, we provide an analytical study able to give a parametric constraint sufficient to avoid asymptotic individual collapse. In this respect, we have to neglect the alignment velocity contribution and to focus only on attractive-repulsive dynamics to assure the existence of large-time equilibrium configurations. Under this assumption, the individual velocity vector $\boldsymbol{\omega}_i(t)$, defined in (11.2), can be specified and rewritten in the following form

$$\boldsymbol{\omega}_i(t) = \alpha_i^{\text{attr}}\mathbf{w}_i^{\text{attr}}(t) + \alpha_i^{\text{rep}}\mathbf{w}_i^{\text{rep}}(t) = v_i \sum_{\substack{j=1 \\ j\neq i}}^{N} h^{\text{int}}\left(|\mathbf{x}_j(t)-\mathbf{x}_i(t)|\right)\frac{\mathbf{x}_j(t)-\mathbf{x}_i(t)}{|\mathbf{x}_j(t)-\mathbf{x}_i(t)|} \quad i=1,\dots,N, \tag{11.14}$$

where $\alpha_i^{\text{rep}} + \alpha_i^{\text{attr}} = 1$ (cf. Eq. (11.3)) and

$$h^{\text{int}}\left(|\mathbf{x}_j(t)-\mathbf{x}_i(t)|\right) = h^{\text{rep}}\left(|\mathbf{x}_j(t)-\mathbf{x}_i(t)|\right) + h^{\text{attr}}\left(|\mathbf{x}_j(t)-\mathbf{x}_i(t)|\right), \tag{11.15}$$

with

$$h^{\text{rep}} = \begin{cases} -\alpha^{\text{rep}} & 0 < |\mathbf{x}_j(t)-\mathbf{x}_i(t)| \leq d_{\text{rep}} \\ 0 & \text{otherwise,} \end{cases} \tag{11.16}$$

$$h^{\text{attr}} = \begin{cases} \alpha^{\text{attr}} & d_{\text{align}} < |\mathbf{x}_j(t)-\mathbf{x}_i(t)| \leq d_{\text{attr}} \\ 0 & \text{otherwise.} \end{cases} \tag{11.17}$$

It has been shown that the H-stability characteristics of the potential associated to the interaction kernel h^{int}, which will be hereafter denoted by u^{int}, determine the large-time spatial organization of the particle system. In particular, we recall that if u^{int} is H-stable, the minimal interparticle distance at the equilibrium is bounded below by a finite fixed positive value (regardless of the total amount of particles N). In other words, if u^{int} is H-stable, the individuals do not asymptotically overlap. In this respect, a criterion to detect

the H-stability of a scalar potential has been given in [13], and already applied to the case of honeybee swarms in the First Part of this Thesis (see Theorems 5.2.1 and 5.2.3 in Chapter 5). Accordingly, we can state the following:

Theorem 11.3.1. *The interaction potential u^{int} related to the pairwise interaction kernel h^{int} defined in Eqs. (11.15)-(11.17) is H-stable if the following parametric relation holds*

$$\frac{d_{\text{attr}}^3 - d_{\text{align}}^3}{d_{\text{rep}}^3 + d_{\text{attr}}^3 - d_{\text{align}}^3} < \alpha_{\text{rep}} < 1, \quad \textit{or equivalently}, \quad 0 < \alpha^{\text{attr}} < \frac{d_{\text{rep}}^3}{d_{\text{rep}}^3 + d_{\text{attr}}^3 - d_{\text{align}}^3}. \tag{11.18}$$

Proof. We have first to derive the potential $u^{\text{int}} : \mathbb{R} \to \mathbb{R}$ associated to the kernel h^{int}, i.e.,

$$u^{\text{int}}(r) = \begin{cases} -\alpha^{\text{rep}} r + C_1, & \text{if } 0 < r \leq d_{\text{rep}}; \\ C_2, & \text{if } d_{\text{rep}} < r \leq d_{\text{align}}; \\ \alpha^{\text{attr}} r + C_3, & \text{if } d_{\text{align}} < r \leq d_{\text{attr}}; \\ C_4, & \text{if } r > d_{\text{attr}}. \end{cases}$$

where $r := |\mathbf{x}_j(t) - \mathbf{x}_i(t)|$. The constants of integration $C_1, C_2, C_3, C_4 \in \mathbb{R}$ have then to be estimated in order to guarantee (i) the continuity of the potential $u^{\text{int}}(r)$ and (ii) the fact that it is essentially negligible for large enough interparticle distances (i.e., $\lim_{r\to 0} u^{\text{int}}(r) = 0$). Both conditions are in fact necessary hypotheses for Theorem 11.3.1, as clearly stated in [13]. By simple algebraic calculations, we have that C_4 can be taken equal to 0 and the other constants result

$$\begin{aligned} C_1 &= \alpha^{\text{attr}} d_{\text{align}} - \alpha^{\text{attr}} d_{\text{attr}} + \alpha^{\text{rep}} d_{\text{rep}}; \\ C_2 &= \alpha^{\text{attr}} d_{\text{align}} - \alpha^{\text{attr}} d_{\text{attr}}; \\ C_3 &= -\alpha^{\text{attr}} d_{\text{attr}}, \\ C_4 &= 0, \end{aligned}$$

so that the interaction potential rewrites as

$$u^{\text{int}}(r) = \begin{cases} -\alpha^{\text{rep}} r + \alpha^{\text{attr}} d_{\text{align}} - \alpha^{\text{attr}} d_{\text{attr}} + \alpha^{\text{rep}} d_{\text{rep}}, & \text{if } 0 < r \leq d_{\text{rep}}; \\ \alpha^{\text{attr}} d_{\text{align}} - \alpha^{\text{attr}} d_{\text{attr}}, & \text{if } d_{\text{rep}} < r \leq d_{\text{align}}; \\ \alpha^{\text{attr}} r - \alpha^{\text{attr}} d_{\text{attr}}, & \text{if } d_{\text{align}} < r \leq d_{\text{attr}}; \\ 0, & \text{if } r > d_{\text{attr}}. \end{cases}$$

Recalling the Definition 1.1 in [13], we can affirm that u^{int} is H-stable when

$$\int_0^{+\infty} u^{\text{int}}(r)\, r\, dr = \frac{1}{2} \lim_{r \to 0} u^{\text{int}}(r) > 0.$$

In this respect, with some simple algebraic calculations, we obtain

$$\int_0^{+\infty} u^{\text{int}}(r)\, r\, dr = \frac{\alpha^{\text{rep}} d_{\text{rep}}^3 + \alpha^{\text{attr}} (d_{\text{align}}^3 - d_{\text{attr}}^3)}{6} > 0,$$

which is non negative if

$$\frac{\alpha^{\text{rep}}}{\alpha^{\text{attr}}} > \frac{d_{\text{attr}}^3 - d_{\text{align}}^3}{d_{\text{rep}}^3}. \tag{11.19}$$

Finally, recalling that $\alpha_i^{\text{rep}} + \alpha_i^{\text{attr}} = 1$, we can rewrite (11.19) only in terms of the repulsive (respectively, the adhesive) coefficient α_i^{rep} (respectively, α_i^{attr}):

$$\frac{d_{\text{attr}}^3 - d_{\text{align}}^3}{d_{\text{rep}}^3 + d_{\text{attr}}^3 - d_{\text{align}}^3} < \alpha_{\text{rep}} < 1, \quad \text{or equivalently,} \quad 0 < \alpha^{\text{attr}} < \frac{d_{\text{rep}}^3}{d_{\text{rep}}^3 + d_{\text{attr}}^3 - d_{\text{align}}^3},$$

which is exactly the thesis of the Theorem. □

Condition (11.18) allows to subdivide the segment s defining the permitted parameter space $(\alpha_i^{\text{rep}}, \alpha_i^{\text{attr}})$ into two parts, each resulting in a distinct stability characterization of the interaction kernel h^{int}, see Fig. 11.3. In particular, pairs of α-values falling within the dashed part s_2 of the segment satisfy Eq. (11.18) and assure an asymptotic non-collapsed configuration of the system. For the sake of completeness, the non-dimensional counterparts of constraints (11.18) reads as:

$$\frac{\overline{d}_{\text{attr}}^3 - \overline{d}_{\text{align}}^3}{1 + \overline{d}_{\text{attr}}^3 - \overline{d}_{\text{align}}^3} < \alpha_{\text{rep}} < 1, \quad \text{or equivalently,} \quad 0 < \alpha^{\text{attr}} < \frac{1}{1 + \overline{d}_{\text{attr}}^3 - \overline{d}_{\text{align}}^3}. \tag{11.20}$$

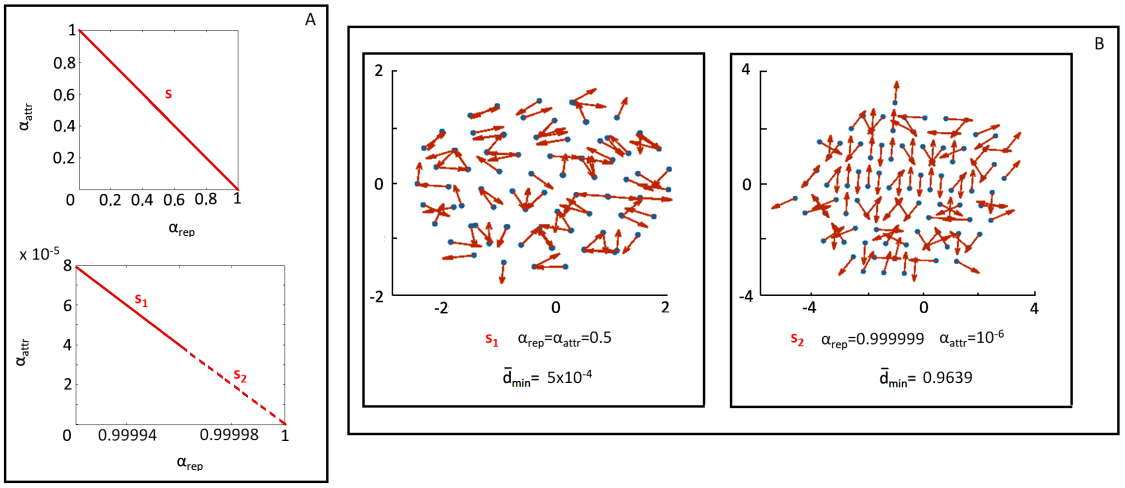

Figure 11.3 (A-top panel) In the absence of the alignment velocity component, the set of permitted values of the weights $\alpha^{(\cdot)}$s (i.e., those satisfying constraint (11.3)) defines the segment s, reproduced by the red line. (A-bottom panel) The H-stability condition of the repulsive/attractive velocity contributions divides s in two segments, i.e., s_i $(i = 1,2)$, identifying distinct asymptotic behavior of the animal group, as provided by Theorem 11.3.1. In particular, if the values of α_{rep} and α_{attr} satisfy condition (11.18) (or its non-dimensional counterpart (11.20)), then the system does not collapse but stabilizes in a large-time equilibrium configuration characterized by finite and positive interindividual distances. (B) Large-time system patterns (taken at $\bar{t} = 2000$) resulting from two representative pairs of coefficients $\alpha^{(\cdot)}$s (one for each subregion). Again, the quantity $\overline{d}_{\text{min}}$ is introduced in Definition (11.2.1).

The above analytical considerations can be supported by numerical results. In this respect, we perform a pair of representative computational tests that reproduce the evolution of a homogeneous population of $N = 100$ component individuals, whose dynamics are only regulated by adhesive and repulsive stimuli. The values of the individual speed and of the extension of the interaction regions, as well as the initial condition of the system, are exactly the same as those employed in the previous Section. As shown in Fig. 11.3, if the weights $\alpha^{(\cdot)}$s do not satisfy the H-stability condition (i.e., fall within s_1), then the particle cluster asymptotically collapses, as confirmed by the corresponding $\overline{d}_{\text{min}} = 5 \times 10^{-4}$. On the other hand, if the values of the two coefficients satisfies the H-stability constraint (i.e., fall within s_2), then the animal group stabilizes in a well-spaced configuration characterized by the absence of individual overlap. Interestingly, in this case, the large-time minimal interparticle distance $\overline{d}_{\text{min}} = 0.9639$ falls within the range $(\overline{d}_{\text{rep}} - \varepsilon; \overline{d}_{\text{rep}} + \varepsilon)$, introduced in Definition 11.2.1 (recalling that $\overline{d}_{\text{rep}} = 1$).

The *coupling* between the analytical and the numerical results proposed in this Section allows therefore to conclude that, in the absence of the alignment velocity component, an asymptotic crystalline configuration of the system is *a priori* assured by H-stable repulsive/attractive kernels, i.e., by pairs of weights $(\alpha^{\text{rep}}, \alpha^{\text{attr}})$ satisfying condition (11.20). It is finally useful to remark that, as far as we know, a similar study has been never done in the case of interaction potential characterized by constraints and interdependence between the characteristic parameters.

11.4 Prey - predator dynamics: model and results

We now incorporate heterogeneity in the animal system by introducing the presence of a single predator, labeled by the identification number $i = 100$ (so that the overall number of agents remains unaltered). In this respect, the remaining set of individuals hereafter constitutes a group of prey chased by the hunter. In nature, we can observe a wide variety of predator-prey interactions: however, a common characteristic is the emergence of empty space around the predator, due to the obvious tendency of the other individuals to move away, as commented again in [19] and references therein and shown in Fig. 6.1 (C-D). This behavior can be implemented in our model by the inclusion of a proper avoidance term in the prey dynamical rules: in this respect, we have that $\mathcal{J}_i = \{\text{rep, align, attr, escape}\}$ and

$$\overline{\boldsymbol{\omega}}_i(\bar{t}) = \alpha_i^{\text{rep}}(\bar{t})\overline{\mathbf{w}}_i^{\text{rep}}(\bar{t}) + \alpha_i^{\text{align}}(\bar{t})\overline{\mathbf{w}}_i^{\text{align}}(\bar{t}) + \alpha_i^{\text{attr}}(\bar{t})\overline{\mathbf{w}}_i^{\text{attr}}(\bar{t}) + \alpha_i^{\text{escape}}(\bar{t})\overline{\mathbf{w}}_i^{\text{escape}}(\bar{t}), \tag{11.21}$$

for $i \in \{1, ..., 99\}$. In particular, the directional velocity contribution $\overline{\mathbf{w}}_i^{\text{escape}}$ reads as

$$\overline{\mathbf{w}}_i^{\text{escape}}(\bar{t}) = \frac{\overline{\mathbf{x}}_i(\bar{t}) - \overline{\mathbf{x}}_{100}(\bar{t})}{|\overline{\mathbf{x}}_i(\bar{t}) - \overline{\mathbf{x}}_{100}(\bar{t})|}, \tag{11.22}$$

which is actually active if $|\overline{\mathbf{x}}_i(\bar{t}) - \overline{\mathbf{x}}_{100}(\bar{t})| \leq \overline{d}_{\text{escape}}$, being $\overline{d}_{\text{escape}}$ set equal to $\overline{d}_{\text{attr}}$, see again Fig. 11.1 (A). The term in (11.22) is indeed a *long-range* repulsive contribution since it enters the picture as soon as the predator falls within the visual region of the i-th prey. We in fact recall that the extension of the attraction region can be interpreted as an individual gaze depth. The weights of the behavioral stimuli included in (11.21) have finally to satisfy constraint (11.3), i.e.,

$$\alpha_i^{\text{rep}}(\bar{t}) + \alpha_i^{\text{align}}(\bar{t}) + \alpha_i^{\text{attr}}(\bar{t}) + \alpha_i^{\text{escape}}(\bar{t}) = 1 \tag{11.23}$$

for any particle $i = 1, ..., 99$ and time $\bar{t}$.

The dynamics of the predator are described by a first-order model as well, under the assumption that it is only subjected to the hunting stimulus. In mathematical terms, $\mathcal{J}_{100} = \{\text{pred}\}$ while, in the usual non-dimensional form, Eqs. (11.1)-(11.2) can be rewritten as

$$\frac{d\overline{\mathbf{x}}_{100}(\bar{t})}{d\bar{t}} = \bar{v}_{100}(\bar{t})\alpha_{100}^{\text{pred}}(\bar{t})\overline{\mathbf{w}}_{100}^{\text{pred}}(\bar{t}), \tag{11.24}$$

where obviously $\alpha_{100}^{\text{pred}}(\bar{t}) = 1$ for any $\bar{t}$. To specify the velocity contribution in Eq. (11.24), we can observe that, in general, the predator is attracted and consequently oriented by the group of prey: however, different hunting strategies can be identified. For instance, the *confused* predator does not have the ability to identify and attack a single individual within a set of agents [74, 59]. In this respect, its chasing direction points towards the center of mass of the population of prey, where all of them are equally targeted (if seen). From a modeling perspective, this amounts in defining:

$$\overline{\mathbf{w}}_{100}^{\text{pred}}(\bar{t}) = \overline{\mathbf{w}}_{100}^{\text{pred, conf}}(\bar{t}) = \frac{\displaystyle\sum_{j\in\mathcal{N}_{100}^{\text{pred}}(\bar{t})} (\overline{\mathbf{x}}_j(\bar{t}) - \overline{\mathbf{x}}_{100}(\bar{t}))}{\left|\displaystyle\sum_{j\in\mathcal{N}_{100}^{\text{pred}}(\bar{t})} (\overline{\mathbf{x}}_j(\bar{t}) - \overline{\mathbf{x}}_{100}(\bar{t}))\right|}, \tag{11.25}$$

with

$$\mathcal{N}_{100}^{\text{pred}}(\bar{t}) = \left\{ j = 1, \ldots, 99 : 0 < |\overline{\mathbf{x}}_j(\bar{t}) - \overline{\mathbf{x}}_{100}(\bar{t})| \leq \overline{d}_{\text{pred}} \right\}, \tag{11.26}$$

where $\overline{d}_{\text{pred}}$ is the non-dimensional extension of the predation region, that can be assimilated to the hunter visual depth, see also Fig. 11.1 (B).

In other cases (e.g., in other species of animals), the predator is *not confused* by the presence of multiple prey, being it able to target a specific individual within the group and to change strategy accordingly. For instance, it can chase the agent which, at a given time, is the closest to its position, i.e.,

$$\overline{\mathbf{w}}_{100}^{\text{pred}}(\bar{t}) = \overline{\mathbf{w}}_{100}^{\text{pred, non conf}}(\bar{t}) = \frac{\overline{\mathbf{x}}_{j*}(\bar{t}) - \overline{\mathbf{x}}_{100}(\bar{t})}{\left|\overline{\mathbf{x}}_{j*}(\bar{t}) - \overline{\mathbf{x}}_{100}(\bar{t})\right|}, \tag{11.27}$$

with

$$j* : |\overline{\mathbf{x}}_{j*}(\bar{t}) - \overline{\mathbf{x}}_{100}(\bar{t})| = \min_{\substack{j=1,\ldots,99 \\ j\in\mathcal{N}_{100}^{\text{pred}}(\bar{t})}} |\overline{\mathbf{x}}_j(\bar{t}) - \overline{\mathbf{x}}_{100}(\bar{t})|.$$

Simulation details and numerical results. Multispecies dynamics are located within the planar space. The values of the non-dimensional parameters characterizing the behavioral rules of the group of prey remain unaltered with respect to the Section 11.2, given their independency from both time and individual specificity, i.e., $\overline{v}_i = 1$, $\overline{d}_{\text{rep}} = 1$, $\overline{d}_{\text{align}} = 8$ and $\overline{d}_{\text{escape}} = \overline{d}_{\text{attr}} = 30$ for any $i = 1, ..., 99$ and $\bar{t}$. For the sake of simplicity, we also assume that the predator has the same physiological characteristics as its prey: we therefore fix $\overline{d}_{\text{pred}} = \overline{d}_{\text{attr}} = 30$ and $\overline{v}_{100}(\bar{t}) = 1$ for any $\bar{t}$.

The group of prey is initially arranged within the same round area of diameter equal to 6 used in the previous set of simulations, with random positions and velocity directions. The predator is initially placed at a significant distance from the cluster of individuals however with at least a prey within its hunting region, i.e., $\mathcal{N}_{100}(\bar{t} = 0) \neq \emptyset$. Furthermore, the initial orientation of the hunter points to the center of mass of the group of targets, see Fig. 11.1 (C). The predator is finally assumed to catch a target when their relative non-dimensional distance drops below 10^{-2}.

The dynamics of the heterogenous system are then numerically studied upon variations of (i) predator hunting strategy and (ii) hierarchy of prey behavioral preferences which are quantified, as seen, by the weights $\alpha^{(\cdot)}$, being $(\cdot) \in \{\text{rep, align, attr, escape}\}$. In particular, we hereafter focus on representative cases characterized by the fact that one (or more) prey behavioral stimuli significantly overcome the others. With the terminology "significantly overcome", we arbitrarily mean that the corresponding α-value(s) is (are) at least two-fold higher than the others. The resulting simulation outcomes are then analyzed qualitatively (i.e., in terms of prey escape strategies) and quantitatively (i.e., in terms of time needed by the predator to eventually reach a target individual, hereafter defined as $\bar{t}_{\text{p}}$).

As shown in Fig. 11.4, when the prey agents are mainly subjected to the escape stimulus (i.e., $\alpha^{\text{escape}} \gg \alpha^{\text{rep}} = \alpha^{\text{align}} = \alpha^{\text{attr}}$), they are able to avoid the attack of both confused and not confused predators. In particular, they quickly move away from the approaching hunters without wasting time to organize in a crystalline configuration or to align towards a preferred direction. In this respect, the group of prey randomly dissociates in disorganized colonies of different sizes with the predators falling within the empty space in between them and therefore being unable to reach any target, as shown also by the insets i1 and i2 in Fig. 11.4.

Differentiated phenomenologies instead emerge if the prey group is in an attraction regime (i.e., $\alpha^{\text{attr}} \gg \alpha^{\text{rep}} = \alpha^{\text{align}} = \alpha^{\text{escape}}$). The confused predator falls and oscillates

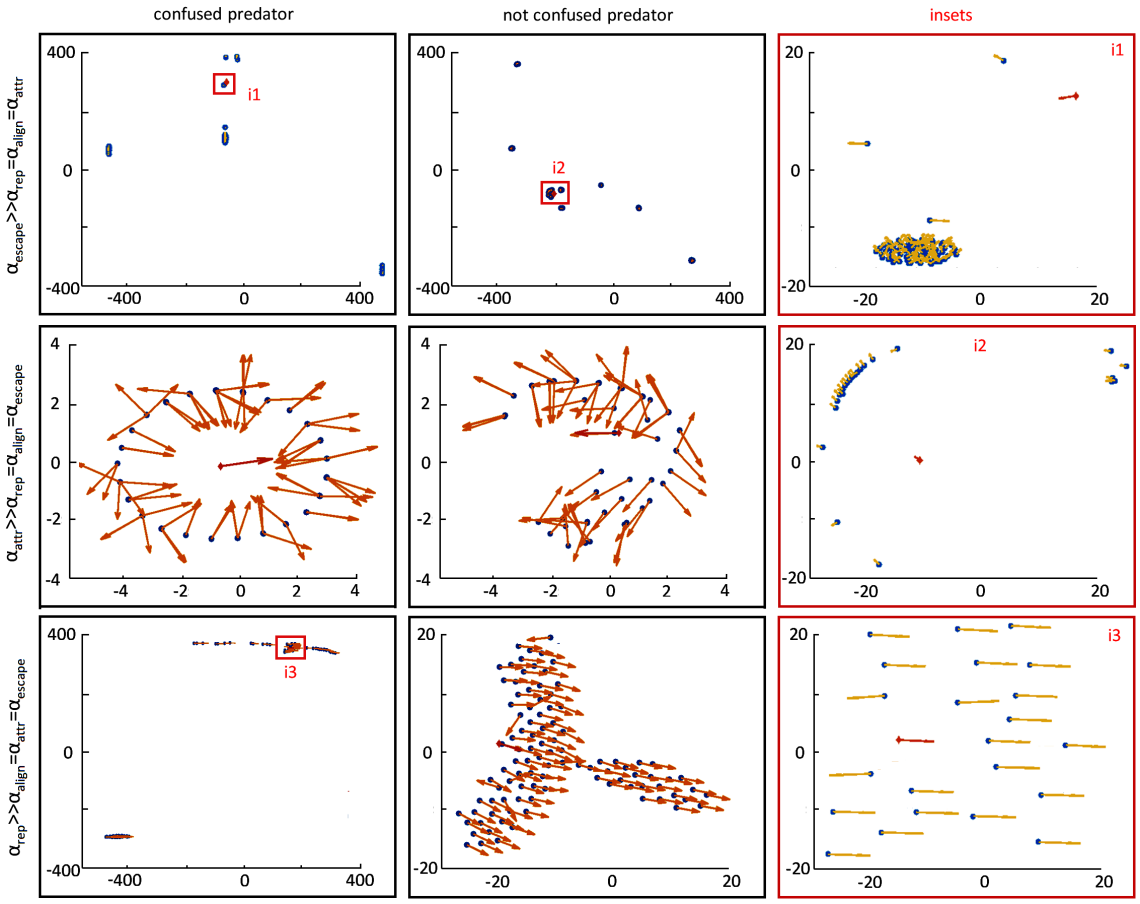

Figure 11.4 Large-time (i.e., taken at $\bar{t} = 100$) representative dynamics of the heterogenous animal system for different hierarchies of prey behavioral stimuli and predator strategies (confused vs. not confused). The panels of the right column reproduce zoomed views of the selected insets. As usual, arrows indicate the actual velocity of both prey individuals (blue dots) and predator (red diamond).

at the center of a ring of radially escaping individuals, which still maintain a collective connection (see the left-middle panel in Fig. 11.4). The confused hunter is in fact unable to choose an optimal direction of attack, lying at the center of mass of the set of prey locations. Such an evasion pattern has been numerically captured and analytically constructed and justified in a similar model [19]. The prey agents perform almost the same strategy in the case of a not confused predator, organizing in a half-moon of escaping agents. However, as shown in the center panel in Fig. 11.4, the tendency to remain in an almost compact configuration delays their evasive manoeuvres: the hunter has therefore enough time to catch at least one target. In this respect, Fig. 11.6 (B-left panel) shows that the predation time $\bar{t}_p$ decreases upon increments in the attraction stimulus of the prey (with respect to

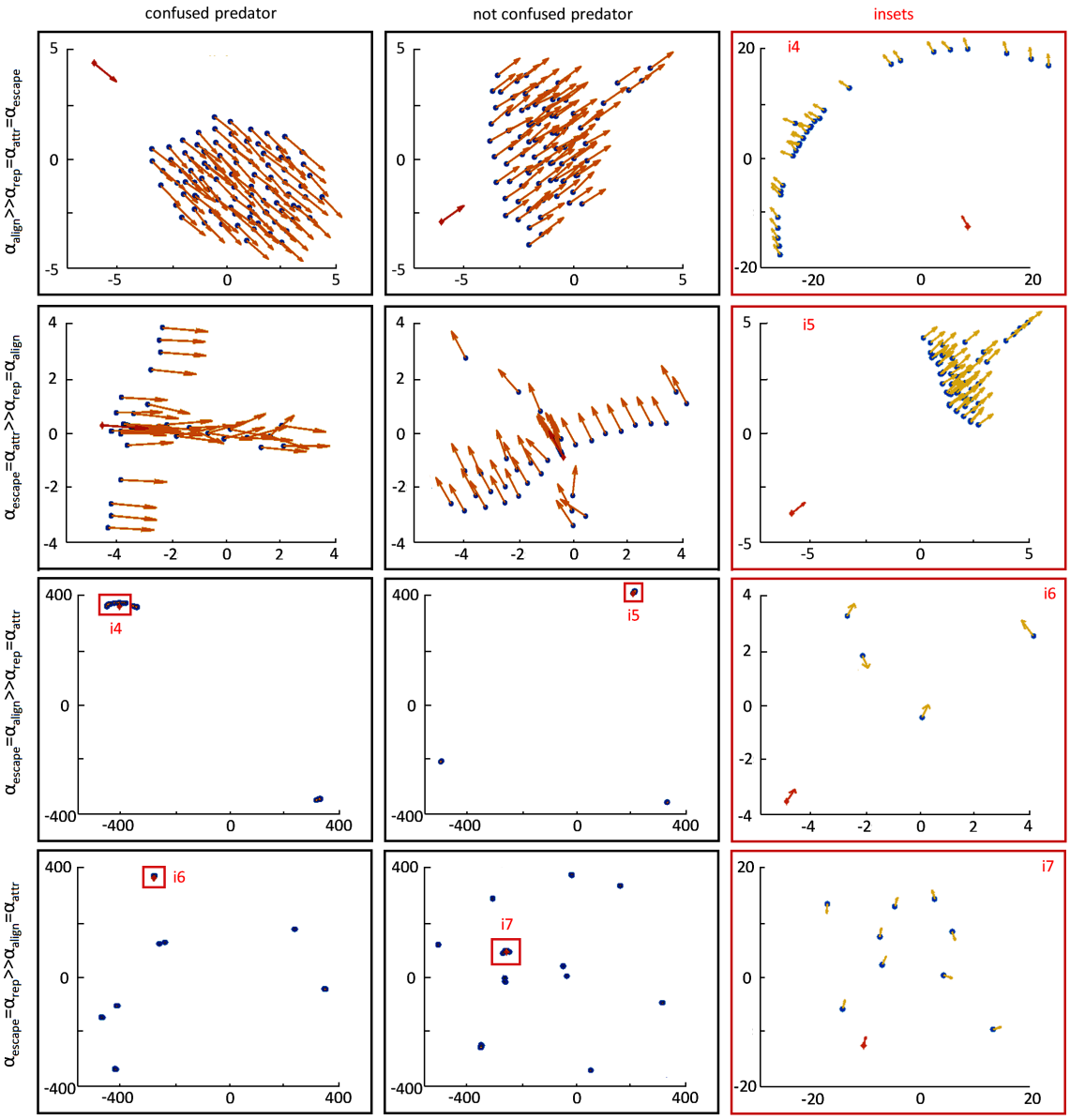

Figure 11.5 Large-time (i.e., taken at $\bar{t} = 100$) representative dynamics of the heterogenous animal system for different hierarchies of prey behavioral stimuli and predator strategies (confused vs. not confused). The panels of the right column reproduce zoomed views of the selected insets. As usual, arrows indicate the actual velocity of both prey individuals (blue dots) and predator (red diamond).

the other behavioral inputs), until stabilizing around a non-dimensional threshold value close to 4. Half-moon evasive patterns in the case of a predator pointing the center of the target cluster has been obtained also in the work by Lee and colleagues [72] which will be reviewed in more details in the conclusive chapter.

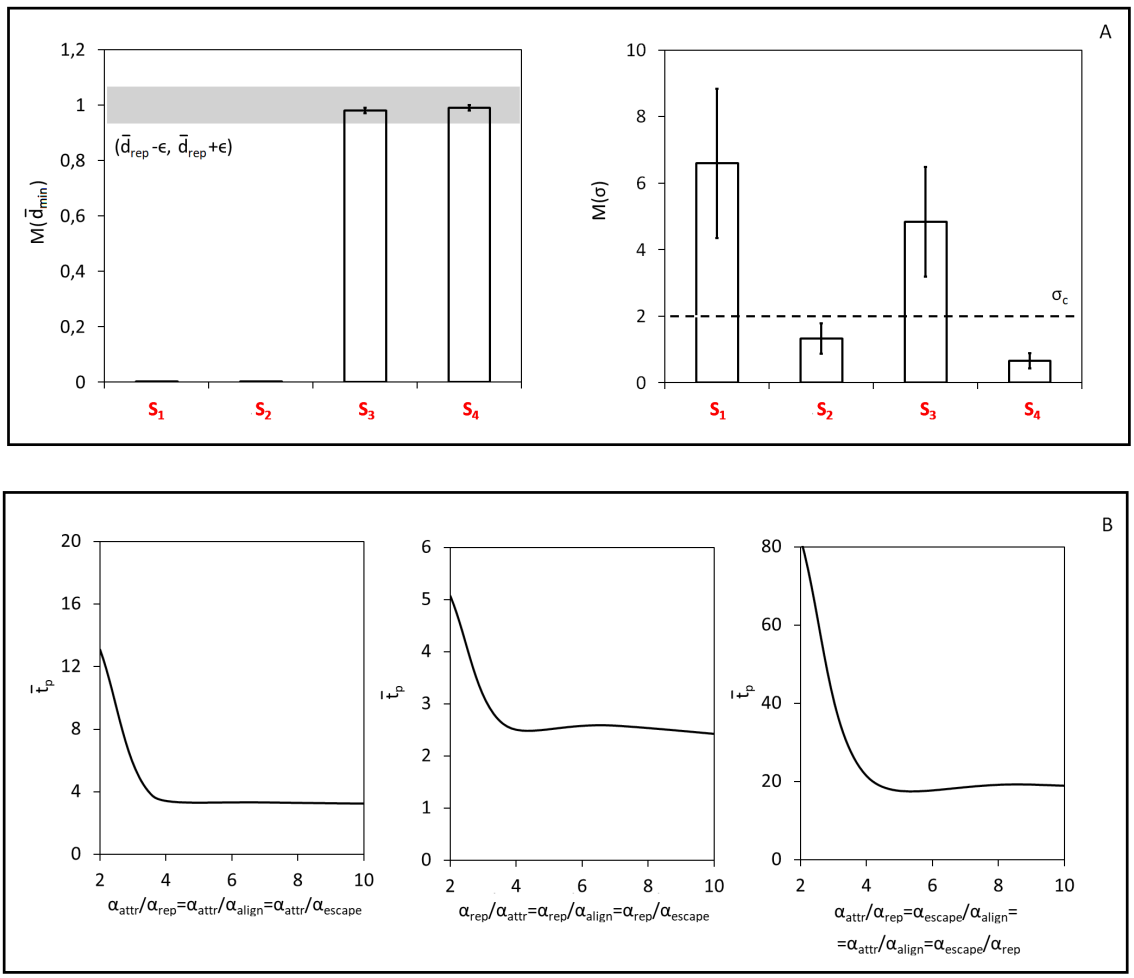

Figure 11.6 Quantitative analysis of the dynamics of both the homogeneous and the heterogeneous systems. (A) For each subregion $\mathcal{S}_i$ ($i = 1, ..., 4$) of the permitted parameter space, the mean and the standard deviation of the asymptotic (i.e., taken at $\bar{t} = 2000$) quantities introduced in Definition 11.2.1 are evaluated over a set of 10 representative numerical realizations resulting from randomly chosen $\alpha^{(\cdot)}$-triplets. For the sake of consistency throughout the text, notation $M(a)$ defines in fact the mean of the quantity a, with $a \in \{\bar{d}_{\min}, \sigma\}$. (B) Time needed by the predator to reach a target upon variations in the ratio between the magnitude of prey behavioral stimuli. Each curve is a *natural cubic spline* interpolating numerical data.

A too large repulsion stimulus (i.e., $\alpha^{\text{rep}} \gg \alpha^{\text{align}} = \alpha^{\text{attr}} = \alpha^{\text{escape}}$) has a negative effect in the case of not confused predator: in order to maintain a comfort space, some prey may in fact turn back and go in the direction of the hunter, which is therefore facilitated in its purpose (see the left-bottom panel in Fig. 11.4). Increasing differences between prey preference for interagent avoidance and the other behavioral stimuli reduce the time

needed by the predator to reach a target, as captured by the central plot in Fig. 11.6 (B). Also in this case a threshold value for $\bar{t}_p$ emerges, which is just below 3. The confused predator is instead not able to take advantage of this prey phenomenology, as captured by the inset i3 in Fig. 11.4.

The prey group safely moves away from both types of predator when they are able to synchronize their movement, regardless of their spacing and escape stimulus (i.e., $\alpha^{\text{align}} \gg \alpha^{\text{rep}} = \alpha^{\text{attr}} = \alpha^{\text{escape}}$), see top panels in Fig. 11.5. In fact, as soon as some individuals within the population are able to perceive the presence and the location of the predator, they start to evade in the opposite direction: such an information is then quickly transmitted to the rest of group and allows all animals to behave accordingly. Such a collective phenomenology represents an example of *coordinated* defense mechanism.

A coupling between sufficiently high escape and attraction stimuli (i.e., $\alpha^{\text{escape}} = \alpha^{\text{attr}} \gg \alpha^{\text{rep}} = \alpha^{\text{align}}$) is detrimental for prey in the case of not confused predator. The tendency to remain somewhat compact in fact delays the evasive strategy: in particular, some individuals fall behind the rest of the group and are unable to avoid the attack of the focused hunter. In such a parameter regime, increments of the difference between the pair of more relevant stimuli and the others lead to decrements of the predation time $\bar{t}_p$, which finally stabilizes around a limit value close to 20, see right panel in Fig. 11.6 (B). This threshold is much larger than the corresponding quantities obtained in the previous parameter setting: this is probably a consequence of the fact that in this case the prey individuals are subjected also to a substantially high preservation stimulus. Such a hierarchy of prey preferred behavior does not represent instead a sufficient advantage for the confused predator, which is still unable to point out and chase any single agent.

The co-presence of significant alignment and escape stimuli (i.e., $\alpha^{\text{escape}} = \alpha^{\text{align}} \gg \alpha^{\text{rep}} = \alpha^{\text{attr}}$) is instead sufficient for the set of prey to avoid both confused and not confused predators. In particular, the groupmates organize in more or less compact clusters, each of them having a preferred direction of evasion. In this respect, the confused hunter undergoes an almost uneffective Brownian motion, being unable to choose and follow a single subgroup of prey (see the inset i4 in Fig. 11.5). On the other hand, the not confused predator, after an initial crawling, opts to follow a single cluster of targets but it can not reach the component individuals, which are already too far from its position (see the inset i5 in Fig. 11.5).

Dispersion in small aggregates is also the prey's successful strategy when mainly guided by repulsion and escape tendencies (i.e., $\alpha^{\text{escape}} = \alpha^{\text{rep}} \gg \alpha^{\text{align}} = \alpha^{\text{attr}}$). It is

however useful to notice that, in this case, prey agents belonging to the same (well-spaced) cluster can undergo uncorrelated movement, as captured by the insets i6 and i7 in Fig. 11.5.

Summing up, we can conclude that confusion completely drops predator ability to hunt its targets, regardless of their strategy, as also experimentally confirmed in [5, 59, 66]. From a prey perspective, alignment represents a significant strategic advantage. On the other hand, excessive grouping stimuli are detrimental since they make it easier for the predator to spot and attack prey, which proceed slowly to remain in visual-contact with the mates. The tendency to maintain a comfort spacing is instead negative if not accompained by a similar or a larger (in term of intensity) escape strategy. We finally remark, for the sake of completeness, that prey and predator have the same speed. Of course, a different hypothesis in this respect may result in variations of the simulation results.

11.5 Conclusive remarks

Populations of intelligent living entities are mainly characterized by the fact that the component agents are not passively prone to external forces but rather undergo active decision-based processes according to individual behavioral preferences and mutual interactions.

In this respect, the description of the collective organization and motion of animal groups has become of increasing interest also for the modeling community and treated with different techniques (as specified in Chapter 2).

This topic has been here addressed with a microscopic particle approach able to distinguish speed and orientation. In particular, the latter has been assumed to be the result of competing stimuli, each of them simply weighted by a coefficient ($\alpha^{(\cdot)}$) that defines a sort of individual preference. The sum of the α-coefficients has been fixed equal to one in order to account for a balance between individual movement traits while avoiding their simultaneous minimization/maximization.

In the case of a homogeneous population of animals, a numerical analysis of the model has then allowed to point out the hierarchy of behavioral inputs (i.e., attraction, repulsion and movement synchronization) eventually resulting in a large-time non-collapsed configuration of the system and/or in fully aligned dynamics.

Our approach has been then enriched to include the effect on collective dynamics of the presence of predators. In this respect, a confused hunter, being unable to single out and chase a preferred target, has been shown to constantly fail in its purpose (at least under the assumption that it has the same physical characteristics as its prey, such as the speed). Such simulation results are in agreement with experimental studies [5, 74, 59] and have been also captured by similar mathematical approaches dealing with schools of fish [105] and swarming prey [19, 69, 68, 78]. On the opposite, the search of an aligned movement has been shown to represent an escape advantage for the prey group in the case of not confused predator. Evasive manoeuvres are instead delayed and impeded by individual preference towards cohesion. Interactions within heterogenous systems have been recently analyzed in several other contexts, i.e., not strictly related to the animal world, including crowd dynamics, in particular in the perspective of groups with leaders [29], and cell migration, e.g., in the case the coexistence of different cell lineages and phenotypes [24, 103].

We here remark that, in principle, the computational results presented in this Chapter depend on the initial condition of the particle system. However, we have observed that the simulation outcomes obtained by keeping the same initial density of agents (i.e., the initial number of animals and diameter of the population), while randomly varying individual position and orientation, did not significantly differ. In this respect, the plots relative to the predation time shown in Fig. 11.6 (B) are obtained from a single numerical realization for each parameter setting. The absence of error bars in the figure, according to us, avoids unnecessary graphical overcomplications as well.

Keeping fixed its basic structure, our model can be easily extended to include a possibly large spectrum of individual behavioral rules: this would simply amount in adding the proper contribution in Eq. (11.2). It would be also possible to deal with a variability in the weights α. For instance, the prey's escape stimulus, quantified by coefficient α^{escape}, may increase when the predator is sufficiently close, while it may decrease becoming negligible when the hunter is substantially far. In this respect, interesting data can be obtained from experimental works. For instance, Herbert and co-workers in [56] demonstrate that, in the case of shoaling fish, the presence of a hunter increases the cohesion within the group, while decreasing dispersion and interindividual spacing. Further, it seems that the tendency and the intensity of the alignments processes are not affected. To employ these results in our model, we would have to keep fixed α^{align}, while simultaneously decrease α^{rep} and increase α^{attr}.

Of course, in nature, predators of different species may have more or less sophisticated hunting strategies, as they can have the ability to target a single prey according to a given characteristic (e.g., age or physical limitations) and not only according to its distance. This aspect can be introduced in the proposed modeling framework by defining a state variable that, for each agent, describes the characteristic of interest, thereby introducing a differentiation within the set of prey. Finally, the application to specific groups of animals is straightforward, since it would only require the inclusion of proper empirical information on individual speed, extension of the interaction regions, and relative behavioral preferences (i.e., hierarchies of α values).

Chapter 12

Comparison with the pertinent literature

We now discuss similarities and differences between our model and analogous published discrete/microscopic approaches. The second-order model proposed by Cucker and Smale in [31, 30] to study flocking phenomena only accounts for an alignment mechanism that forces each individual to adjust its orientation to the groupmates. In particular, the tendency to move in the same direction is set to be higher for close enough individuals, whereas it decreases in the case of pairs of distant agents. An interesting extension of this approach is discussed in [18] and deals with role differentiation within the animal population. In particular, the emergence of some instantaneous leaders (defined as individuals whose movement is not affected by others) can be observed by introducing anisotropy in the synchronization process, i.e., by assuming that each animal interacts only with the groupmates falling within a given visual cone. A further proposed model development is the addition of stochastic perturbations in individual dynamics. As commented again in [18], a noise contribution can be also included in the second-order particle model developed by D'Orsogna and coworkers which, in its original version, accounts for a self propulsion term, a friction contribution (following Rayleigh's law) and a classical Morse potential for attractive/repulsive pairwise interactions [40].

The analysis and classification of the collective motion of identical interacting particles is the topic also of the well-known Vicsek's model [97]. In particular, it assumes that flocking phenomena are due to alignment mechanisms (described by a term similar to our Eq. (11.6)), with uncertainties arising from a random contribution in individual

velocity. This approach is then extended in [50] with the introduction of a Lennard-Jones-type potential to represent repulsive and attractive dynamics. Interestingly, Gregoire and colleagues weight each velocity contribution by a parameter that, at variance with our work, can independently vary in $\mathbb{R}$. Another difference with respect to our model relies in the fact that the extension of the interaction regions are significantly smaller so that the particles interact strictly locally.

The influence of a hunter on group collective dynamics is deeply investigated by particle-based models as well. For instance, in [19], each prey is assumed to be subjected to an increasingly linear attraction towards groupmates and to a hyperbolic repulsion both towards groupmates and towards the predator. The cohesive term and the velocity component relative to hunter avoidance are multiplied by coefficients varying in $\mathbb{R}^+$, whereas the repulsion between prey individuals has a constant unitary weight. Predator dynamics are then completely determined by an attraction term which has a hyperbolic or a more than hyperbolic law. In particular, the hunter is simultaneously attracted by all prey, i.e., it is confused according to our terminology. In the work by Chen and Kolokolnikov, all velocity component finally rely on an Euclidean metric, i.e., they depend on the relative distance between the pair of interacting agents.

In [72], predator-prey interactions are instead tackled by a second-order particle approach, eventually applicable to the case of birds attacking crabs and whales attacking small fishes. In particular, Lee and coworkers assume that prey individuals are subjected to alignment, attraction, repulsion, friction, and hunter escape forces. A random component is also accounted for. Also in this case, each term has a distinct form. For instance, the tendency of a generic agent to synchronize its movement with a groupmate is set to be proportional to the inverse of the square of their mutual distance. Repulsive and attractive behavior are instead given by a Morse-like potential (that depends on the relative position of the pair of interacting particles). A friction force, proportional to the present individual speed, is employed to prevent prey from moving too quickly (this is not necessary in our approach since the speed is possibly limited by a threshold value). Finally, the escape stimulus of each agent is modelled by an $\exp^{-1}$-based function accounting for the presence of the predator within an given region. The hunter is finally set to point towards the center of mass of the group of prey (i.e., it has a *confused* strategy).

The approaches reviewed so-far share with our model the main principles underlying animal movement, i.e., repulsion, attraction, alignment and eventually predator avoidance. However, some relevant differences emerge: in fact, in all these works, the speed closely

depends on the modulus of the vector establishing the direction of motion and/or each contribution taken into account has a substantially distinct mathematical law. These two aspects make our work conceptually closer to the following group of microscopic models dealing with group dynamics.

In 1987, Reynolds published a well-known agent-based approach to simulate flocking phenomena of bird-like individuals (named with the acronym BOIDs) [83]. Therein, each particle is moved by attraction, repulsion, and alignment stimuli. In particular, each behavioral trait is mathematically given by an orientation unit vector multiplied by a weight (as in our case, cf. Eq. (11.2)). However, in the BOID model, the weights are allowed to independently vary, i.e., no constraint on their relationship (e.g., on their sum) is established. An agent may therefore simultaneously maximise or minimize all its behavioral stimuli which, according to us, is somehow unrealistic. Furthermore, in the approach by Reynolds, the resultant velocity vector is not normalized: accordingly, its modulus gives the agent speed, if a threshold values is not exceeded. In this perspective, speed and orientation are not decoupled. The BOID model is then extended in [35] by including an additional escape rule with the same mathematical structure as the other three classical contributions. Further, Delgado-Mata and coworkers multiply each velocity component by a factor that accounts for the emotional state of the animals (e.g., fear). Also in this case, the velocity vector of each agent in not normalized thereby establishing its speed.

In the work by Couzin and colleagues [27, 28], the velocity of each individual is instead established by a constant speed and an orientation unit vector, exactly as in our approach. However, the direction of movement is determined in a slightly different way. In fact, a generic agent, characterized by an anisotropic visual cone, is set to be subjected *only* to repulsion if it detects another mate within its avoidance region. Otherwise, it is set to be subjected to both attraction and alignment towards the groupmates falling within the corresponding interaction areas: in this case the resultant orientation vector is given by the mean of the two contributions. Perturbations are employed by modifying the direction of movement at a randomly chosen extent: however, an agent is not allowed to undergo a complete change in its orientation, due to a constraint on the turn-around angle. At variance with our approach, Couzin and colleagues therefore do not weight individual behavioral preferences; rather, repulsion is the primary stimulus, whereas alignment and attraction equally affect animal dynamics.

Couzin and another group of coworkers perform and describe in [57] an interesting experiment, where a predator bluegill sunfish is allowed to hunt mobile virtual targets in

a controlled environment. In particular, the prey agents are assumed to move following almost the set of rules defined in [27, 28]. Each agent is in fact subjected either to repulsion *or* to the balance between three traits: it can align, ignore, and be attracted by the groupmates. In this respect, the resultant direction of motion of a virtual prey, in the absence of repulsion, is given by a weighted sum of the three contributions, where the weights, as in our case, sum up to one. However, differently from our work, such three behavioral inputs are simultaneously present within the same interaction region (for instance, in our case the alignment and the attraction areas do not overlap). Predator strategy is then analyzed upon variations in target type of motion, which ranges from solitary random walk to the formation and the maintenance of aggregations, eventually coupled with coordinated polarized movement. Their empirical evidence shows that the predation risk is reduced in the case of prey exhibiting a balance between attraction and orientation. Such outcomes are in partial agreement with our numerical results: they are in fact consistent in highlighting the advantage given by a relevant synchronization stimulus but fail to reproduce the disadvantages emerging from the tendency towards group cohesion. A possible explanation of this discrepancy is due to the fact that in our model the virtual prey individuals react to the presence of the predator. In [57], it is also observed that the predator preferentially attaches small groups of targets and individuals located at the edge of the prey aggregate.

The approaches by Couzin and colleagues are extended in [104] to describe escape and foraging manoeuvres in a selfish herd. In particular, all agents are set also to move away from the position of the predator and/or towards the location of a food source. Further, Wood and Ackand multiply each velocity contribution by a weight, that is allowed to freely and independently vary: this is an analogy with the Reynlods' BOID model but differently with respect to our approach. Therefore, also in this case, implausible situations may in principle occur: e.g., a prey may simultaneously maximize the competing stimuli of predator avoidance and food search. Finally, in the work by Wood and Ackland, the predator points to the closest pray, i.e., it is *non-confused*. We finally remark that the alignment term proposed in [27, 28, 57, 104] has exactly the same form as the one given here in Eq. (11.6). However, in their works, the attraction and repulsion contributions slightly differ from ours. In fact, they normalize each term of the sum of vectors at the numerator (and at the denominator) of Eqs. (11.8) and (11.4). However, in all these works, interparticle interactions are based on an Euclidean metric.

These second group of models share with our approach several ingredients. However, as previously commented, some differences emerge as well. In this respect, we can conclude

that our model combines and modifies at various extents concepts and ingredients already present in the literature.

For the sake of completeness, we finally recall that spatial organization and collective motion of systems of animals, also in the presence of escape stimuli, can be approached with lattice-based models. This is the case, for instance, of the series of works by the group of Kamimura (refer to [62, 61, 65, 75, 77] and of the so-called swarm Lattice-Gas Cellular Automata (swarm LGCA) introduced by Deutsch in [36].

Bibliography

[1] Aoki, I. (1980). An analysis of the schooling behavior of fish: Internal organization and communication process. *Bulletin of the Ocean Research Institute-University of Tokyo (Japan). no. 12.*

[2] Avitabile, A., Morse, R., and Boch, R. (1975). Swarming honey bees guided by pheromones. *Annals of the Entomological Society of America*, 68(6):1079–1082.

[3] Ballerini, M., Cabibbo, N., Candelier, R., Cavagna, A., Cisbani, E., Giardina, I., Lecomte, V., Orlandi, A., Parisi, G., Procaccini, A., et al. (2008). Interaction ruling animal collective behavior depends on topological rather than metric distance: Evidence from a field study. *Proceedings of the national academy of sciences*, 105(4):1232–1237.

[4] Barbaro, A. B., Taylor, K., Trethewey, P. F., Youseff, L., and Birnir, B. (2009). Discrete and continuous models of the dynamics of pelagic fish: application to the capelin. *Mathematics and Computers in Simulation*, 79(12):3397–3414.

[5] Bazazi, S., Ioannou, C. C., Simpson, S. J., Sword, G. A., Torney, C. J., Lorch, P. D., and Couzin, I. D. (2010). The social context of cannibalism in migratory bands of the mormon cricket. *Plos One*, 5(12):e15118.

[6] Beekman, M., Fathke, R. L., and Seeley, T. D. (2006). How does an informed minority of scouts guide a honeybee swarm as it flies to its new home? *Animal Behaviour*, 71(1):161–171.

[7] Bernardi, S. and Colombi, A. (2018). A particle model reproducing the effect of a conflicting flight information on the honeybee swarm guidance. *Communications in Applied and Industrial Mathematics*, 9(1):159–173.

[8] Bernardi, S., Colombi, A., and Scianna, M. (2018a). A discrete particle model reproducing collective dynamics of a bee swarm. *Computers in biology and medicine*.

[9] Bernardi, S., Colombi, A., and Scianna, M. (2018b). A particle model analysing the behavioural rules underlying the collective flight of a bee swarm towards the new nest. *Journal of biological dynamics*, 12(1):632–662.

[10] Boeddeker, N., Dittmar, L., Stürzl, W., and Egelhaaf, M. (2010). The fine structure of honeybee head and body yaw movements in a homing task. *Proceedings of the Royal Society of London B: Biological Sciences*, 277(1689):1899–1906.

[11] Burger, M., Capasso, V., and Morale, D. (2007). On an aggregation model with long and short range interactions. *Nonlinear Analysis: Real World Applications*, 8(3):939–958.

[12] Cañizo, J. A., Carrillo, J. A., and Rosado, J. (2011). A well-posedness theory in measures for some kinetic models of collective motion. *Mathematical Models and Methods in Applied Sciences*, 21(03):515–539.

[13] Cañizo, J. A., Carrillo, J. A., and Patacchini, F. S. (2015). Existence of compactly supported global minimisers for the interaction energy. *Archive for Rational Mechanics and Analysis*, 217(3):1197–1217.

[14] Carrillo, J. A., Colombi, A., and Scianna, M. (2017). Adhesion and volume constraints via nonlocal interactions lead to cell sorting. *arXiv preprint arXiv:1706.08969*.

[15] Carrillo, J. A., Delgadino, M. G., and Mellet, A. (2016). Regularity of local minimizers of the interaction energy via obstacle problems. *Communications in Mathematical Physics*, 343(3):747–781.

[16] Carrillo, J. A., D'orsogna, M., and Panferov, V. (2008). Double milling in self-propelled swarms from kinetic theory.

[17] Carrillo, J. A., Fornasier, M., Rosado, J., and Toscani, G. (2010a). Asymptotic flocking dynamics for the kinetic cucker–smale model. *SIAM Journal on Mathematical Analysis*, 42(1):218–236.

[18] Carrillo, J. A., Fornasier, M., Toscani, G., and Vecil, F. (2010b). Particle, kinetic, and hydrodynamic models of swarming. *Mathematical modeling of collective behavior in socio-economic and life sciences*, pages 297–336.

[19] Chen, Y. and Kolokolnikov, T. (2014). A minimal model of predator–swarm interactions. *Journal of The Royal Society Interface*, 11(94):20131208.

[20] Choi, Y., Lui, R., and Yamada, Y. (2003). Existence of global solutions for the shigesada-kawasaki-teramoto model with weak cross-diffusion. *Discrete and Continuous Dynamical Systems*, 9(5):1193–1200.

[21] Chuang, Y.-l., D'orsogna, M. R., Marthaler, D., Bertozzi, A. L., and Chayes, L. S. (2007). State transitions and the continuum limit for a 2d interacting, self-propelled particle system. *Physica D: Nonlinear Phenomena*, 232(1):33–47.

[22] Colombi, A. and Scianna, M. (2017). Modelling human perception processes in pedestrian dynamics: a hybrid approach. *Royal Society open science*, 4(3):160561.

[23] Colombi, A., Scianna, M., and Alaia, A. (2017a). A discrete mathematical model for the dynamics of a crowd of gazing pedestrians with and without an evolving environmental awareness. *Computational and Applied Mathematics*, 36(2):1113–1141.

[24] Colombi, A., Scianna, M., and Preziosi, L. (2017b). Coherent modelling switch between pointwise and distributed representations of cell aggregates. *Journal of mathematical biology*, 74(4):783–808.

[25] Colombi, A., Scianna, M., and Tosin, A. (2015). Differentiated cell behavior: a multiscale approach using measure theory. *Journal of mathematical biology*, 71(5):1049–1079.

[26] Conway, E. D. and Smoller, J. A. (1977). Diffusion and the predator-prey interaction. *SIAM Journal on Applied Mathematics*, 33(4):673–686.

[27] Couzin, I. D., Krause, J., Franks, N. R., and Levin, S. A. (2005). Effective leadership and decision-making in animal groups on the move. *Nature*, 433(7025):513–516.

[28] Couzin, I. D., Krause, J., James, R., Ruxton, G. D., and Franks, N. R. (2002). Collective memory and spatial sorting in animal groups. *Journal of theoretical biology*, 218(1):1–11.

[29] Cristiani, E., Piccoli, B., and Tosin, A. (2014). *Multiscale modeling of pedestrian dynamics*, volume 12. Springer.

[30] Cucker, F. and Smale, S. (2007a). Emergent behavior in flocks. *IEEE Transactions on automatic control*, 52(5):852–862.

[31] Cucker, F. and Smale, S. (2007b). On the mathematics of emergence. *Japanese Journal of Mathematics*, 2(1):197–227.

[32] Degond, P., Génieys, S., and Jüngel, A. (1998). A steady-state system in non-equilibrium thermodynamics including thermal and electrical effects. *Mathematical methods in the applied sciences*, 21(15):1399–1413.

[33] Degond, P. and Motsch, S. (2008a). Continuum limit of self-driven particles with orientation interaction. *Mathematical Models and Methods in Applied Sciences*, 18(supp01):1193–1215.

[34] Degond, P. and Motsch, S. (2008b). Large scale dynamics of the persistent turning walker model of fish behavior. *Journal of Statistical Physics*, 131(6):989–1021.

[35] Delgado-Mata, C., Martinez, J. I., Bee, S., Ruiz-Rodarte, R., and Aylett, R. (2007). On the use of virtual animals with artificial fear in virtual environments. *New Generation Computing*, 25(2):145–169.

[36] Deutsch, A. (1995). Towards analyzing complex swarming patterns in biological systems with the help of lattice-gas cellular automata. *Journal of Biological Systems*, 3(04):947–955.

[37] Deutsch, A., Dormann, S., et al. (2005). *Cellular automaton modeling of biological pattern formation*. Springer.

[38] Di Costanzo, E., Natalini, R., and Preziosi, L. (2015). A hybrid mathematical model for self-organizing cell migration in the zebrafish lateral line. *Journal of mathematical biology*, 71(1):171–214.

[39] Diwold, K., Schaerf, T. M., Myerscough, M. R., Middendorf, M., and Beekman, M. (2011). Deciding on the wing: in-flight decision making and search space sampling in the red dwarf honeybee apis florea. *Swarm Intelligence*, 5(2):121–141.

[40] D'orsogna, M. R., Chuang, Y.-L., Bertozzi, A. L., and Chayes, L. S. (2006). Self-propelled particles with soft-core interactions: patterns, stability, and collapse. *Physical review letters*, 96(10):104302.

[41] Drasdo, D. et al. (2003). On selected individual-based approaches to the dynamics in multicellular systems. *Multiscale modeling*, pages 169–203.

[42] Dyer, J. R., Ioannou, C. C., Morrell, L. J., Croft, D. P., Couzin, I. D., Waters, D. A., and Krause, J. (2008). Consensus decision making in human crowds. *Animal Behaviour*, 75(2):461–470.

[43] Eaton, R. C. and Emberley, D. S. (1991). How stimulus direction determines the trajectory of the mauthner-initiated escape response in a teleost fish. *Journal of Experimental Biology*, 161(1):469–487.

[44] Fetecau, R. and Guo, A. (2012). A mathematical model for flight guidance in honeybee swarms. *Bulletin of mathematical biology*, 74(11):2600–2621.

[45] Fetecau, R. C., Huang, Y., and Kolokolnikov, T. (2011). Swarm dynamics and equilibria for a nonlocal aggregation model. *Nonlinearity*, 24(10):2681.

[46] Fornasier, M., Haskovec, J., and Toscani, G. (2011). Fluid dynamic description of flocking via the povzner–boltzmann equation. *Physica D: Nonlinear Phenomena*, 240(1):21–31.

[47] Galiano, G., Jüngel, A., and Velasco, J. (2003). A parabolic cross-diffusion system for granular materials. *SIAM Journal on Mathematical Analysis*, 35(3):561–578.

[48] Giardina, I. (2008). Collective behavior in animal groups: theoretical models and empirical studies. *HFSP journal*, 2(4):205–219.

[49] Graham, J. (1992). The hive and the honeybee, dadant & sons. *Hamilton, Illinois*.

[50] Grégoire, G., Chaté, H., and Tu, Y. (2003). Moving and staying together without a leader. *Physica D: Nonlinear Phenomena*, 181(3-4):157–170.

[51] Gurney, W., Blythe, S., and Nisbet, R. (1980). Nicholson's blowflies revisited. *Nature*, 287(5777):17–21.

[52] Ha, S.-Y., Liu, J.-G., et al. (2009). A simple proof of the cucker-smale flocking dynamics and mean-field limit. *Communications in Mathematical Sciences*, 7(2):297–325.

[53] Ha, S.-y. and Tadmor, E. (2008). From particle to kinetic and hydrodynamic descriptions of flocking. In *Kinetic and Related Methods*, number 2, pages 415–435.

[54] Hager, M. C. and Helfman, G. S. (1991). Safety in numbers: shoal size choice by minnows under predatory threat. *Behavioral Ecology and Sociobiology*, 29(4):271–276.

[55] Handegard, N. O., Boswell, K. M., Ioannou, C. C., Leblanc, S. P., Tjøstheim, D. B., and Couzin, I. D. (2012). The dynamics of coordinated group hunting and collective information transfer among schooling prey. *Current biology*, 22(13):1213–1217.

[56] Herbert-Read, J. E., Rosén, E., Szorkovszky, A., Ioannou, C. C., Rogell, B., Perna, A., Ramnarine, I. W., Kotrschal, A., Kolm, N., Krause, J., et al. (2017). How predation shapes the social interaction rules of shoaling fish. *Proceedings of the Royal Society B: Biological Sciences*, 284(1861):20171126.

[57] Ioannou, C. C., Guttal, V., and Couzin, I. D. (2012). Predatory fish select for coordinated collective motion in virtual prey. *Science*, 337(6099):1212–1215.

[58] Janson, S., Middendorf, M., and Beekman, M. (2005). Honeybee swarms: how do scouts guide a swarm of uninformed bees? *Animal Behaviour*, 70(2):349–358.

[59] Jeschke, J. M. and Tollrian, R. (2007). Prey swarming: which predators become confused and why? *Animal Behaviour*, 74(3):387–393.

[60] Joie, J., Lei, Y., Colin, T., Durrieu, M.-C., Poignard, C., and Saut, O. (2013). Modelling of migration and orientation of endothelial cells on micropatterned polymers.

[61] Kamimura, A. and Ohira, T. (2010). Group chase and escape. *New Journal of Physics*, 12(5):053013.

[62] Kamimura, A. and Ohira, T. (2019). Group chase and escape. In *Group Chase and Escape*, pages 43–75. Springer.

[63] Katz, Y., Tunstrøm, K., Ioannou, C. C., Huepe, C., and Couzin, I. D. (2011). Inferring the structure and dynamics of interactions in schooling fish. *Proceedings of the National Academy of Sciences*, 108(46):18720–18725.

[64] Kim, J. U. (1984). Smooth solutions to a quasi-linear system of diffusion equations for a certain population model. *Nonlinear analysis*, 8(10):1121–1144.

[65] Kobayashi, T. J. and Kamimura, A. (2012). Theoretical aspects of cellular decision-making and information-processing. In *Advances in Systems Biology*, pages 275–291. Springer.

[66] Krause, J., Ruxton, G. D., Ruxton, G. D., Ruxton, I. G., et al. (2002). *Living in groups*. Oxford University Press.

[67] Kuang, Y. and Gourley, S. A. (2003). Wavefronts and global stability in a time-delayed population model with stage structure. In *Proceedings of the Royal Society of London A: Mathematical, Physical and Engineering Sciences*, volume 459, pages 1563–1579. The Royal Society.

[68] Kunz, H. and Hemelrijk, C. K. (2003). Artificial fish schools: collective effects of school size, body size, and body form. *Artificial life*, 9(3):237–253.

[69] Kunz, H., Züblin, T., and Hemelrijk, C. K. (2006). On prey grouping and predator confusion in artificial fish schools. In *Proceedings of the Tenth International Conference of Artificial Life. MIT Press, Cambridge, Massachusetts*.

[70] Landeau, L. and Terborgh, J. (1986). Oddity and the 'confusion effect'in predation. *Animal Behaviour*, 34(5):1372–1380.

[71] Latty, T., Duncan, M., and Beekman, M. (2009). High bee traffic disrupts transfer of directional information in flying honeybee swarms. *Animal Behaviour*, 78(1):117–121.

[72] Lee, S.-H., Pak, H., and Chon, T.-S. (2006). Dynamics of prey-flock escaping behavior in response to predator's attack. *Journal of theoretical biology*, 240(2):250–259.

[73] Lindauer, M. (1955). Schwarmbienen auf wohnungssuche. *Zeitschrift für vergleichende Physiologie*, 37(4):263–324.

[74] M. Jeschke, J. and Tollrian, R. (2005). Effects of predator confusion on functional responses. *Oikos*, 111(3):547–555.

[75] Milton, J. G., Fuerte, A., Bélair, C., Lippai, J., Kamimura, A., and Ohira, T. (2013). Delayed pursuit-escape as a model for virtual stick balancing. *Nonlinear Theory and Its Applications, IEICE*, 4(2):129–137.

[76] Neill, S. and Cullen, J. M. (1974). Experiments on whether schooling by their prey affects the hunting behaviour of cephalopods and fish predators. *Journal of Zoology*, 172(4):549–569.

[77] Nishi, R., Kamimura, A., Nishinari, K., and Ohira, T. (2012). Group chase and escape with conversion from targets to chasers. *Physica A: Statistical Mechanics and its Applications*, 391(1-2):337–342.

[78] Olson, R. S., Hintze, A., Dyer, F. C., Knoester, D. B., and Adami, C. (2013). Predator confusion is sufficient to evolve swarming behaviour. *Journal of The Royal Society Interface*, 10(85):20130305.

[79] Parrish, J. K. and Edelstein-Keshet, L. (1999). Complexity, pattern, and evolutionary trade-offs in animal aggregation. *Science*, 284(5411):99–101.

[80] Penzhorn, B. (1984). A long-term study of social organisation and behaviour of cape mountain zebras equus zebra zebra. *Zeitschrift für Tierpsychologie*, 64(2):97–146.

[81] Pitcher, T. J. and Wyche, C. J. (1983). Predator-avoidance behaviours of sand-eel schools: why schools seldom split. In *Predators and prey in fishes*, pages 193–204. Springer.

[82] Ramaswamy, S. (2010). The mechanics and statistics of active matter. *Annu. Rev. Condens. Matter Phys.*, 1(1):323–345.

[83] Reynolds, C. W. (1987). Flocks, herds and schools: A distributed behavioral model. In *Proceedings of the 14th annual conference on Computer graphics and interactive techniques*, pages 25–34.

[84] Ruelle, D. (1969). *Statistical mechanics: Rigorous results*. World Scientific.

[85] Schultz, K. M., Passino, K. M., and Seeley, T. D. (2008). The mechanism of flight guidance in honeybee swarms: subtle guides or streaker bees? *Journal of Experimental Biology*, 211(20):3287–3295.

[86] Scianna, M. and Preziosi, L. (2012). Multiscale developments of the cellular potts model. *Multiscale Modeling & Simulation*, 10(2):342–382.

[87] Seeley, T. D. (2010). *Honeybee democracy*. Princeton University Press.

[88] Seeley, T. D. (2014). *Honeybee ecology: a study of adaptation in social life*. Princeton University Press.

[89] Seeley, T. D. and Buhrman, S. C. (1999). Group decision making in swarms of honey bees. *Behavioral Ecology and Sociobiology*, 45(1):19–31.

[90] Seeley, T. D., Morse, R. A., and Visscher, P. K. (1979). The natural history of the flight of honey bee swarms. *Psyche*, 86(2-3):103–114.

[91] Seidl, R. and Kaiser, W. (1981). Visual field size, binocular domain and the ommatidial array of the compound eyes in worker honey bees. *Journal of Comparative Physiology A: Neuroethology, Sensory, Neural, and Behavioral Physiology*, 143(1):17–26.

[92] Sumpter, D. J. (2010). *Collective animal behavior*. Princeton University Press.

[93] Toner, J. and Tu, Y. (1995). Long-range order in a two-dimensional dynamical xy model: how birds fly together. *Physical Review Letters*, 75(23):4326–4329.

[94] Topaz, C. M. and Bertozzi, A. L. (2004). Swarming patterns in a two-dimensional kinematic model for biological groups. *SIAM Journal on Applied Mathematics*, 65(1):152–174.

[95] Topaz, C. M., Bertozzi, A. L., and Lewis, M. A. (2006). A nonlocal continuum model for biological aggregation. *Bulletin of mathematical biology*, 68(7):1601–1623.

[96] Traniello, J. F. (1989). Foraging strategies of ants. *Annual review of entomology*, 34(1):191–210.

[97] Vicsek, T., Czirók, A., Ben-Jacob, E., Cohen, I., and Shochet, O. (1995). Novel type of phase transition in a system of self-driven particles. *Physical review letters*, 75(6):1226.

[98] Visscher, P. K. and Seeley, T. D. (2007). Coordinating a group departure: who produces the piping signals on honeybee swarms? *Behavioral Ecology and Sociobiology*, 61(10):1615–1621.

[99] von Foerster, H. (1959). Some remarks on changing populations. *The kinetics of cellular proliferation*, pages 382–407.

[100] Ward, A. J., Sumpter, D. J., Couzin, I. D., Hart, P. J., and Krause, J. (2008). Quorum decision-making facilitates information transfer in fish shoals. *Proceedings of the National Academy of Sciences*, 105(19):6948–6953.

[101] Waters, A., Blanchette, F., and Kim, A. D. (2012). Modeling huddling penguins. *PLoS one*, 7(11).

[102] Weihs, D. and Webb, P. W. (1984). Optimal avoidance and evasion tactics in predator-prey interactions. *Journal of Theoretical Biology*, 106(2):189–206.

[103] Wolansky, G. (2002). Multi-components chemotactic system in the absence of conflicts. *European Journal of Applied Mathematics*, 13(6):641–661.

[104] Wood, A. J. and Ackland, G. J. (2007). Evolving the selfish herd: emergence of distinct aggregating strategies in an individual-based model. *Proceedings of the Royal Society B: Biological Sciences*, 274(1618):1637–1642.

[105] Zheng, M., Kashimori, Y., Hoshino, O., Fujita, K., and Kambara, T. (2005). Behavior pattern (innate action) of individuals in fish schools generating efficient collective evasion from predation. *Journal of theoretical biology*, 235(2):153–167.